Characterization of VKORC1L1 with respect to VKORC1

Dissertation

zur

Erlangung des Doktorgrades (Dr. rer. nat.)

der

Mathematisch-Naturwissenschaftlichen Fakultät

der

Rheinischen Friedrich-Wilhelms-Universität Bonn

vorgelegt von

Kerstin Liphardt

aus

Grimma

Bonn, September 2018

Angefertigt mit Genehmigung der Mathematisch-Naturwissenschaftlichen Fakultät der Rheinischen Friedrich-Wilhelms-Universität Bonn

1. Gutachter: Prof. Dr. med. Johannes Oldenburg

2. Gutachter: Prof. Dr. rer. nat. Gabriele M. König

Tag der Promotion: 25. Juni 2019

Erscheinungsjahr: 2019

Dieser Weg wird kein leichter sein, dieser Weg wird steinig und schwer.

Für meine Familie

Abstract

Vitamin K reduction is essential and catalyzed by two enzymes *in vitro*. Vitamin K 2,3-epoxide reductase complex subunit 1 (VKORC1) reduces vitamin K to sustain γ-carboxylation of vitamin K dependent (VKD) proteins. This modification is important to physiologically activate all VKD proteins, which are involved in blood coagulation, bone and glucose metabolism. Inhibition of VKORC1 by oral anticoagulants (OACs) is clinically used in therapy and prevention of thrombosis. However, OACs also inhibit the isozyme VKORC1-like1 (VKORC1L1), which may have antioxidative properties and is suspected to reduce vitamin K to scavenge reactive oxygen species.

Specific inhibition data for various OACs were examined by means genetically engineered *VKOR* deficient HEK 293T cells. Inhibition profile differed in terms of therapeutic OACs with 4-hydroxycoumarin and 1,3-indandione backbone. In contrast, rodenticides investigated showed similar susceptibility for both enzymes. To explain the distinct inhibition pattern *in silico* and *in vitro* analysis was performed which identified a warfarin binding site in VKORC1L1 other than VKORC1 binding site.

The function of VKORC1L1 *in vivo* is still unclear. In order to check the effect of the absence of the enzyme, we generated *Vkorc1l1*$^{-/-}$ mouse by CRISPR/Cas9 gene editing. Those mice were viable in homozygous state, in contrast to *Vkorc1*$^{-/-}$ mice, and showed normal fertility. However, they were slender and smaller in size and showed reduced cholesterol and glucose levels in plasma compared to their wild type littermates. Further phenotyping is needed to describe those mice in more detail.

Zusammenfassung

Die Reduktion von Vitamin K ist essentiell und wird durch zwei Enzyme katalysiert. Die Vitamin K 2,3-Epoxid Reduktase Complex Untereinheit 1 (VKORC1) reduziert Vitamin K welches für die γ-Carboxylierung von Vitamin K abhängigen Proteinen benötigt wird. Durch die post-translationale Modifikation werden alle Vitamin K abhängigen Proteine physiologisch aktiviert, welche in der Blutgerinnung als auch u.a. im Knochen- und Glukosestoffwechsel eine Rolle spielen. Orale Antikoagulantien (OAKs) hemmen spezifisch die VKORC1 und werden in der Therapie und Prävention von Thrombosen eingesetzt. Neben der VKORC1 existiert ein Isoenzym, die VKORC1-like 1 (VKORC1L1), welches ebenfalls durch OAKs gehemmt werden kann. Diesem Enzym werden anti-oxidative Eigenschaften zugeschrieben, denn durch die Reduktion von Vitamin K können reaktive Sauerstoffspezies unschädlich gemacht werden.

Um das Inhibitionsprofil verschiedener OAKs zu untersuchen wurden HEK 293T Zellen genetisch manipuliert, so dass eines oder beide Enzyme ausgeschaltet waren. Dabei zeigte sich, dass die VKORC1 (im Vergleich zu VKORC1L1) wesentlich sensitiver gegenüber den therapeutischen OAKs der Gruppen der 4-Hydroxycoumarine und 1,3-Indandione ist. Im Gegenteil dazu zeigten die untersuchten Rattengifte eine gleich hohe Wirksamkeit für beide Enzyme. Um der Ursache der unterschiedlichen Wirksamkeiten nachzugehen wurden *in silico* und *in vitro* Analysen durchgeführt. Es konnte gezeigt werden, dass VKORC1 und VKORC1L1 unterschiedliche Warfarin-Bindungsstellen haben.

Die Funktion der VKORC1L1 *in vivo* ist noch nicht bekannt. Um den Einfluss des Enzyms im Mausmodell zu untersuchen wurde eine *Vkorc1l1*$^{-/-}$ Maus mittels der CRISPR/Cas9 Technologie generiert. Im Gegensatz zu *Vkorc1*$^{-/-}$ Mäusen zeigten die *Vkorc1l1*$^{-/-}$ Mäuse keine Auffälligkeiten, was ihre Lebensfähigkeit und Fruchtbarkeit angeht. Allerdings sind sie kleiner und schmaler und weisen reduzierte Cholesterol- und Glucosespiegel im Plasma auf. Um genauere Aussagen treffen zu können ist es nötig den Phänotyp der *Vkorc1l1*$^{-/-}$ Mäuse genauer zu charakterisieren.

Table of contents

List of abbreviations

°C	degree celsius
3'UTR	3' untranslated region
4HC	4-hydroxycoumarin
aa	Amino acid
ALP/AP	Alkaline phosphatase
ALT	Alanine aminotransferase
Amp	Ampicillin
AST	Aspartate aminotransferase
BHK	Baby hamster kidney cells
BHQ1	Black Hole Quencher 1
BLAST	Basic local alignment search tool
C1	VKORC1
Cas	CRISPR associated
cDNA	copy/ complementary DNA
CHAPS	3-[(3-Cholamidopropyl)dimethylammonio]-1-propanesulfonate
CO_2	Carbon dioxide
CRISPR	Clustered Regularly Interspaced Short Palindromic Repeats
crRNA	CRISPR RNA
C-terminus	Carboxy-terminus
d, h, min, s	Day, hour, minute, second
ddNTP	Dideoxyribonucleotide triphosphate
dest.	destillatus
DEXA	Dual-energy X-Ray absorptiometry
DNA	deoxyribonucleic acid
dNTP	deoxynucleotide triphosphate
DSB	Double strand break
dsDNA	Double stranded DNA
DTT	Dithiothreitol
E. coli	*Escherichia coli*
e.g.	exempli gratia, for example
ECG	Electrocardiogram
ER	Endoplasmatic reticulum
ERGIC	ER-Golgi intermediate compartment 53 kDa protein
ES cells	Embryonic stem cells
et al.	et altera
F	Factor (e.g. FII ,FVII)
FAM	Fluorescein amidite
g	Gram
Gas6	Growth arrest-specific gene 6
GGCX	γ-glutamyl carboxylase
Gla	γ-carboxy glutamate
Glu	Glutamate (glutamic acid)
GRP	Gla-rich protein
GTH	Gesellschaft für Thrombose und Hämostase
HCT	Hematocrit
HEK	Human embryonic kidney cells
hFIX	Human FIX
HGB	Hemoglobin
HR	Homologous recombination
HRP	Horseradish peroxidase

hVKORC1	Human VKORC1
hVKORC1L1	Human VKORC1L1
i.e.	id est
IC_{50}	Half maximal inhibitory concentration
IC_{80}	Eighty percent inhibitory concentration
Indels	Insertion and deletion
ISTH	International society of thrombosis and hemostasis
K>O	Vitamin K 2,3-epoxide
kb	Kilo bases
kDa	kilo dalton
KH_2	Vitamin K hydroquinone
k_i	Inhibitory constant
k_m	Michaelis constant
KO	knockout
L1	VKORC1L1
LDH	Lactate dehydrogenase
M	molar, mol per liter
m, µ, n, p	milli-, mikro-, nano-, pico-
MCH	Mean corpuscular hemoglobin
MCHC	Mean corpuscular hemoglobin concentration
MCV	Mean corpuscular volume
MGP	Matrix Gla protein
MK4	Menaquinone 4
MPV	Mean platelet volume
mRNA	messenger RNA
MWCO	Molecular weight cut-off
Myc tag	polypeptide protein tag derived from the c-myc gene product
NHEJ	Non-homologous end joining
NK cells	Natural killer cells
NQO1	NAD(P)H:Quinon akzeptor oxidoreduktase
nt	Nucleotide
N-terminus	Amino terminus
OAC	Oral anticoagulant
OCN	Osteocalcin
PAM	Protospacer adjacent motif
PCR	Polymerase chain reaction
PDI	Proteindisulfid isomerase
PDW	platelet distribution width
pH	potential hydrogen
PLT	Platelet count
PRGP	Proline-rich Gla protein
qPCR	Quantitative PCR
RBC	Red blood cell count
RDW	Red blood cell distribution width
RNA	Ribonucleic acid
ROS	Reactive oxygen species
rpm	Revolutions per minute (U/min)
RT	Room temperature
SD	Standard deviation
SEM	Standard error of mean
sgRNA	Single guide RNA
siRNA	Small interfering RNA
SpCas9	*Streptococcus pyogenes* Cas9
ssRNA	Single stranded RNA
TF	Tissue factor
TFPI	Tissue factor pathway inhibitor

TIBC	Total iron binding capacity
TM domain	Transmembrane domain
TMG	Transmembrane Gla protein
UBIAD1	UbiA prenyltransferase domain-containing protein 1
UDG	Uracil-DNA glycosylase
UIBC	Unsaturated iron binding capacity
US	United States
v/v	volume per volume
VKCFD1 / 2	Vitamin K clotting factor deficiency type 1 / type 2
VKD	Vitamin K dependent
VKOR	Vitamin K 2,3-epoxid reductase
VKORC1	Vitamin K 2,3-epoxide reductase complex subunit 1
VKORC1L1	Vitamin K 2,3-epoxide reductase complex subunit 1 – like 1
VKR	Vitamin K 2,3 reductase
v_{max}	Maximal velocity
w/v	weight per volume
WBC	White blood cell count
WT	Wild type
xg	Gravity 9,81 m/s^2

1 Introduction

1.1 Blood coagulation

Hemostasis is defined as a physiological response to blood vessel injury and bleeding. It involves the concerted action of vasculature, platelets, and plasma factors and is divided into primary and secondary hemostasis. The primary hemostasis rapidly initiates after endothelial damage and is characterized by vascular contraction, platelet adhesion, and formation of a soft aggregate plug. The secondary hemostasis is initiated following the release of tissue factor (TF) and involves a complex sequence of events known as the blood coagulation cascade (see Figure 1). This process encompasses serial steps where each coagulation factor (F) activates another in a chain reaction that finally results in the conversion of fibrinogen to fibrin. The main goal of secondary hemostasis is to stabilize the soft plug of primary hemostasis and therefore to facilitate the arrest of the hemorrhage.

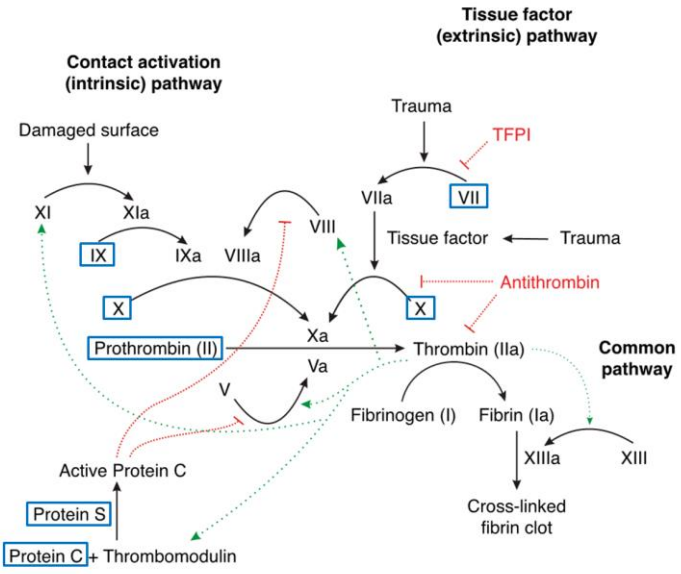

Figure 1: Blood coagulation cascade of secondary hemostasis.
The intrinsic and extrinsic pathways merge in the common pathway, which is characterized by the activation of FX and subsequent cross-linking of fibrin monomers. Feedback mechanisms are shown in red (negative) and green (positive). Vitamin K dependent proteins are boxed in blue (Figure taken and modified from https://en.wikipedia.org/wiki/Coagulation visited on 13-Jan-2018)

1.2 Vitamin K

The discovery of vitamin K resulted from experiments by Henrik Dam and coworkers who investigated dietary deficiency diseases [1]. When chick was fed in a fat and cho-

lesterol-free diet, they developed large subcutaneous and intramuscular hemorrhages. The disease phenotype was not prevented by administration of ascorbic acid as well as vitamin A, C and D. In the 1930's Dam proposed that the antihemorrhagic factor causing the bleeding phenotype was a fat soluble vitamin, which he called vitamin K (K stands for German/Scandinavian Koagulation) [2]. Vitamin K is important for the function of numerous proteins within the body [3]. Three different forms of vitamin K (named K_1 to K_3) are existing, whereby K_1 (phylloquinone) and K_2 (menaquinone, MK-4 through MK-13, dependent on the length of the isoprene side chain) are naturally occurring and K_3 is of synthetic origin. The parent structure of all K vitamins is 2-methyl-1,4 naphthoquinone, the K vitamins differ in the side chain in C3 position (Figure 2). Vitamin K_1 is mainly found in green leafy vegetables as well as olive and soybean oil, whereas vitamin K_2 is present in meat (beef), butter, egg yolks, cheese and fermented soybeans (reviewed in [4]). For healthy adults, adequate intakes of vitamin K range from 55 to 90 µg/d for adult women and 65–120 µg/d for adult men [5].

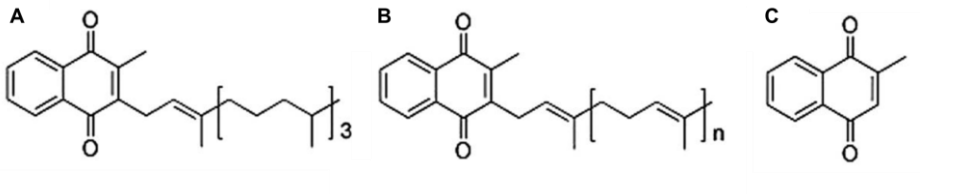

Figure 2: Forms of vitamin K.
A: phylloquinone (vitamin K_1), which is the primary dietary source; B: menaquinones (vitamin K_2), which can vary in length from MK-4 to MK-13; C: menadione (vitamin K_3), which is supplemented to animal food [4].

Vitamin K deficiency can occur in persons of any age due to different reasons (malnutrition, disease-associated). However, infants are at higher risk for hemorrhagic disease [6]. The vitamin K content of human milk is low and only little vitamin K crosses the placenta. Furthermore, the newborn's reservoir of vitamin K is small and expression of coagulation factors is low but increases during first months of life. Thus, vitamin K deficiency can result in hemorrhage, which is counteracted by vitamin K prophylaxis at the time of birth [6].

Vitamin K_1 is the primary dietary source for human beings and is poorly absorbed but has a high hepatic concentration. In contrast, menaquinones are mainly found in extrahepatic tissues, which are converted from vitamin K_1. Nakagawa and colleagues identified UBIAD1 (UbiA prenyltransferase domain-containing protein 1) being responsible for conversion of K_1 to MK-4 [7].

1.3 Vitamin K cycle

The dietary source of vitamin K is vitamin K quinone (K), which needs to be reduced to vitamin K hydroquinone (KH_2) for post-translational modification of vitamin K dependent (VKD) proteins. KH_2 serves as cofactor for γ-glutamyl carboxylase (GGCX), the enzyme responsible for γ-carboxylation and thus biological activation of VKD proteins. GGCX oxidizes KH_2 to vitamin K 2,3-epoxide (K>O), while simultaneously adding CO_2 to glutamic acid (Glu) of vitamin K dependent proteins to form γ-carboxyglutamic acid (Gla). K>O in turn is recycled by VKORC1 (vitamin K 2,3-epoxide reductase complex subunit 1) to KH_2 to serve for another γ-carboxylation as cofactor. The cyclic process of vitamin K reduction by VKORC1 and KH_2 oxidation by GGCX is known as vitamin K cycle (Figure 3) [8].

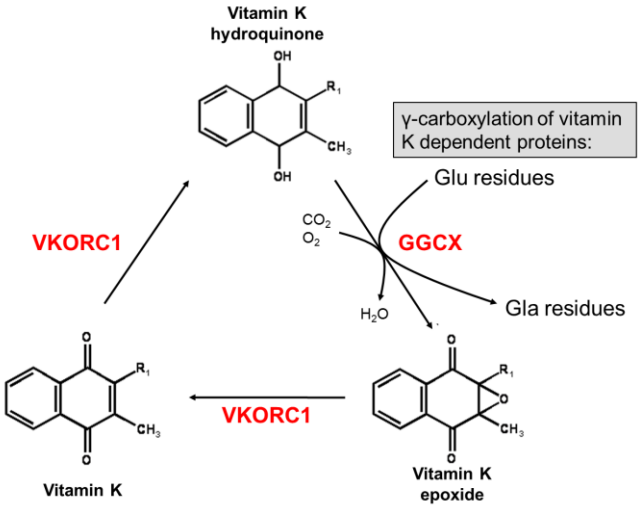

Figure 3: Overview of the vitamin K cycle.
VKORC1 catalyzes the reduction of vitamin K quinone to hydroquinone, which serves as substrate for γ-carboxylation of vitamin K dependent proteins. By carboxylation of glutamic acid residues those proteins get biologically activated. During γ-carboxylation, vitamin K hydroquinone is oxidized to K epoxide, which is reduced to hydroquinone via K quinone by VKORC1. The recycled vitamin K hydroquinone is again available as a co-factor of GGCX. Modified from [8].

Generally, VKORC1 and GGCX are the key enzymes participating in cyclic conversion of vitamin K. However, at least two other proteins are known to be able to reduce KH_2. VKORC1L1 (vitamin K 2,3-epoxide reductase complex subunit 1 like 1), a paralog of VKORC1, was shown to utilize K_1 as well as K_1>O to drive γ-carboxylation of a reporter protein *in vitro* [9, 10].

In addition, it has been speculated that NAD(P)H:quinone oxidoreductase 1 (NQO1) might function as a bypass enzyme in the vitamin K cycle. Although NQO1 has been shown to catalyze the reduction of menadione *in vitro* [11], it is expected that NQO1 is not responsible for γ-carboxylation of VKD proteins in the classical vitamin K cycle [12].

1.4 Proteins of the vitamin K cycle

1.4.1 GGCX

Recycling of vitamin K provides KH_2, which is an important co-factor of GGCX. During γ-carboxylation the γ-hydrogen of the glutamate is abstracted, followed by the addition of CO_2 [13]. Simultaneously, GGCX oxidizes KH_2 to K>O to provide the energy required for γ-carboxylation [14]. GGCX is an integral ER membrane glycoprotein comprised of five (or seven) transmembrane domains, whereby the N-terminus resides in the cytoplasm and C-terminus in the ER lumen [15]. Mutations in the *GGCX* gene (NG_011811.29) can cause vitamin K-dependent clotting factors deficiency type 1 (VKCFD1, OMIM #277450). Besides affecting hemostasis, clinical manifestations have been linked to mutations in *GGCX* causing Pseudoxanthoma elasticum (PXE)-like phenotype. Zhu *et al.* found that *Ggcx*$^{+/-}$ mice developed normally, exhibited normal survival and fertility, and showed normal plasma levels of VKD coagulation factors [16]. However, only 50% of *Ggcx*$^{-/-}$ offspring survived to term and those that were born succumbed to massive intraabdominal hemorrhage shortly after birth [16].

1.4.2 VKORC1

The *VKORC1* gene (NG_011564.1) encodes vitamin K 2,3-epoxide reductase complex subunit-1, a small transmembrane protein of the ER, which was identified 2004 independently by two groups [17, 18]. The gene contains 3 exons, spans approximately 5 kb and is mapped to chromosome 16p11.2. The mRNA has a size of about one kb and encodes a protein of 163 amino acids with a calculated relative molecular mass of 18 kDa. The crystallographic structure of human VKORC1 (hVKORC1) is not solved until now. *In silico* analysis based on bacterial homologue *Synechococcus* sp. (synVKOR) [19] revealed, depend on the algorithm used, a three or four transmembrane (4TM) model (Figure 4) [20, 21]. Recently, the membrane topology of VKORC1 was investigated by Cao and coworkers and confirmed the 4TM model [22]. In the 4TM model, N- and C-terminus face the cytosol. The loop is located between TM1 and TM2 and resides in the ER lumen.

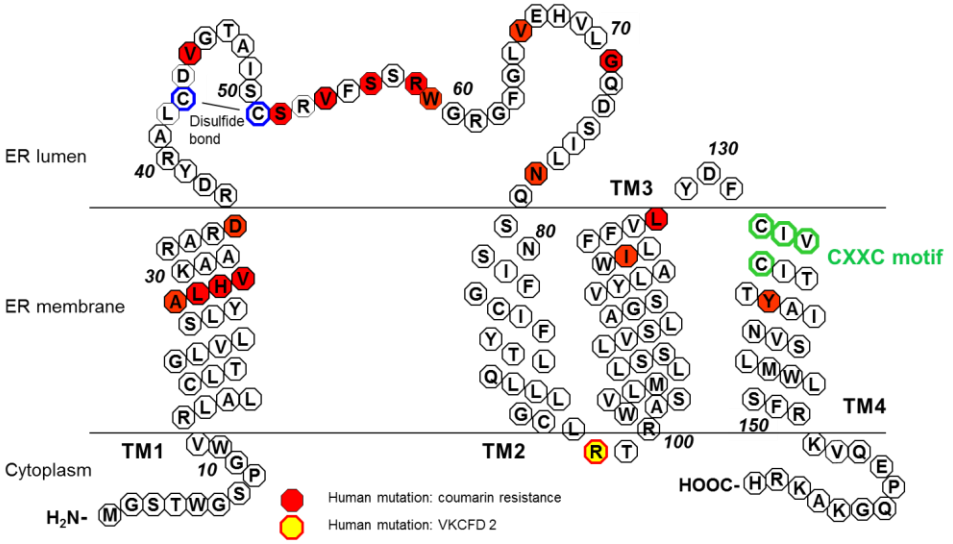

Figure 4: Four transmembrane model of hVKORC1.
The protein passes the membrane four times, whereby N- and C-terminus are located in the cytoplasm. The loop between the first two TMs contains the conserved cysteines Cys43 and Cys51 and resides in the ER lumen. The active center (CXXC motif) is situated in the fourth TM. In addition, red labeled circles represent human mutations leading to coumarin resistance, yellow circle show the mutation associated with VKCFD 2 (modified from [23]).

The ability of vitamin K recycling is highly conserved among species and VKORC1 homologues are found in bacteria, archaea, plants and mammals but not in yeast and fungi [24]. Characteristic for all VKOR (vitamin K 2,3-epoxide reductase) homologs is the CXXC motif in the active site which is essential for reduction of quinone substrates [25]. The cysteines 132 and 135 of the CXXC motif form a disulfide bridge that becomes reduced for catalytic activity. Additionally, there are two other cysteines located in the loop (Cys43 and Cys51) and a conserved serine at amino acid position 57 (or threonine in some VKORC1 homologues) in the large loop of VKORC1 [26]. The loop cysteines are thought to participate in an electron relay in which a redox partner first reduces the Cys43–Cys51 disulfide bond to generate free thiols that then reduce the Cys132–Cys135 disulfide bond, thus leading to activation of VKORC1 [26]. These four cysteines and the serine/threonine are absolutely conserved and define proteins of the VKOR family.

In close proximity to the CXXC motif the hydrophobic Thr138-Tyr139-Ala140 (TYA) motif is located. Mutations in these particular amino acids show resistance to coumarins *in vitro* and *in vivo* suggesting being involved in drug binding [27].

Up to now, only one mutation in VKORC1 has been described to cause a bleeding phenotype. VKCFD2 (vitamin K-dependent clotting factors deficiency type 2, OMIM #607473) is triggered by a point mutation in the *VKORC1* gene, whereby arginine at position 98 is substituted by tryptophan. The phenotype is characterized by reduced

VKD blood coagulation factor levels and can be reversed by oral administration of K_1 leading to increased serum K_1>O level [28], but the mechanism by which vitamin K supplementation rescues VKD coagulation factor levels is not understood.

Beside the VKCFD2 phenotype, 26 mutations in *VKORC1* have been assigned with different requirements of oral anticoagulants (OACs) for stable anticoagulation (OMIM #12270) [21, 29]. The inhibitory profile of these mutations were assessed in a recently described cell-based FIX assay [30] and revealed increased half-maximal inhibitory concentration (IC_{50}) over a range of 2.5-fold and 8.5-fold compared to wild-type VKORC1, reflecting clinical OAC resistance phenotypes that range from moderate to severe resistance [21].

Spohn and colleagues generated VKORC1-deficient mice in order to investigate the deleterious effect of the enzyme on blood coagulation. *Vkorc1*$^{-/-}$ were born at the expected Mendelian ratio, appeared normal, but died between postpartal day P1 and P20. Heterozygous VKORC1-deficient (*VKORC1*$^{+/-}$) mice developed normally, showed normal survival rate and fertility and were phenotypically indistinguishable from their wild-type littermates [31, 32]. To rescue the lethal phenotype non-physiological high doses of vitamin K quinone was devised to bypass the vitamin K cycle (30–50 µg vitamin K per offspring per day, orally administered). In this rescue approach the survival rate of *Vkorc1*$^{-/-}$ mice was indistinguishable from their heterozygous and wild-type littermates. However, VKD clotting factor activities remained significantly reduced in *Vkorc1*$^{-/-}$ mice compared to their wild-type and heterozygous littermates. Cessation of supplementation led to death of *Vkorc1*$^{-/-}$ mice within one week. Beside the bleeding phenotype, a significant reduction in length of the long bones of both *Vkorc1*$^{-/-}$ and *Vkorc1*$^{+/-}$ mice compared to their wild-type littermates was observed [31].

Expression studies in rodents revealed a predominant mRNA occurrence in liver, underlining the importance of vitamin K cycle in the context of blood coagulation since the coagulation factors are synthesized and activated in the liver. However, *VKORC1* is expressed in other tissues as well [12] and was almost not influenced by age in rats [33].

1.4.3 VKORC1L1

By database search with the sequence of VKORC1 as query, Rost and colleagues identified VKORC1L1 (VKORC1-like 1) as a paralog of VKORC1 [17]. *VKORC1L1* is mapped to chromosome 7 and spans about 86 kb. The gene (NC_000007.14) consists of three exons yielding a protein of 176 amino acids. The intronic sequences between exon 1/2 and exon 2/3 have a size of 75 kb and 5.3 kb, respectively. The human protein shares 50% identity with VKORC1 and approximately 97% identity with mouse and rat

Vkorc1l1. It is expected that VKORC1L1 is also comprised of four transmembrane domains with a loop segment between the first and the second TM domain (Figure 5). Both termini are located in the cytoplasm, whereas the loop resides in the lumen of the ER [22, 34].

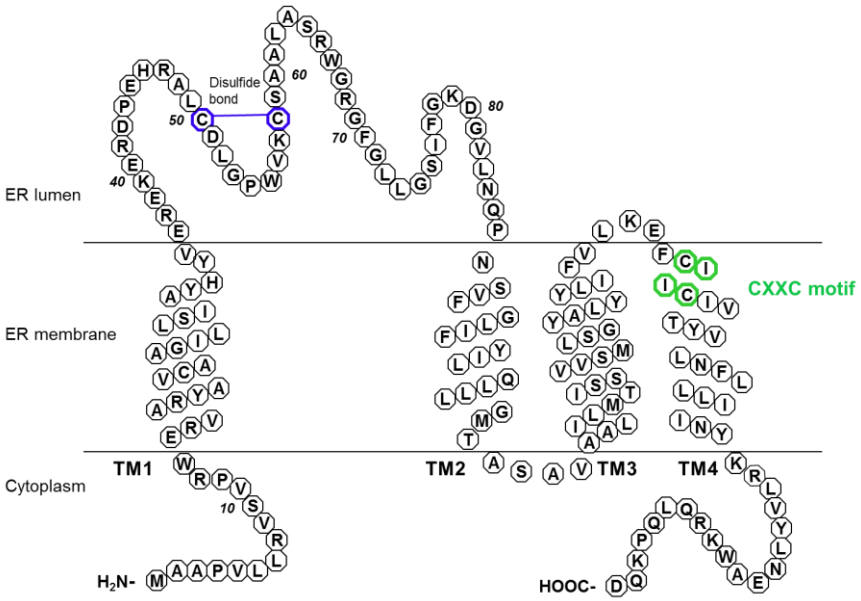

Figure 5: A topological model for human VKORC1L1.
The model is based on sequence alignment to a prokaryotic VKOR homolog protein structure. Cysteines in loop important for disulfide bridge are shown in blue, the catalytic center (CXXC motif) is given in green [10].

By protein sequence alignment of VKORC1 and VKORC1L1 loop cysteines were identified at amino acid positions 50 and 58 in VKORC1L1. The enzyme also comprises an active center (CXXC motif), located at amino acids 139 to 142. Tie and colleagues have examined loop cysteines and concluded from their experiments that the conserved loop cysteines Cys50 and Cys58 participate in active site regeneration through an intramolecular pathway [34, 35].

Up to now, no disease has been associated with mutations in *VKORC1L1* gene. Furthermore, polymorphisms in *VKORC1L1* are not connected with different OAC dose requirements as known for *VKORC1* [36]. The group of Ferron generated *Vkorc1l1* knockout mice to investigate the impact of the absent enzyme. When *Vkorc1l1*$^{+/-}$ mice were intercrossed, littermates were born at the expected Mendelian ratio. There was no evidence of hemorrhage in *Vkorc1l1*$^{-/-}$ mice at any age, and they all survived to adulthood [32].

The physiological function of VKORC1L1 is under debate since the isozyme of VKORC1 is able to provide KH_2 for γ-carboxylation of a reporter protein *in vitro* [9, 33], i.e. VKORC1L1 can produce KH_2 utilizing K and K>O as substrate. However, VKORC1L1 is

not able to rescue the bleeding phenotype in *Vkorc1*$^{-/-}$ mice [31]. Furthermore, Ferron investigated the ability to rescue *Vkorc1*$^{-/-}$ genotype in osteoblasts of OCN-specific *Vkorc1*$^{-/-}$ mice. Serum measurement of osteocalcin (OCN) revealed decreased Gla-OCN and increased Glu-OCN levels, whereas circulating levels of total OCN were unaffected compared to controls. In contrast, measurement in OCN-specific *Vkorc1l1*$^{-/-}$ mice revealed no difference on the circulating levels of Gla-, Glu-, or total OCN. A double knockout of both enzymes in an OCN-specific manner revealed the same levels of OCN as measured in OCN-specific *Vkorc1*$^{-/-}$ mice. Here again, the phenotype of low Gla-OCN and high Glu-OCN was reversible by K_1 but not K_1>O supplementation [32].

Westhofen and colleagues postulated that VKORC1L1 is involved in antioxidation by scavenging reactive oxygen species (ROS). By induction of oxidative stress *in vitro* *VKORC1L1* expression was dramatically upregulated. Furthermore, total VKOR enzymatic activity (reflecting VKORC1 and VKORC1L1 enzyme activity) was strongly enhanced. These results suggest that oxidative stress impacts *VKORC1L1* expression, thus intracellular levels of KH_2 may directly or indirectly counteract ROS and ROS-induced protein damage [10].

1.5 Vitamin K dependent proteins

About 30 years after its discovery the physiological function of vitamin K was resolved in 1974 when Stenflo and colleagues described the presence of a glutamate residue in prothrombin that is modified to Gla (γ-carboxyglutamic acid) [37]. Since then, at least 14 more proteins have been identified containing Gla residues, which build the so-called VKD protein family. VKD proteins can be grouped whether they are synthesized in- or outside the liver (i.e. hepatic and extrahepatic VKD proteins). The distinct Gla residues are located typically in the amino-terminal domain of the protein, for which there is a high degree of amino acid sequence identity in all vitamin K dependent proteins [38]. The Gla residues, modified by GGCX, are required for calcium binding and the calcium mediated action of the proteins and thus essential for biological activity.

1.5.1 Vitamin K dependent coagulation factors

Well characterized vitamin K dependent proteins are proteins belonging to the coagulation cascade. They are synthesized and activated in the liver [39]. The group is comprised of seven proteins that contain 9 to 13 glutamic acid residues in the Gla domain, which are all modified during γ-carboxylation. The Gla residues enable Ca^{2+}-mediated binding of the proteins to negatively charged phospholipid surfaces provided by blood platelets and endothelial cells at the site of injury [40]. The pro-coagulant factors pro-

thrombin (factor II), factors VII, IX, and X participate in the coagulation cascade resulting in the formation of a fibrin clot. In contrast, proteins C, S, and Z have an anticoagulant effect [40].

1.5.2 Vitamin K dependent proteins beyond coagulation

Beyond the VKD coagulation factors, there are other proteins with widespread physiologic function which require γ-carboxylation for their biological activity.

Gas6 (growth arrest-specific gene 6) shows high similarities with protein S [41], however they diverge in their steroid-hormone binding domain. Gas6 is a ligand of receptor tyrosine kinases leading to phosphorylation of proteins at tyrosine residues. Gas6 has many functions, as it is involved in cell proliferation [42], protection against apoptosis [43], and bone differentiation and resorption [44]. Furthermore, it was shown that *Gas6*$^{-/-}$ mice are protected against thrombosis (by preventing the formation of stable platelet plugs) but did not suffer from bleeding [45]. All of the eleven glutamic acid residues in the Gla domain are γ-carboxylated.

Osteocalcin (OCN) is produced by osteoblasts and the γ-carboxylated form binds to hydroxylapatite in the extracellular matrix of bone [46]. OCN is modified at three glutamic acid residues, whereby five residues are located within the Gla domain. Beside the contribution in bone metabolism, undercarboxylated OCN acts as a hormone in glucose homeostasis, energy expenditure, male fertility, brain development, and cognition [32].

Matrix Gla protein (MGP) is synthesized in many soft tissues, with the highest levels of expression in heart, lung, kidney and cartilage [47]. Like OCN, MGP is also found in extracellular bone matrix. The major role of MGP is the inhibition of soft-tissue calcification which was clearly demonstrated by Luo and co-workers. *Mgp*$^{-/-}$ mice were indistinguishable from their littermates during first two weeks of life. At the age of two months KO mice died due to hemorrhage caused by the rupture of thoracic or abdominal aorta [48].

Like MGP, GRP (Gla-rich protein) serves as an important inhibitor of vascular calcification, too [49]. GRP is characterized by 15 glutamic acid residues located in the Gla domain and is distributed in bone, cartilage, skin and vasculature [50].

Another protein suggested to be vitamin K dependent is periostin, a protein whose expression is developmentally regulated and is associated with bone, heart, and dental ligament ontogeny [51]. However controverse results with regard to the γ-carboxylation of periostin are existing [52, 53].

Some years ago, four VKD proteins harboring a transmembrane domain have been identified [54, 55], namely proline-rich Gla protein 1 (PRGP1) and PRGP2 as well as transmembrane Gla protein 3 (TMG3) and TMG4 (also named PRGP3 and 4). Those proteins are expressed in various tissues including brain and kidney [55]. Current studies have shown that PRGP4 may be included in autism and mental retardation in the context of a rare genetic disorder WAGR (Wilm's tumor, aniridia, genitourinary malformations and mental retardation) syndrome [56]. Furthermore, *PRGP4* was identified as one of the top 10 up-regulated genes in response to three common food allergens [57]. However, the biochemical function of these proteins remains to be elucidated.

1.6 Oral anticoagulants

Conditions being treated with oral anticoagulants (OACs) include atrial fibrillation, mechanical heart valves, venous or arterial thromboembolism, and ventricular assist devices [58]. OACs exert their effect by inhibition of VKORC1 activity [59], which reduces the availability of KH_2, thus leading to impaired γ-carboxylation of VKD proteins *in vivo*. In addition, VKORC1L1 was also shown to be susceptible to warfarin treatment [10, 33].

For many decades, substances like warfarin have been the only choice for long-term treatment of before mentioned diseases [60]. More recently, new drugs as direct thrombin inhibitors (e.g. dabigatran) and direct factor Xa inhibitors (e.g. rivaroxaban) are used in antithrombotic therapy. These direct oral anticoagulants (DOACs) act specifically against the active site of one clotting factor, thereby inhibiting the turnover of natural substrates [61]. The chemical compounds used in this study belong to the first generation of OACs and have a 4-hydroxycoumarin or 1,3-indanione backbone.

The matrix of 4-hydroxycoumarins is coumarin (Figure 6), which is a plant-derived natural product with a variety of pharmacological functions including anti-inflammatory, anticoagulant, antibacterial, antioxidative and anticancer properties [62]. Another naturally occurring 4-hydroxycoumarin is ferulenol which is much more potent than coumarin. Ferulenol is synthesized by *Ferula communis* L. and can cause hemorrhage in mammals [63].

In the 1930s Karl Link identified dicoumarol (Figure 6) as the causative agent of the sweet clover disease, a hemorrhagic disorder in cattle. Thereby, coumarin is oxidized by molds (*Asperigillus* or *Penicillium*) in spoiled hay to dicoumarol (3,3'-methylenebis-(4-hydroxycoumarin)) [64]. Further research of Link and colleagues revealed synthetic 4-hydroxycoumarin compounds with anticoagulant activity, were warfarin (named in honor to Wisconsin Alumni Research Foundation, WARF) was the most potent agent out of 150 substances. Warfarin was promoted in 1948 as a rodenticide and later shifted to

clinical application [65]. The most prominent patient treated with warfarin after myocardial infarction was President Dwight Eisenhower in 1955. Since then, more synthetic coumarins have been approved for treatment and prevention of thrombosis. For oral anticoagulation therapy, warfarin is the drug of choice in the US, acenocoumarol (Southern Europe and Asia) and phenprocoumon (Europe) are used as well (Figure 6).

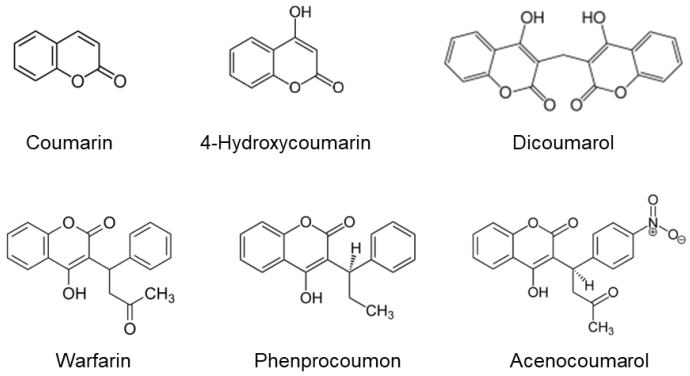

Figure 6: Chemical structure of coumarin-based oral anticoagulants.
Coumarin is a naturally occurring agent which can be oxidized to 4-hydroxycoumarin and dicoumarol by microorganisms. Warfarin, acenocoumarol and phenprocoumon are OACs of synthetic origin.

A second compound class of OACs is represented by 1,3-indandiones. Thereof, fluindione represents 70% of oral anticoagulant prescriptions in France (Figure 7) [66].

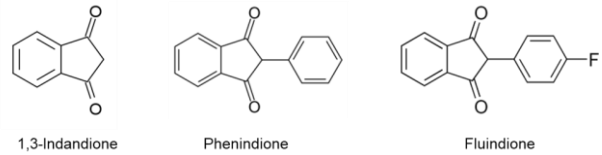

Figure 7: Chemical structure of oral anticoagulants with a 1,3-indandione backbone.

Dosing of oral anticoagulants depends on type of coumarin used and the pharmacogenetic and pharmacokinetic profile of a patient. The metabolism of coumarins depends on hepatic microsomal monooxygenases, mainly CYP2C9 [67–69]. Approximately 40% of phenprocoumon is excreted non-metabolized, whereas acenocoumarol and warfarin are almost completely metabolized [67]. In contrast, little is known about the metabolism of 1,3-indandiones. CYP2C9 haplotypes were shown to have only little impact indicating a minor effect on metabolism of those compounds [66].

The half-lifes of the OACs differ markedly. Of the therapeutically used OACs phenprocoumon displays the longest half-life (about 150 h). Half-lifes of warfarin and fluindione are intermediate (~40 h and 69 h, respectively) whereas acenocoumarol harbors the shortest time (about 6 h) [67, 70].

Originally, coumarins were used for rodent control, because the drug is colorless and odorless with a delayed onset of action. Initially, warfarin was introduced as a pesticide against rats and mice (and is still in use as rodenticide). In the 1950s and 1960s rodenticides with increased potency and half-live were established [71]. In the early 1960s, it was recognized that some rodent strains developed resistance against the “first generation” rodenticides [72, 73]. Thus, a second generation of rodenticides (also called super-warfarins) was introduced in the 1970s solving the problem only partially [74]. By substituting the methyl group of 4-hydroxycoumarin with long, phenyl side-chains these compounds were shown to be more potent with a longer time of action [75].

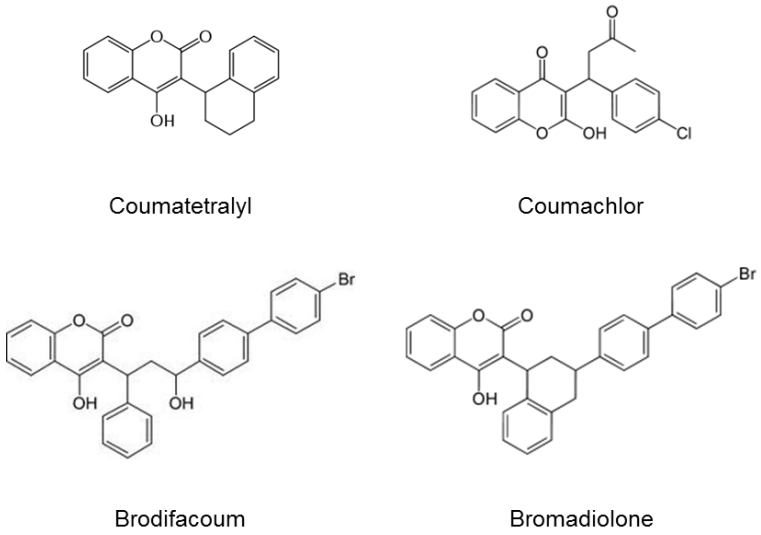

Figure 8: Chemical structure of rodenticides with 4-hydroxycoumarin backbone.
Coumatetralyl and coumachlor belong to the 1st generation of rodenticides, whereas brodifacoum and bromadiolone, introduced as super-warfarins, belong to the 2nd generation of rodenticides.

In contrast to the therapeutically used OACs, the half-lives of rodenticides amount a few up to several days in rats [76]. Pharmacokinetic data in men are only available as case reports of intentional or accidental poisoning. Olmos and Lopez reported a case of brodifacoum intoxication, their analysis revealed a half-life of 56 days [77]. Intoxication requires acute treatment with vitamin K_1 and fresh frozen plasma followed by long term administration of high doses of vitamin K_1 until poisoning resolve [71].

1.7 Aim of the study

In vitro, vitamin K is recycled by two enzymes, VKORC1 and VKORC1L1, which serves as co-factor for γ-carboxylation of vitamin K dependent proteins. *In vivo*, VKORC1 is the key enzyme in liver for vitamin K recycling. Studies highlighting the function of VKORC1L1 *in vivo* and *in vitro* are sparsely available. Therefore the aim of the study was to characterize VKORC1L1 *in vitro* and *in vivo*.

In vitro, both VKOR enzymes are sensitive to warfarin treatment leading to reduced enzyme activity and hence lower KH_2 availability. In a first approach, their susceptibility to various OACs was analyzed by means of genetically engineered cells which allow individual review of VKOR enzyme. Based on the inhibition studies further analysis aimed to identify the binding pattern of warfarin to VKORC1L1.

The second part of this thesis addresses the impact of VKORC1L1 *in vivo*. *Vkorc1l1* knockout mice were generated by CRISPR/Cas9 technology. In contrast to *Vkorc1* knockout mice, *Vkorc1l1* knockout mice are viable. *Vkorc1l1*$^{-/-}$ mice are slender and showed altered glucose and cholesterol plamsa levels. Further characterization of *Vkorc1l1* knockout mice will give insight to biochemical and pathophysiological function of Vkorc1l1 in mice.

2 Materials

2.1 Reagents and chemicals

All the chemicals used were purchased at *pro analysis* grade.

4-hydroxycoumarin	Dr. Ehrenstorfer GmbH, Wesel
Acenocoumarol	Cayman, Ann Arbor, MI, USA
Acetic acid	Merck, Darmstadt
Acryl/bisacrylamide solution	Sigma-Aldrich, Munich
Agar	Sigma-Aldrich, Munich
Agarose	Biozym Scientific GmbH, Oldendorf
Ampicillin	Sigma-Aldrich, Munich
APS	Sigma-Aldrich, Munich
BigDye terminator	Life Technologies, Darmstadt
Brodifacoum	Sigma-Aldrich, Munich
Bromadiolon	Sigma-Aldrich, Munich
Cefemandole	Sigma-Aldrich, Munich
Cephalosporin C	Sigma-Aldrich, Munich
Chloroform	Fluka, Neu Ulm
cOmplete mini, EDTA-free	Roche Diagnostics, Mannheim
Coumachlor	Sigma-Aldrich, Munich
Coumarin	Sigma-Aldrich, Munich
Coumatetralyl	Sigma-Aldrich, Munich
Dade Owren's Veronal Buffer	Siemens Healthcare GmbH, Erlangen
Dicoumarol	Merck, Darmstadt
DMEM, MEM, OptiMEM	Life Technologies, Darmstadt
DMSO	Merck, Darmstadt
DNA ladder (100 bp, 1 kb)	Fermentas, St. Leon-Rot
DNA loading dye	Fermentas GmbH, Leon-Rot
dNTPs	Fermentas GmbH, Leon-Rot
DreamTaq DNA polymerase	Fermentas GmbH, Leon-Rot
EDTA	Sigma-Aldrich, Munich
Ethanol	Merck, Darmstadt

Ethidium bromide	Fluka, Neu Ulm
FBS – SeraPlus	PAN Biotech, Aidenbach
FIREPol® DNA polymerase	Solis Biodyne, Tartu, Estonia
Fluindione	BOC Sciences, NY, USA
Glycerol	Merck, Darmstadt
Glycine	Merck, Darmstadt
HPLC–grade water	Merck, Darmstadt
iProof High-Fidelity DNA Polymerase	Bio-Rad Laboratories, Munich
Isopropanol	Merck, Darmstadt
Kanamycin	Sigma-Aldrich, Munich
LB broth (Lennox)	Sigma-Aldrich, Munich
LB broth with agar (Lennox)	Sigma-Aldrich, Munich
Methanol	Merck, Darmstadt
Midori green	Biozym Scientific GmbH, Oldendorf
Moxalactam	Sigma-Aldrich, Munich
NEAA	Life Technologies, Darmstadt
NP-40	Sigma-Aldrich, Munich
Penicillin/streptomycin	Life Technologies, Darmstadt
PfuTurbo DNA polymerase	Agilent Technologies, Santa Clara, CA, USA
Phenindione	Sigma-Aldrich, Munich
Phenprocoumon	Roche Diagnostics, Mannheim
Proteinase K	Qiagen, Hilden
SDS	Sigma-Aldrich, Munich
SOC medium	Life Technologies, Darmstadt
Tris	Sigma-Aldrich, Munich
Triton X-100	Sigma-Aldrich, Munich
Trizol®	Life Technologies, Darmstadt
Trypsin-EDTA (0.05%)	Life Technologies, Darmstadt
Tween-20	Sigma-Aldrich, Munich
Vitamin K_1	Sigma-Aldrich, Munich
Vitamin K_1 epoxide	Sigma-Aldrich, Munich
Warfarin	Sigma-Aldrich, Munich

2.2 Laboratory equipment

3130xl capillary sequencer	Life Technologies, Applied Biosystems, Karlsruhe
7500 Fast Real-Time PCR	Life Technologies, Applied Biosystems, Karlsruhe
Centrifuge (5430R-X)	Eppendorf, Wesseling-Berzdorf
Centrifuge (3-16PK)	Sigma Laborzentrifugen GmbH, Osterode am Harz
Chemi doc (Gel Doc XR+)	Bio-Rad Laboratories, Munich
Microscope	Carl Zeiss Microscopy GmbH, Göttingen
Nano-Drop ND 1000	Peqlab Biotechnologie GmbH
Neubauer chamber	Neubauer, DE
Power supply	Biometra, GE healthcare, Munich
Thermomixer	Eppendorf, Wesseling-Berzdorf
Thermocycler (MJ Research)	Bio-Rad Laboratories, Munich
Thermocycler (T3000)	Biometra, GE healthcare, Munich
Water bath (Thermostat 2761)	Eppendorf, Wesseling-Berzdorf
96-well plate reader	Synergy 2, BioTek Germany, Bad Friedrichshall

2.3 Consumables

Labware:

Centrifuge tubes (15 and 50 ml)	Greiner Bio-One GmbH, Solingen
CryoTube vials	VWR International GmbH, Langenfeld
Filtertips, 10, 200, 1000 µl	Sarstedt, Nürbrecht
Petri dishes	Greiner Bio-One GmbH, Solingen
PCR 8-stripes	Thermo Fischer Scientific, Waltham, MA, USA
Plates for cell culture (6- and 96-well)	Greiner Bio-One GmbH, Solingen
Serological pipettes	Sarstedt, Nürbrecht
Reaction tubes (1,5 and 2 ml)	Eppendorf, Wesseling-Berzdorf

Commercially available kits:

BigDye Terminator v1.1, Life technologies, Darmstadt

Omniscript® Reverse Transcription Kit, Qiagen, Hilden

Plasmid Mini and Midi Kit, Qiagen, Hilden

Qiaquick Gel Extraction Kit, Qiagen, Hilden

RNeasy Mini Kit, Qiagen, Hilden

RNase-Free DNase Set, Qiagen, Hilden

GenElute™ Mammalian Genomic DNA Miniprep Kit, Sigma-Aldrich, Munich

The CellTiter 96® AQueous One Solution Cell Proliferation Assay, Promega Corporation, Madison, WI, USA

qScript cDNA Synthesis Kit, Quanta Biosciences/VWR, Langenfeld

AgPath-ID One-Step RT-PCR Kit, Applied Biosystems/Thermo Fisher Scientific, Waltham, MA, USA

TaqMan® Gene Expression Master Mix, Applied Biosystems/Thermo Fisher Scientific, Waltham, MA, USA

2.4 Vectors

pIRES	Clontech, Saint-Germain-en-Laye, France
pCMV6-XL4 Human F9, NM_000133.2 (SC126517)	Origene, Rockville, MD, USA
pX330-U6-Chimeric_BB-CBh-hSpCas9	Addgene, Cambridge, MA, USA
pCDNA 3.1 myc/His	Life Technologies, Karlsruhe

2.5 Antibodies

anti-c-myc	Sigma-Aldrich, Munich
ERGIC-53	Santa Cruz Biotechnology, Heidelberg
goat anti-mouse HRP-conjugated	Santa Cruz Biotechnology, Heidelberg

2.6 Buffers and solutions

„Stripping“ buffer	1000 ml: 15 g Glycin, 1 g SDS, 10 ml Tween 20, pH 2.2
10x TBS	0.1 M Tris pH 7.7, 1.5 M NaCl
10x Transfer buffer	250 mM Tris pH 8.3, 1.92 M glycine, 0.1% w/v SDS
1x Cathode buffer	0.1 M Tris, 0.1 M tricine, 0.1% w/v SDS
1x DreamTaq buffer	100 µl 10x DreamTaq buffer, 20 µl 10 mM dTNP mix, 880 µl water

50x TAE buffer	2 M Tris pH 8.5, 50 mM acetic acid, 50 mM EDTA
5x Anode buffer	0.2 M Tris pH 8.9
Blocking solution	2.5 g skim milk powder, 50 ml TBS-Tween, 25 µl Tween-20
Lysis buffer for mouse tails	50 mM Tris pH 8.0, 50 mM KCl, 2.5 mM EDTA, 0.45% NP-40, 0.45% Tween-20, 0.2 mg/ml Proteinase K
Lysis buffer for western blot	50 mM Tris-HCl pH 8.0, 150 mM NaCl, 1% NP-40
MiSeq lysis buffer	10 mM Tris pH 7.5, 1 mM $CaCl_2$, 3 mM $MgCl_2$, 1 mM EDTA, 1% Triton X-100, 0.2 mg/ml Proteinase K (added prior to use)
MiSeq lysis buffer	10 mM Tris pH 7.5, 1 mM $CaCl_2$, 3 mM $MgCl_2$, 1 mM EDTA, 1% Triton X-100, 0.2 mg/ml Proteinase K (added prior to use)
TBS-Tween	100 ml 10xTBS, 900 ml a.d., 50 µl Tween-20
TrisCl-SDS buffer	3 M Tris pH 8.45, 0.3% w/v SDS

2.7 Media for bacterial cultures

Ten g of Luria-Bertani (LB) Lennox broth or 17.5 g of LB Broth with agar were suspended in 500 ml water and autoclaved for 15 minutes at 121°C to sterilize. The broth/agar was supplemented with 75 mg/l of ampicillin after liquid was cooled down to ~ 50°C. LB broth and agar plates were stored at 4°C.

2.8 Media for cell culture

Complete DMEM (including 4.5 g/l D-glucose, L-glutamine and pyruvate) or complete MEM (including Earle's salts and L-glutamine) was supplemented with 1% v/v penicillin/streptomycin, 1% v/v NEAA and 10% FBS.

Expression medium for FIX assay was comprised of OptiMEM supplemented with 0.25 % w/v BSA (sterile filtrated) and 2.5 mM $CaCl_2$ (sterile filtrated). Before use, vitamin K_1 or vitamin K_1 2,3-epoxide was added to a final concentration of 12 µM. Therefore, 6.1 µl of 200 mM K_1 or K_1>O stock (in DMSO or ethanol) solution was added to 100 ml of expression medium. Stock solutions of 10 mM of 4-hydroxycoumarins and 1,3-indandiones were prepared in ethanol and dilution series (10 mM, 5 mM, 2.5 mM, 1.25 mM, 500 µM, 250 µM, 125 µM, 50µM, 25 µM, 12.5 µM, 5µM, 2.5 µM, 1.25 µM) were prepared. In the

assay, each compound was diluted 1:5000 in expression medium including 12 µM K_1 or K_1>O with the respective pre-dilution.

Freezing medium contained 50% complete medium, 40% FBS and 10% sterile DMSO.

2.9 Primers

Primers were designed using online software tools and synthesized by Eurofins MWG Operon (Ebersberg) in desalted quality (HPSF). List of primers is given in the appendix.

2.10 Software

Dissertation preparation	• Microsoft Office 2008
	• Citavi 5 (version 5.2.0.8; Swiss Academic Software GmbH, Wädenswil, Switzerland)
	• SnapGene Viewer 1.3.3
Primer design	• Oligo Calc (www.basci.northwestern.edu/biotools/oligocalc.html)
	• Primer3web version 4.0.0 (http://primer3.ut.ee/)
Sequence analysis	• GeneMapper® v.4.1 (Life Technologies, Applied Biosystems)
	• SeqScape v2.5 (Applied Biosystems)
	• FinchTV (Geospiza, Inc., Seattle, WA, USA)
	• Gentle (Magnus Manske, Cologne)
Sequence search	• BLAST (Basic Local Alignment Search Tool) (www.ncbi.nlm.nih.gov/BLAST/)
Data analysis	• Kaleidagraph 4.5.2 (Synergy Software, Reading, PA, USA)
	• GraphPad Prism 5 (version 5.01, GraphPad Software Inc., La Jolla, CA, USA)
	• Image Lab™ Software 5.1 (Bio-Rad Laboratories, Munich)
In silico analysis	• YASARA platform [78]
	• Chimera platform [79]

3 Methods

3.1 General methods

3.1.1 Site-directed mutagenesis

Site-directed mutagenesis is a method to create specific, targeted changes in double stranded plasmid DNA. Therefore primers are designed which contain the desired mutation and are about 30 bp long [80]. For amplification the PFU polymerase was used, an enzyme having 5'-3'polymerase activity and 3'-5' exonuclease activity, which is an important proof reading feature. By proof reading an incorrect base pair is recognized, excised and replaced by the correct base. PFU polymerase works more accurate but slower (2 min per 1 kb) in comparison to polymerases without this feature (Figure 9).

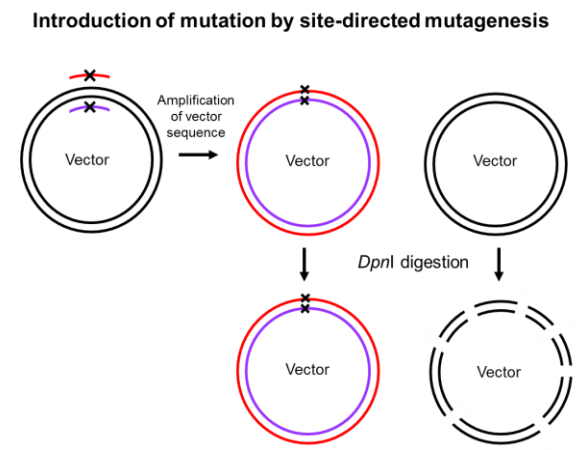

Figure 9: Chart for site-directed mutagenesis.
After denaturation during PCR primers containing desired mutation hybridize to the original plasmid and the polymerase amplifies the complete vector. Afterwards, parent plasmids are digested by *Dpn*I, whereby amplified plasmids remain intact.

The reaction was set up as follows:

	Volume in µl
1x PFU buffer	23
Template (10 ng/µl)	1
Forward primer (20 µM)	0.5
Reverse primer (20 µM)	0.5
PFU Polymerase (2.5 U/µl)	0.5
dH_2O	11.5
Total	**25**

The PCR protocol for the amplification was as follows:

Step 1	95°C	3 min	
Step 2	95°C	30 s	Repeat 15x
Step 3	60°C	1 min	
Step 4	68°C	2 min/kb	
Step 5	95°C	30 s	Repeat 15x
Step 6	60°C	1 min	
Step 7	68°C	2 min/kb + 2 min	

3.1.2 RF cloning

Cloning can be performed without use of restriction enzymes. In restriction free (RF) cloning the desired DNA fragment is integrated via PCR [81]. The DNA fragment to be inserted is called megaprimer and contains overlapping sequences complementary to vector sequence (see Figure 10). The megaprimers were amplified using iProof high-fidelity DNA polymerase and can have a size up to 3 kb. This thermostable polymerase possesses a proofreading activity that accurately amplifies long products from a variety of DNA templates. Primers used for amplification contained 30 bp of vector sequence and 20 bp of target DNA. The resulting PCR products were purified by gel extraction (3.1.8) and are then ready to use for RF-PCR. During RF-PCR the megaprimer hybridizes with the single stranded plasmid and the *Taq* polymerase synthesizes the complementary strand (Figure 10). The PCR products were subsequently incubated with *Dpn*I to destroy the parent plasmid (3.1.3). By means of this technique fragments of interest can be inserted, deleted or exchanged.

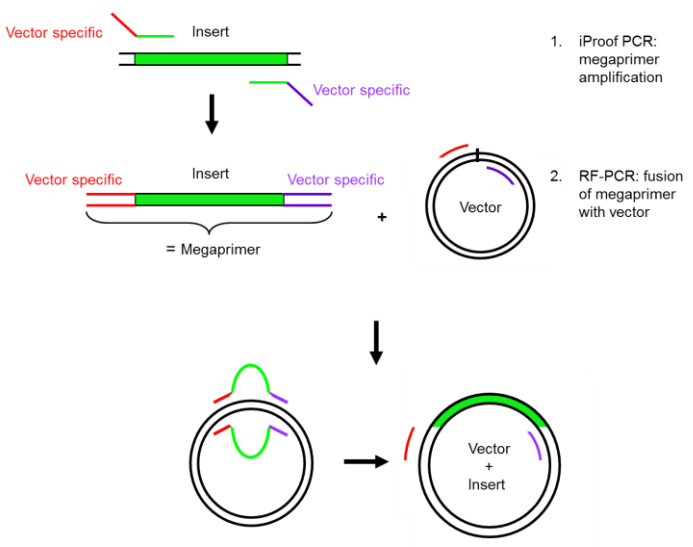

Figure 10: Chart for restriction-free cloning. In the first PCR the megaprimer containing complementary sequences of the target vector is generated. The second PCR (RF-PCR) was used to fuse the megaprimer with the vector which results in an insertion of the DNA.

The PCR was set up as follows:

	Volume in µl
5x HF buffer	4
dNTP Mix (2.5 mM each)	1.6
Forward primer (20 µM)	0.5
Reverse primer (20 µM)	0.5
Template DNA (10 ng/µl)	1.5
iProof polymerase (5 U/µl)	0.5
dH_2O	11.5
Total	**20**

The PCR protocol for the amplification was as follows:

Step 1	98°C	30 s	
Step 2	98°C	10 s	
Step 3	55-65°C	30 s	Repeat 35x
Step 4	72°C	1 min/kb	
Step 5	72°C	10 min	

PCR products were analyzed by gel electrophoresis and respective bands were cutted and extracted (3.1.7). The DNA concentration of the extracted fragment was determined (3.1.11). The megaprimer was used in the RF-PCR, the components were set up as described below:

	Volume in µl
5x Phusion HF buffer	4
dNTP Mix (2.5 mM each)	1.6
Megaprimer (50 -100 ng/µl)	1
Vector (10 ng/µl)	1.5
Phusion High-Fidelity DNA-Polymerase (2 U/µl)	0.5
dH_2O	11.5
Total	**20**

The PCR protocol for the amplification was as follows:

Step 1	98°C	2.5 min	
Step 2	98°C	30 s	
Step 3	60°C	1 min	Repeat 30x
Step 4	72°C	6 min	
Step 5	72°C	7 min	

3.1.3 *Dpn*I digestion

*Dpn*I is an endonuclease which specifically cuts methylated and hemi-methylated DNA at 5´-Gm^{6}ATC-3´. Bacteria methylate their own DNA to discriminate between self and foreign DNA. Plasmids amplified in *E.coli* are methylated, whereby plasmids amplified by PCR are not. Therefore, plasmids amplified by PCR (either by site directed mutagenesis or RF cloning) are not susceptible to *Dpn*I digestion but the original plasmid, which was multiplied in *E.coli.* To the PCR product (20 or 25 µl) 10 U *Dpn*I were added and incubated for 1 h at 37°C. Afterwards, the mixture was transformed into *E.coli* (see 3.1.5).

3.1.4 Manufacturing of competent *E.coli* Top10 cells

To enable the cells to take up circular DNA they have to be made competent. Cells can be made electroporation-competent, whereby plasmids are introduced by application of an electric current. In contrast, chemically competent cells are transformed by heat shock. To make bacteria chemically competent, the following protocol was used. A 5 ml culture of *E.coli* Top10 cells was grown in LB media overnight. In the morning, the culture was transferred to 200 ml LB medium and incubated at 37°C for 2-4 h. When the turbidity, measured at 600 nm, reached 0.5 to 0.6, the bacterial culture was transferred to four 50 ml falcons and centrifuged at 5000 rpm for 10 min at 4°C. Each pellet was resuspended in 9 ml of pre-chilled 100 mM $MgCl_2$ and incubated for 25 min on ice, whereby the number of falcons was reduced to two. After centrifugation (4000 rpm, 10 min, 4°C), each pellet was resuspended in 2 ml 100 mM $CaCl_2$/15% glycerol and united to have one suspension. The cells were aliquoted (50 µl) in pre-chilled eppis and stored at -80°C until use.

3.1.5 Transformation of *E.coli*

Plasmids generated by mutagenesis (see 3.1.1) or RF-cloning (section 3.1.2) were introduced into competent *E.coli* Top10 cells (3.1.4) for replication. Therefore competent cells were thawed on ice and 5 µl of plasmid was added to the cells, mixed gently, and incubated for 30 minutes on ice. Followed by a heat-shock for 30 seconds in a 42°C water bath, cells were chilled on ice for 5 minutes. Afterwards, 200 µl SOC medium was added to the cells, followed by incubation for 1h at 37°C at ~200 rpm. Finally, cells were plated on LB-agar plates containing the appropriate antibiotic (75 µg/ml final concentration) and the plates were incubated upside down at 37°C overnight.

3.1.6 Colony PCR

For verification of cloning or mutagenesis, target DNA was amplified using FIREPol® DNA polymerase. Therefore, clones were picked with a pipette tip and placed into 10 µl of water. After assembly of the PCR reaction mix, 1 µl of the bacterial solution was added to the PCR mix. After successful amplification of desired sequence, 200 µl of LB medium including antibiotic was added and stored at 4°C until evaluation of sequencing. The primers used for amplification were located up- and downstream of multiple cloning site to assure amplification of insert and vector boundaries. The composition of the PCR mix for amplification of target sequence was as follows.

	Volume in µl
10x Buffer	2.5
dNTP Mix (10 mM each)	0.5
$MgCl_2$ (25 mM)	2
Forward primer (20 µM)	0.5
Reverse primer (20 µM)	0.5
Formamid	0.5
Colony	1
DNA polymerase (5 U/µl)	0.2
dH_2O	13
Total	**25**

The PCR protocol for the amplification was as follows:

Step 1	95°C	5 min	
Step 2	95°C	30s	Repeat 35x
Step 3	55-65°C	30s	
Step 4	72°C	1 min/kb	
Step 5	72°C	7 min	

PCR products were analyzed on agarose gel (3.1.7) and the product size was verified by comparison with DNA ladder. Products of expected size were selected for sequencing.

3.1.7 Agarose gel electrophoresis

1% (w/v) Agarose gels were prepared in 1x TAE buffer by heating the mixture in a microwave oven. After cooling to ~60°C Midori Green Advance (1:20,000) was added to visualize the DNA. Samples were mixed with 5x loading dye and loaded on the gel. A molecular weight size marker (1 kb or 100 bp ladder) was used depending on the size of

the products. Samples were separated in 1x TAE at 5-10 mA/cm (usually 150 V for 25 min) and were visualized and documented under UV light on a ChemiDoc system.

3.1.8 Gel extraction

PCR products (like megaprimers for RF-cloning) were gel purified using the QIAquick Gel Extraction Kit. Briefly, the products were resolved on agarose gels as described above and the fragments were excised. Gel slices were dissolved in a buffer containing a pH indicator and incubated for 10 minutes at 55°C. The mixture was then applied to the QIAquick spin column, and after several wash steps, the products were eluted in 30 µl water.

3.1.9 Sequencing

Sequencing was performed based on the chain termination method using BigDye terminators, which contains a set of dye terminators labeled with high-sensitivity dyes [82]. Each dye is fluorescent at a different wavelength. Sequencing is based on a mix of these fluorescence-labeled dideoxynucleotides. The excitation of dyes is done via a laser beam followed by a detection of fluorescence by a CCD camera. PCR products (3.1.6) were diluted by the addition of 200 µl water and used in the following sequencing mix:

	Volume in µl
5x BigDye sequencing buffer	1.5
Sequencing primer (5 µM)	0.5
BigDye Terminator sequencing mix	0.5
Diluted PCR product	2
dH_2O	6.5
Total	**11**

The PCR protocol for sequencing was as follows:

Step 1	96°C	1 min	
Step 2	96°C	10 s	Repeat 35x
Step 3	50°C	5 s	
Step 4	60°C	4 min	

The products were subsequently purified by EtOH/NaAc precipitation (10 µl of the sequencing reaction product, 50 µl 96 % EtOH, 10 µl dH_2O and 2 µl of 3M NaAc pH 4.6) followed by centrifugation by 4°C at 4000 rpm for 45 minutes. The pellet was washed once with 70% EtOH for 10 minutes at the same centrifugation conditions and air dried.

Samples were stored at -20° C until they were resuspended in 15 µl water and loaded on the capillary sequencer.

3.1.10 Isolation and purification of bacterial plasmid DNA

After validation of the clones by sequencing, clones were grown overnight in 2-5 ml LB-medium with the appropriate antibiotic. For long term storage stocks were prepared from each colony by pelleting an overnight culture (4000xg, 10 min, 4°C). The pellet was re-suspended in 730 µl LB medium and 130 µl glycerol, mixed well and stored at -80°C for later use.

Dependent on the application plasmid isolation was done on “mini” or “midi” level, whereby the yield on plasmid DNA differed. QIAGEN Plasmid Mini Kit was used for small scale DNA purification with a yield of maximum 20 µg. For higher yields PureLink® HiPure Plasmid Filter Midiprep Kit (Invitrogen) was used. Purification was performed according to manufacturer’s protocol.

In general, plasmid preparation procedure uses the modified alkaline lysis method. Therefore, cells are harvested by centrifugation and lysed under alkaline conditions, and the lysate is subsequently neutralized and adjusted to high-salt binding conditions in one step. After lysate clearing, the sample is ready for purification on the silica membrane. After a wash step plasmid DNA is eluted in high-salt buffer and the DNA is concentrated and desalted by isopropanol precipitation and collected by centrifugation. Afterwards, DNA was washed with 70% ethanol and centrifuged again. Finally, the supernatant was carefully discarded and the pellet was resuspended in appropriate volume of water. DNA concentration was assessed and plasmids were stored at -20°C until use.

3.1.11 Measurements of DNA and RNA concentrations

Nucleic acid concentration and quality was determined by photometry on a Nanodrop® instrument (1 OD_{260nm} = 50 µg double stranded DNA/ml or 1 OD_{260nm} = 40 µg single stranded RNA/ml).

3.1.12 Protein analysis

During electrophoresis proteins are separated on polyacrylamide gels according to their size. The monomer acrylamide is cross-linked with N,N-methylenebis-acrylamide by polymerization initiators APS and TEMED. The separation of molecules is determined by the relative size of the pores formed within the gel. Non-covalent protein interactions are disrupted by a detergent (usually SDS) and disulfide bonds are degraded by DTT or β-mercaptoethanol, leading to size-dependent migration of the proteins in the gel.

For separation of proteins the Mini-PROTEAN Tetra system (Bio-Rad Laboratories) was used with handcast tricine based gels.

Assembly of tricine gels

The gels were prepared and stored up to one week at 4°C in cathode buffer. Volumes given below are sufficient for casting 4 mini gels.

Sealing gel	10% separation gel	Stacking gel
700 µl TrisCl-SDS buffer	3.2 ml water	4.2 ml water
1 ml 30% Acryl/bisacrylamide	6.6 ml 30% Acryl/bisacrylamide	1.2 ml 30% Acryl/bisacrylamide
10 µl 10% w/v APS	6.6 ml TrisCl-SDS buffer	1.8 ml TrisCl-SDS buffer
10 µl TEMED	4 ml 50% v/v glycerol	72 µl 10% w/v APS
	200 µl 10% w/v APS	7.2 µl TEMED
	8 µl TEMED	

Samples were diluted in a 1:1 ratio with tricine sample buffer, incubated at room temperature for 10 min or at 95°C for 5 min, depending on the application. Electrode assembly was filled with cathode buffer, and the tank was filled with 1x anode buffer. The gels were run at 180 V for 30 to 45 min.

Western blot

By western blot proteins can be identified from a complex mixture of proteins by means of specific antibodies.

Proteins were blotted onto polyvinylidene fluoride (PDVF) membrane by tank blot system at 300 mA for 70 min. To block free antibody binding sites the membrane was incubated for 1 h at room temperature or overnight at 4°C in blocking solution. Washing of membrane was performed in TBS-Tween. Incubation with anti-c-myc antibody (1:2000, diluted in TBS-Tween) or anti-ERGIC53 (1:500 in TBS-Tween) was done for 1 h at room temperature or overnight at 4°C. Membrane was washed at least three times for 10 min with TBS-Tween. Secondary antibody (goat anti-mouse HRP conjugated, 1:5000) was incubated for 1 h at room temperature. Membrane was washed as described earlier. For detection HRP substrate was added according to manufacturer's instructions and visualized using ChemiDoc.

For incubation with another antibody the membrane was „stripped" to release bound antibodies. Therefore, membrane was incubated twice with "Stripping" buffer for 10 min and washed afterwards (with PBS twice for 10 min, with TBS-Tween twice for 5 min). Subsequently the membrane was ready to use (starting with blocking solution).

3.1.13 Cultivation of mammalian cells

HEK 293T cells originate from human embryonic kidney cells that were generated in 1973 by transformation of cultures of normal with sheared adenovirus 5 [83].

The adherent growing cells were cultivated in complete DMEM. For maintenance, cells were cultivated on 10 cm dishes and splited once a week in a 1:10 to 1:20 ratio. Therefore, medium was aspirated and 2 ml of trypsin was added to detach the cells. After 2-3 min, 8 ml of complete medium was added to stop trypsinization and the cells were resuspended carefully. For 1:10 ratio, one ml of the cell solution was spread to the desired number of plates and 9 ml of complete medium was added and mixed gently. After 2-3 days medium was changed.

For long-term storage cells were stored in liquid nitrogen. Therefore, cells of a confluent 10 cm dish were trypsinized and pelleted by centrifugation (500xg, 2 min, room temperature). Subsequently, the pellet was resuspended in 3.8 ml freezing medium and divided to two cyro vials and put into a cooling container (Mr. Frosty), which was placed at -80°C overnight. The use of the container provides a –1°C/minute cooling rate required for successful cell cryo preservation and recovery. Afterwards, the vials are stored for long term in liquid nitrogen.

For re-cultivation of frozen cells, vials were thawed at 37°C and directly mixed with 8 ml of complete medium. After 8 to 16 hours the medium was changed to eliminate DMSO contained in freezing medium. Usually, cells were cultivated for one to two weeks prior experimental use.

3.1.14 Cell counting

For cell counting, cells were trypsinized and resuspended in complete DMEM. Afterwards, 10 µl of cell suspension was mixed with 90 µl trypan blue, a diazo dye which is taken up only by dead cells, whereby these cells are stained blue. An aliquot of the mix was loaded on the Neubauer chamber and viable cells (“white” cells) were counted in bright field microscope as depicted in Figure 11.

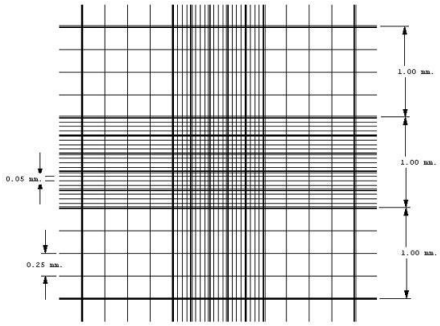

Figure 11: Neubauer-improved chamber counting grid detail.
Cells located in the outer big 4 squares are counted.

For calculation of cell number, the mean of counted cells per big square was multiplied by the dilution factor (which is 10, if diluted as described above) and the chamber factor ($1*10^4$) and gives the number of cells per ml.

3.1.15 Transfection of HEK 293T cells

For transfection of HEK 293T cells, Lipofectamine 2000 was used. This reagent is based on the lipofection, whereby genetic material is injected into a cell by means of liposomes, which are vesicles that can easily merge with the cell membrane since they are made of a phospholipid bilayer. The positive surface charge of the liposomes mediates the interaction of the nucleic acid and the cell membrane, allowing for fusion of the liposome/nucleic acid transfection complex with the negatively charged cell membrane.

One day prior to transfection cells were seeded on 6-well plates to reach a confluency of 80 to 90% on the next day. Per 6-well, 2 µg plasmid DNA was diluted in 150 µl of Opti-MEM and mixed. In a second reaction vial 10 µl of Lipofectamine 2000 was diluted in 150 µl of OptiMEM. The plasmid-OptiMEM mix was added to the diluted Lipofectamine and mixed by inverting. The plasmid-Lipofectamine-OptiMEM mix was incubated for 5 min at room temperature. In the meantime, medium was aspired and 1 ml of OptiMEM was added to the cells. The plasmid-lipid complex was added carefully to the cells and mixed gently. Four hours later the medium was discarded and the cells were incubated with appropriate medium.

3.1.16 CRISPR/Cas9 based gene editing technique

Bacteria and archaea have evolved RNA-mediated adaptive defense systems that protect organisms from invading viruses and plasmids [84, 85]. The **c**lustered **r**egularly **i**nterspaced **s**hort **p**alindromic **r**epeats (CRISPR) system has currently been adapted to genome editing research with a wide spectrum of organisms. Naturally, the system relies on CRISPR RNAs (crRNAs) in complex with CRISPR-associated (Cas) proteins to direct degradation of complementary sequences present within invading viral and plas-

mid DNA. Three types of CRISPR mechanisms have been identified, of which type II from *Streptococcus pyogenes* is the most studied, because single Cas9 along with crRNA and tracrRNA (trans-activating CRIPSR RNA) seems to be sufficient for cleaving the target DNA [86].

Based on the type II CRISPR system an optimized two-component system using single guide RNA (sgRNA) and Cas9 was established [84] (Figure 12). Thereby, sgRNA consists of a fusion between trRNA and crRNA which can be used to produce sequence-specific double strand breaks (DSBs). The target sequence for introduction of DSB consists of a 20-bp DNA sequence complementary to the sgRNA, followed by protospacer adjacent motif (PAM, 5'-NGG-3'). The Cas9 nuclease digests both strands of the genomic DNA three to four nucleotides 5' of the PAM sequence. By introducing different guide RNA sequences, the Cas9 can be programmed to introduce site-specific DNA double-strand breaks virtually anywhere in the genome where a PAM sequence is located. The double-stranded break at the target site induces DNA repair mechanisms, such as non-homologous end joining (NHEJ) that create insertions and deletions leading to a premature stop codon, and homology-directed recombination (HR) for introducing new sequences.

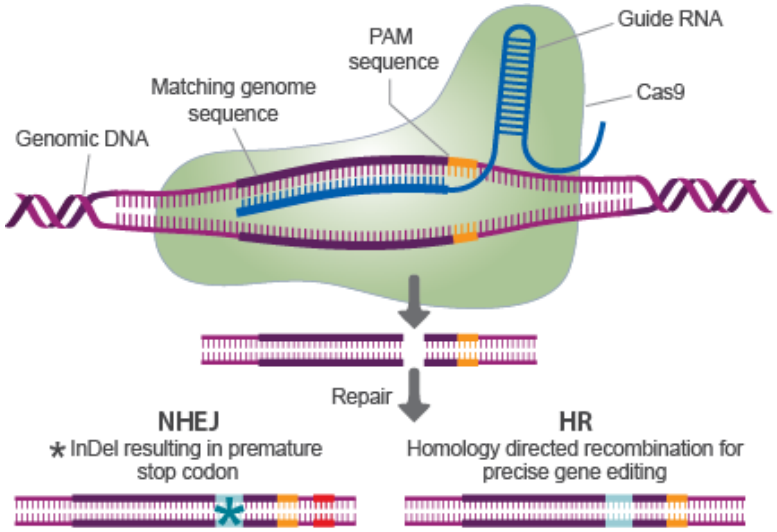

Figure 12: CRISPR Cas9 gene editing tool to modify genomic DNA.
The nuclease Cas9 introduces double stranded breaks, which is repaired non-homologous end joining (NHEJ) or homologous recombination (HR). By NHEJ random insertions or deletions (indels) at the target site are created. By means of recise changes based on template DNA can be introduced. Taken and modified from http://www.transomic.com/Products/transEdit.aspx, visited on 04-Dec-2017.

The CRISPR/Cas9 gene editing tool was used to generate *VKORC1* and *VKORC1L1* knockout HEK 293T cell lines. In addition, the same technique was used to accomplish *VKORC1L1* knockout mice.

3.2 Characterization of VKORC1 and VKORC1L1 *in vitro*

3.2.1 Generation of HEK 293T KO lines

HEK 293T cells were used to knockout *VKORC1*, *VKORC1L1* or both, since those enzymes are able to recycle vitamin K epoxide. The generation of KO cell lines was done by the CRISPR/Cas9 system which allows a highly specific site directed mutagenesis at the target site. CRISPR vector containing the target crRNA was used for transfection of HEK 293T cells. The sequence introduced into the vector was GCTCTACGCGCTG-CACGTGAAGG for *VKORC1* and CCTACCACGTGGAGCGGGAGAAG for *VKORC1L1*. Two days after transfection, cells were seeded on 96-well plates to yield single cell clones. Therefore, cells were trypsinized and complete DMEM was added. After visual inspection, cells were diluted to yield about one single cell per well in a 96 well plate. The suspension was distributed to three to four 96-well plates and once a week medium was changed. Two to three weeks later, cells were grown to confluence and splitted for maintenance and genotyping. Therefore, cells were resuspended in about 50 µl old medium and 5 µl of cell suspension was transferred to two new 96-well plates. The remaining cells were prepared for long-term storage. Therefore, cells were resuspended in freezing medium (composed of 90% FBS, 10% DMSO) and the plates were stored over night at -20°C. Afterwards, the plates were transferred to -80°C for long-term storage.

For genotyping, cells were harvested by aspiration of medium and addition of 100 µl MiSeq lysis buffer. Cells were resuspended and transferred to 96-well PCR plate and lysed by incubation at 65°C for 10 min followed by 15 min at 95°C. Plates were stored at -20°C until use. An aliquot was used for target gene amplification by PCR. The genetic profile was analysed using MiSeq sequencer (Illumina Inc., San Diego, CA, USA) and clones with deleterious VKOR were chosen for further analysis.

3.2.2 FIX cell-based assay

For assessment of inhibitory potential of OACs and related compounds the recently published cell-based FIX activity assay was used [30]. The *in vitro* assay is based on the indirect measurement of VKOR activity by means of FIX, which is γ-carboxylated in the cell if VKOR supplies GGCX with KH_2. Subsequently, FIX is measured by clotting assay, which is a modified aPTT assay. The basic principle of the cell-based assay is shown in Figure 13. Thereby, KO HEK 293T cells are transfected with cDNA of *F9* (see section 3.1.15) and the cells were grown for 3 days in 3 ml expression medium supplemented with K_1 and the respective drug dilution. The supernatant was transferred to VivaSpin columns and centrifuged at 4000 rpm for 20 min at room temperature. The complete

supernatant was transferred to a vial and the column was rinsed with 300 µl of Dade Owren's Veronal buffer. Samples were stored at -40°C until measurement. If double knockout (DKO) cells were used, the bicistronic vector pIRES containing cDNA of *F9* and VKOR variant was transfected. Further steps were performed as described above.

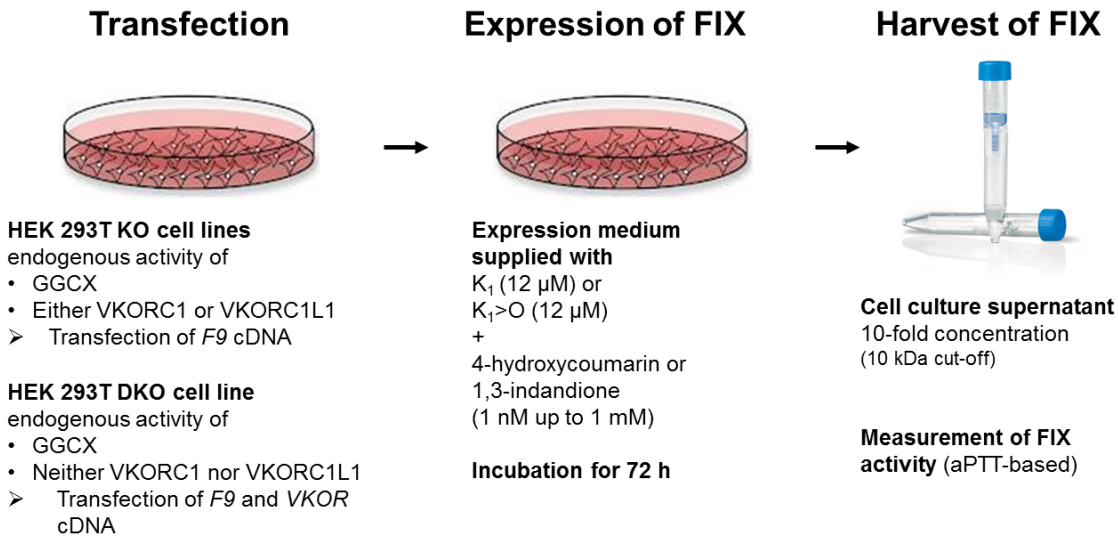

Figure 13: Overview of FIX cell-based assay.
HEK 293T single or double KO cells were transfected with *F9* or with *F9* concomitant with *VKOR* cDNA. Afterwards, cells were grown in expression medium containing K_1 or K_1>O and a respective dilution of 4-hydroxycoumarine or 1,3-indandione. After three days of incubation the cells were harvested by concentration of the cell culture supernatant on VivaSpin columns and FIX activity was assessed using a modified aPTT assay.

The activated partial thromboplastin time (aPTT) is a global screening procedure which is used for the diagnosis of coagulant disorders and therapeutic monitoring of both hemorrhagic and thrombotic disease. To evaluate FIX levels of cell culture samples a modified aPTT was used. Therefore, 50 µl of FIX-deficient plasma was mixed with 20 µl of the sample and 75 µl of Actin FSL, which contains purified soy and rabbit brain phosphatides with plasma activator. The addition of calcium ions triggers the coagulation process, and the clotting time is measured on a coagulation analyzer BCS XP. By means of a calibration curve of standard pool plasma, values are given in percent FIX activity.

3.2.3 Measurement of cell viability

The influence of oxidative stress on different cell lines was assessed using the CellTiter 96® AQueous One Solution Cell Proliferation Assay, which is a colorimetric method to determine the number of viable cells. Thereby, a tetrazolium compound (MTS) is converted exclusively by viable cells into formazan, which can be measured at 490 nm. WT, *VKORC1* KO and *VKORC1L1* KO and DKO HEK 293T cells were seeded on 96 well

plates ($5*10^5$ cell/ml). Four hours later, different concentrations of H_2O_2 (0 to 100 µM) or 50 µM H_2O_2 combined w/o K_1 (12 µM) and w/o warfarin (500 nM) were added. After 18 h, 15 µl of MTS reagent was added and incubated for 2 h in a humidified, 5% CO_2 atmosphere. Finally, the absorbance at 490 nm was measured with a 96-well plate reader. For calculations, mean values were made and blank values subtracted. To normalize, control (i.e. cells without treatment) was set to 100%.

3.2.4 Molecular modeling of VKORC1 and VKORC1L1

Two different approaches were adopted to model the human VKORC1 and VKORC1L1 proteins. A homology model of VKORC1 was previously constructed based on the X-ray crystal structure of the bacterial homologue (*Synechococcus* sp.) of VKORC1 (PDB ID: 3KP9) (http://www.pdb.org/pdb/home/; accessed on 12-Dec-2012) and 3.6 Å resolution using YASARA (version12.9.27) homology modeling program [19, 21, 78]. The model of human VKORC1L1 (hVKORC1L1) was generated in an automated manner on the I-TASSER modeling server (http://zhanglab.ccmb.med. umich.edu/I-TASSER/; accessed on 21-Oct-2015) [19, 87]. Although mostly default parameters were applied for modeling on this server, the 3.6 Å resolution X-ray crystallographic structure of 3KP9 was assigned as a guiding template for modeling on this server. Of five generated models, the best one was chosen based on the calculated C-score of -0.46 (models with C-score >-1.5 are considered to be topologically correct with respect to protein fold). Comparison of backbone Cα alignment between the model and template structures was assessed using Mustang function embedded in YASARA. Stereochemical parameter quality of both models and their template structure 3KP9 was assessed and compared using the MOLPROBITY server (http://molprobity.biochem.duke.edu/; accessed on 25-Dec-2015). The models were refined using a short 500 ps simulation (AMBER03 force field) in a solvated environment. The model with the lowest energy was chosen as the final model. Since VKORC1 and VKORC1L1 are transmembrane proteins, further simulations were performed by first identifying hydrophobic amino acid and subsequently embedding the protein (in a simulation cell) in a 70% phosphatidylcholine and 30% phophatidylethanolamine membrane using YASARA. The simulation cell was then solvated with water, avoiding water from entering between the lipid molecules. An equilibration simulation lasting 250 ps was done to further artificially stabilize the membrane in order to adapt to the protein and appropriate density without being damaged. Post equilibration, a 100 ns simulation was run with AMBER03 force field parameters and from the resulting trajectory the structure with the lowest energy was chosen as the final models for hVKORC1 and hVKORC1L1 for further docking analysis.

We used the automated AutoDock module (© 1989-2013 by The Scripps Research Institute) with default settings for small molecule docking embedded in YASARA to search for possible warfarin interaction sites on hVKORC1 and hVKORC1L1 models [78, 88]. Structure data format files (.sdf) for the ligands acenocoumarol (CID 54676537), bromadiolone (CID 547539), brodifacoum (CID 54680676), coumachlor (CID 54682651), coumatetralyl (CID 54678504), dicoumarol (CID 54676038), fluindione (CID 68942), phenindione (CID 4760), phenprocoumon (CID 54680692), S-warfarin (CID 54688261) were downloaded from the Pubchem database (https://pubchem.ncbi.nlm.nih.gov/search/; accessed on 25-Sep-2015) and converted to PDB format (.pdb) on YASARA using the AUTOSMILES function. All ligands were flexibly docked onto the model of hVKORC1L1 and hVKORC1. Docking poses on hVKORC1L1 were selected on the basis of pseudo-energy scoring function as well as the relative orientation of positively charged stabilizing arginine residues in the ER lumenal loop towards the negatively charged aromatic rings of warfarin. Docking on hVKORC1 for all ligands except warfarin were chosen on the basis of their similarity to a favorable docking position identified for warfarin on hVKORC1 [21]. All selected docks were subjected to 100 ns of membrane embedded simulation. The docked complexes with the lowest energy in the simulation trajectory were picked as the final docked structures and analyzed for identifying the putative binding residues.

3.3 Generation of VKORC1L1 KO mice

3.3.1 Strategy for integration of loxP sites into *Vkorc1l1* locus

To study the biological impact of VKORC1L1, we generated *Vkorc1l1* transgenic mice. By means of the CRISPR/*Cas*9 gene editing system, loxP sites will be integrated flanking exon 2 (Figure 14). Therefore, sgRNAs were designed to bind up- and downstream exon 2. Oligo donor DNAs contain the loxP site and 60 bp overhangs on each side adjoining DSBs introduced by *Cas*9. In case of DNA repair without integration of donor DNAs exon 2 (and adjacent regions) will be deleted.

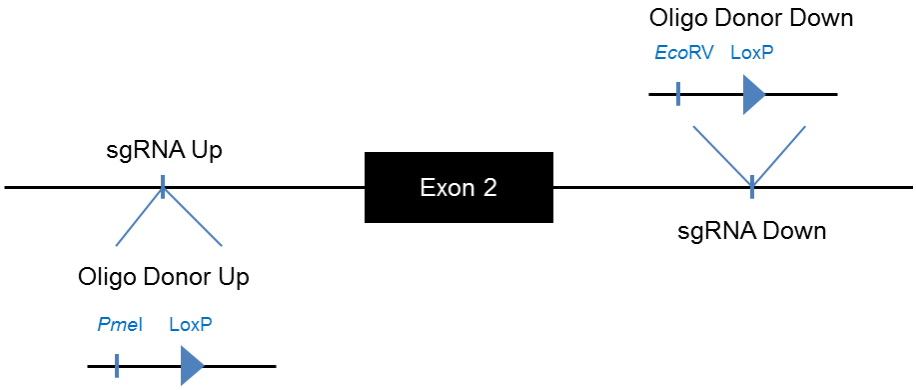

Figure 14: Design of the CRISPR/Cas9 targeting muriune *Vkorc1l1* locus
sgRNAs complementary to the target sequence are located up- and downstream of exon 2. Oligo donor DNAs comprised of loxP sites, complementary sequences of the target and a site for restriction enyzmes are used for integration of loxP sites.

The experimental design and preparation of the samples for microinjection was done in collaboration with Dr. Noelia Fradejas Villar at the Institute of Biochemistry and Molecular Biology, University Bonn. For cloning the vector px330 containing a human codon-optimized SpCas9 (*Streptococcus pyogenes*) and chimeric guide RNA expression was used (Figure 15) [89].

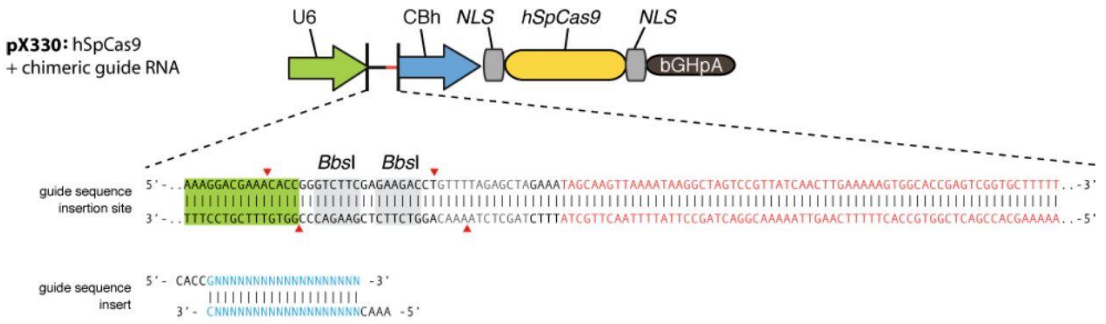

Figure 15: pX330-U6-Chimeric_BB-CBh-hSpCas9 vector design. Taken from https://www.addgene.org/42230/ visited on 13-Jan-2018.

After amplification of the *Cas*9 and sgRNAs, the products were *in vitro* transcribed and purified. Prior to use, the components were mixed in order to avoid clotting of the needle during microinjection.

	Volume in µl
Cas9 mRNA (100 ng/µl)	1
sgRNAs (50 ng/µl)	Each 0.5
Oligo donor ssDNA (100 ng/µl)	Each 0.5
Nuclease-free water	2

Microinjection was performed in collaboration with the animal facility at the University Hospital Bonn. Therefore, components of CRISPR/Cas9 were injected in BL6 oocytes (pronucleus). Approximately three weeks later pups were born and weaned another three weeks later. At the age of 8 to 10 weeks heterozygous mice were mated with BL6 mice in order to verify germline mutation. Subsequently, mice were mated with BL6 for backcrossing to “dilute” possible off-target effects.

3.3.2 Genotyping of transgenic mice

Mice were kept under standard housing conditions in a 12 hour light-dark cycle with food and water *ad libitum* in accordance with local and state regulations concerning animal research. Mouse tail biopsies were used for genotyping. Therefore, about 2 mm of tail were cut and transferred into a 1.5 ml vial. For lysis of the tissue, 200 µl mouse tail lysis buffer containing 200 µg/ml proteinase K was added and incubated over night at 55°C followed by heat inactivation at 80°C for 30 min. For genotyping, the lysed tails were diluted 1:6 with water. The samples were used directly or stored at -20°C.

Genotyping was performed using two different sets of primers. The scheme of for genotyping is depicted in Figure 16. RFLP-F and RFLP-R primers were used to amplify a 2350 bp product for the WT allele and an 1140 bp for the KO allele. The second set amplifies products which are smaller in size. In the WT allele, all three primers can bind to the DNA, however, the cycling conditions restrict to amplify only the smaller product.

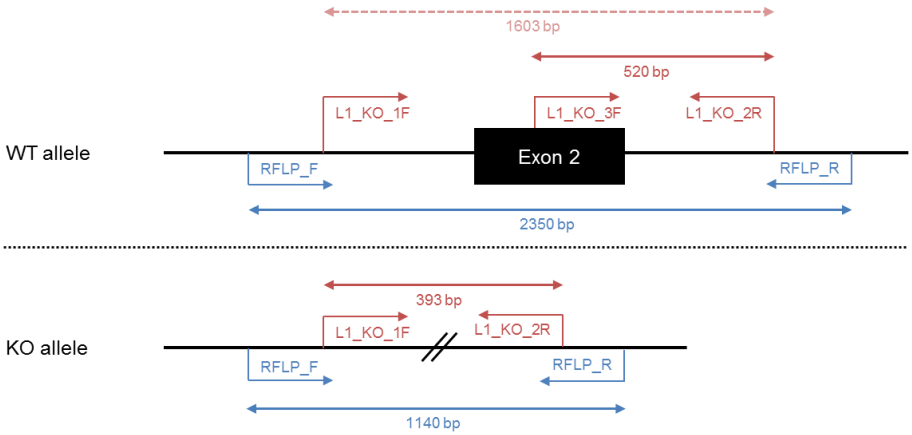

Figure 16: Overview of primers designed to genotype *VKORC1L1* KO mice.
The genotyping were performed with two different sets of primers. RFLP primers (in blue) were used to amplify products of 2.4 kb and 1.1 kb, respectively. L1_KO primers (in claret) were designed to amplify smaller products to shorten PCR running time. Not drawn to scale.

The reaction mix for both PCRs was set as follows:

	Volume in µl
1x DreamTaq buffer	23
Diluted sample (1:6)	2
Primer (each 20 µM)	0.5
Solution S	2
DreamTaq polymerase (5 U/µl)	0.25

The program at the thermocycler for RFLP primers was as follows:

Step 1	95°C	3 min	
Step 2	95°C	30 s	
Step 3	68°C	30 s	Repeat 10x
Step 4	72°C	2 min 30 s	
Step 5	95°C	30 s	
Step 6	66°C	30 s	Repeat 10x
Step 7	72°C	2 min 30 s	
Step 8	95°C	30 s	
Step 9	64°C	30 s	Repeat 15x
Step 10	72°C	2 min 30 s	
Step 11	72°C	7 min	

The program at the thermocycler for L1_KO primers was as follows:

Step 1	95°C	3 min	
Step 2	95°C	30 s	Repeat 35x
Step 3	68°C	30 s	
Step 4	72°C	30 s	
Step 5	72°C	7 min	

For analysis, the products were mixed with 5 µl of loading dye and 10 µl of the mix was loaded on a 1% agarose gel (3.1.7).

3.3.3 Total RNA isolation

For quantitative PCR, total RNA was isolated from tail cut (~5 mm). Therefore, the piece of tail was directly placed in 1 ml Trizol. After homogenization with pistil, 200 µl of chloroform was added and mixed vigorously. By centrifugation (15000 rpm, 4°C, 15 min), the aqueous phase (which contains the RNA) was separated from the organic phase. The upper phase was pipetted into a new cup and mixed with the same volume of 100% ethanol. The next steps were carried out according to manufacturer's instructions using the RNeasy Mini Kit. For digestion of genomic DNA, incubation with RNase-Free DNase was included. Finally, the RNA was eluted in 50 µl RNase-free water and concentration of the sample was determined spectrophotometrically (3.1.11). The samples were stored at -80°C until use.

3.3.4 cDNA synthesis

RNA was reverse transcribed into cDNA using the qScript cDNA Synthesis Kit. The reaction mix contains an optimized blend of random and oligo(dT) primers which allows unbiased first-strand synthesis.

	Volume in µl
5x qScript Reaction Mix	4
RNA (up to 1 µg)	Variable
qScript RT	0.5
dH_2O	Variable
Total	**20**

The mix was incubated at 22°C for 5 min followed by 42°C for 30 min. Subsequent incubation at 85°C for 5 min lead to the inactivation of the enzyme. The samples were stored at -20°C until use.

3.3.5 Quantitative PCR using TaqMan assay

For quantitative PCR (qPCR), the TaqMan assay was used to monitor the increase of PCR products by means of fluorescence in real-time. Thus, the probe contains a fluorescent dye at the 5' end (FAM, Fluorescein amidite) and a quencher (BHQ1, Black Hole Quencher 1) at its 3' end. During PCR the primers and the probe hybridize complementary to the template and the DNA polymerase refills the strand. When the probe is reached, the polymerase cleaves off the probe by its 5'-3' exonuclease activity. During degradation of the probe the fluorescent dye is no longer quenched and a fluorescence signal is detected which is proportional to the number of amplicons.

The primer/probe mix for *Vkorc1l1* contained 10 µM of each primer and 5 µM of the probe. The final concentration in the mix was then 500 nM for primers and 100 nM for the probe, respectively. As an internal control, *Hprt1* (hypoxanthine phosphoribosyltransferase 1, Mm00446968_m1) was used as a housekeeping gene.

AgPath-ID™ One-Step RT-PCR was used to analyze RNA directly. Thereby, the reverse transcription (by ArrayScript™ Reverse Transcriptase) is included in the reaction mix of real-time PCR (by AmpliTaq Gold® DNA Polymerase). Hence, the reverse primers for the respective gene (*Vkorc1l1* or *Hprt1*) were used for cDNA synthesis. The reaction mix was set as follows.

	Volume in µl
2x RT-PCR Buffer	12.5
RNA	1
25x RT-PCR Enzyme Mix	1
Primer/probe mix	1.25
dH_2O	9.25
Total	**25**

The program was as follows:

Step 1	45°C	15 min	cDNA synthesis
Step 2	95°C	10 min	RT inactivation and initial denaturation
Step 3	95°C	15 s	Amplification of target
Step 4	60°C	1 min	
Repeat step 3 to 4 40 times			

Secondly, the samples were analyzed in a two-step quantitative real-time PCR. TaqMan® Gene Expression Master Mix contains beside AmpliTaq Gold® DNA polymerase a uracil-DNA glycosylase (UDG). This enzyme destroys carry-over PCR products by removing any uracil in a single or double stranded amplicon. The reaction mix was set-up as described below.

	Volume in µl
2x TaqMan® Gene Expression Master Mix	12.5
cDNA	2
Primer/probe mix	1.25
dH_2O	10.5
Total	**25**

The program was as follows:

Step 1	50°C	2 min	UDG incubation
Step 2	95°C	10 min	UDG inactivation, polymerase activation and initial denaturation
Step 3	95°C	15 s	Amplification of target
Step 4	60°C	1 min	
Repeat step 3 to 4 40 times			

For evaluation of qPCR, the threshold cycle (C_T) value was determined. Thereby, the C_T value is equal to the cycle number at which the fluorescence crosses the threshold. Therefore, the C_T value represents the detectable amount of amplicon product that has been generated during the early exponential phase of the PCR. The threshold cycle is indirectly proportional to the original relative expression level of the gene of interest.

Samples were analyzed in duplicates and mean values were determined. The ratio of *Vkorc1l1* expression of WT (+/+) to heterozygous KO (+/d) or homozygous KO (d/d) was calculated. Thus, the ratio for WT/WT was set as 1.

$$\Delta C_T = C_{T\,Vkorc1l1} - C_{T\,Hprt1}$$

$$\Delta\Delta C_T = \Delta C_{T+/d} - \Delta C_{T+/+}$$

$$\text{Ratio} = 2^{-\Delta\Delta CT}$$

3.3.6 Phenotypic screen *Vkorc1l1*$^{-/-}$ mice

Vkorc1l1$^{-/-}$ mice were characterized using a standardized, comprehensive phenotyping as established in German Mouse Clinic (GMC) with open access to the scientific community.In the GMC, experts from various fields of mouse physiology and pathology in close cooperation with clinicians work side by side at one location. The examinations comprise the following areas: allergy, behavior, clinical chemistry, dysmorphology, energy metabolism, eye development and vision, host-pathogen interactions, immunology, lung function, molecular phenotyping, neurology, nociception, and pathology. A standardized screen was conducted as depicted in Figure 17.

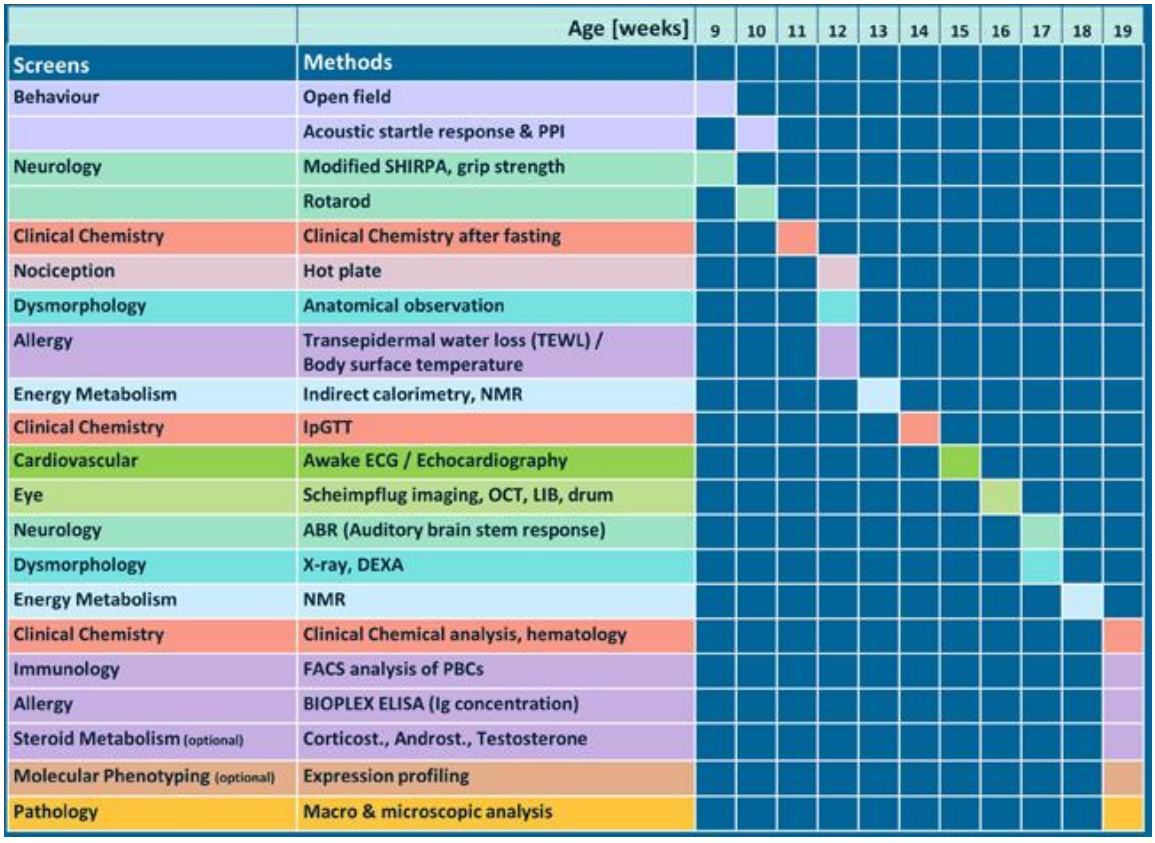

Figure 17: Workflow for primary mouse screening in the German Mouse Clinic.
The picture was taken from the website of the German Mouse Clinic https://www.mouseclinic.de/screens/overview/index.html visited on 25-Sep-2017.

4 Results

4.1 Characterization of VKORC1 and VKORC1L1 *in vitro*

4.1.1 Generation of HEK 293T knockout cell lines

To study VKORC1 and VKORC1L1 independently, knockout (KO) cells of either enzyme were generated by means of CRISPR/Cas9 gene editing system (3.2.1). In addition, a double knockout (DKO) cell line was established to analyze different variants of VKORC1 or VKORC1L1 without sophisticated endogenous VKOR activity.

HEK 293T cells harbor a triploid set of chromosomes 7 and 16, i.e. three copies of *VKORC1* and *VKORC1L1* in HEK 293T cells are present [90]. In Figure 18 the genetic profile of the single and double knockout cell lines is shown. In the *VKORC1* KO cell line (clone 2D1), the gene locus of *VKORC1* showed a 19 bp deletion concomitant with a base substitution resulting in a shortened protein of 88 amino acids (aa). *VKORC1L1* KO (clone 2H2) showed a deletion and an insertion in the *VKORC1L1* gene, which led to a frameshift and resulted in longer proteins (214 and 215 aa, respectively). In DKO cells (clone 1F11), genetic manipulation generated insertion and deletion on *VKORC1* locus, whereby protein was reduced in length (123 aa, 130 aa, and 159 aa, respectively). The *VKORC1L1* locus showed an insertion of one nucleotide (prolonged: 215 aa) and a four nucleotide deletion (shortened: 55 aa).

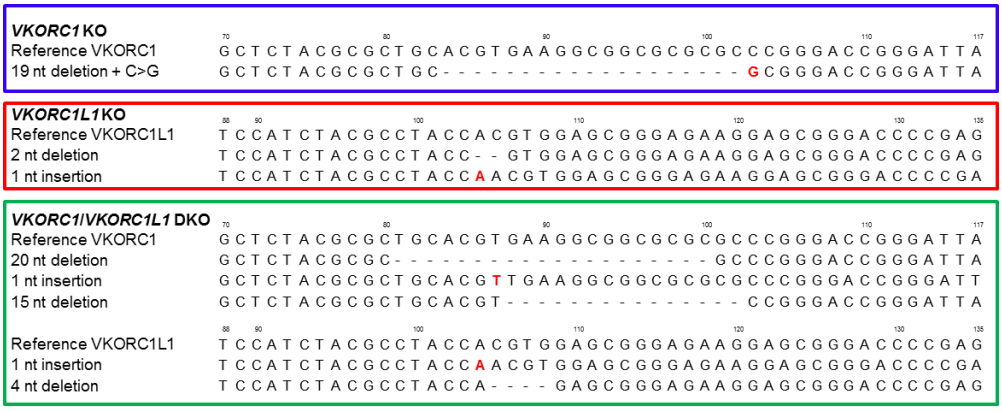

Figure 18: CRISPR/Cas9-mediated gene editing of *VKORC1* (NM_024006.4) and *VKORC1L1* (NM_173517.4) loci in HEK 293T cells.
The wild-type sequence for both genes (c.70-116 of VKORC1 and c.88-131 of VKORC1L1) is shown on the top, deletions are indicated by dashes, insertion and substitution is shown in red.

4.1.2 Characterization of HEK 293T knockout cell lines

In order to verify the ability of *VKORC1* KO and *VKORC1L1* KO cells to activate FIX, h*F9* cDNA was transiently expressed using the previously described cell-based assay [30]. After transfection, cells were supplemented with expression medium containing 12 µM vitamin K_1, supernatant was collected as described in section 3.2.2. For comparison, WT HEK 293T cells were used as a control, because these cells express endogenously *VKORC1* and *VKORC1L1*. When analyzing the enzymes separately by means of *VKORC1L1* KO and *VKORC1* KO cells, both enzymes were able to provide substrate (KH_2) for activation of FIX (Figure 19), as shown by FIX activity of 58% for *VKORC1L1* KO and 41% *VKORC1* KO compared to 51% for WT HEK 293T cells. To completely inactivate vitamin K recycling a DKO HEK 293T cell line was generated, in which *VKORC1* and *VKORC1L1* were silenced. The assessment of FIX yielded no activity (i.e. below detection limit of 0.25% with SEM of zero) in the presence of 12 µM vitamin K_1 (Figure 19).

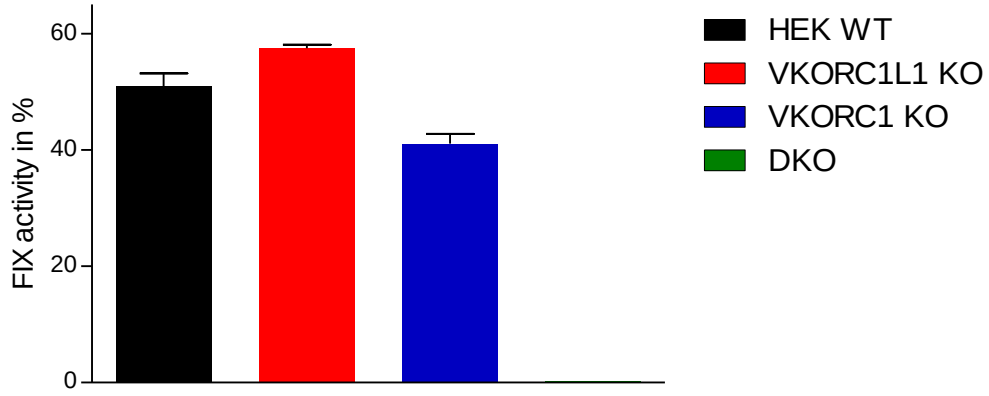

Figure 19: Measurement of FIX activity.
WT, *VKORC1L1* KO and *VKORC1* KO and DKO HEK 293T cells were transfected with h*F9* cDNA and expression medium was supplemented with 12 µM K_1. Three days post transfection cell culture supernatant was harvested and FIX activity was assessed. Measurements were performed in triplicates, error bars represent +/- SEM. FIX activity in DKO cells was below detection limit of 0.25% in all replicates.

HEK 293T cells were analyzed with regard to their expression level of VKORC1 and VKORC1L1. For this purpose cDNAs of both genes were cloned into one vector and a serial dilution was used to yield a standard curve during qPCR. Endogenously, *VKORC1* mRNA exceeded *VKORC1L1* mRNA by approximately 10-fold (Table 1). In *VKORC1* KO cells *VKORC1* mRNA could not be detected. In *VKORC1L1* KO cells mRNA transcripts of *VKORC1L1* were detected, but with lower copy number compared to WT HEK 293T cells. The same was observed in DKO cells, qPCR showed clear amplification curves with a lower copy number for both analytes compared to WT cells. When

VKORC1 or VKORC1L1 were overexpressed in DKO cells, equal copy numbers were detected. In contrast, analysis of protein expression level is difficult due to absent antibodies which can discriminate between both VKOR enzymes.

Table 1: Quantification of *VKORC1* and *VKORC1L1* transcripts in various cell lines.
Endogenous mRNA expression level was determined in HEK 293T, VKORC1 KO, VKORC1L1 KO and DKO cells. In addition, DKO cells after transfection of *VKORC1/VKORC1L1* and *F9* were used for analysis.

Cell line	**Target amplification**	**Copies/µl**
HEK 293T	*VKORC1*	$3.3*10^6$
HEK 293T	*VKORC1L1*	$4.1*10^5$
VKORC1 KO (2D1)	*VKORC1*	Not detected
VKORC1L1 KO (2H2)	*VKORC1L1*	$1.4*10^3$
DKO (1F11)	*VKORC1*	$5.4*10^2$
DKO (1F11)	*VKORC1L1*	$8.4*10^3$
DKO (1F11), transfected with *VKORC1+F9*	*VKORC1*	$6.0*10^8$
DKO (1F11), transfected with *VKORC1L1+F9*	*VKORC1L1*	$5.1*10^8$

4.1.3 Susceptibility of HEK 293T cell lines to oxidative stress

Hydrogen peroxide is present in HEK cells as a metabolite in low concentrations and is spontaneously converted to highly reactive hydroxyl radicals (HO•). To measure the potential to resist oxidative stress, cells were incubated with increasing concentrations of H_2O_2. By adding MTS, the dye is converted only by viable cells into formazan, which can be measured photometrically at 490 nm. Thus, lower extinction values represent for lower number of viable cells.

VKORC1L1 KO cells were compared to *VKORC1* KO and DKO HEK 293T cells, HEK 293T WT cells served as control (Figure 20). The cell lines showed different susceptibilities to H_2O_2 treatment. Incubation with 25 µM H_2O_2 did not result in great variance in comparison to the control, whereby the highest concentration (100 µM) showed markedly reduction of viable cells in all cell lines. A considerable effect of H_2O_2 treatment was seen using concentration higher than 50 µM.

Taken together, *VKORC1L1* KO and DKO cells were most affected by H_2O_2 treatment for concentrations ranging between 50 and 100 µM.

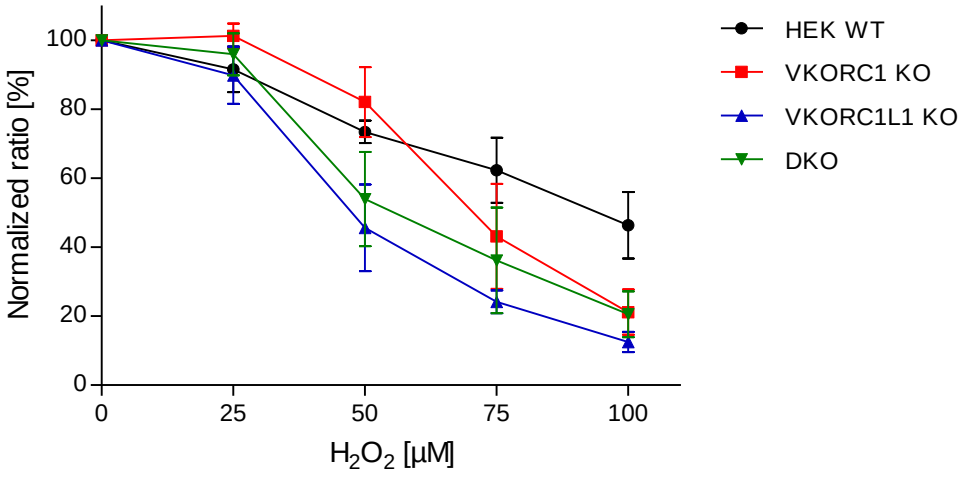

Figure 20: Cell viability in dependence of different H_2O_2 concentrations.
Cells were incubated with different concentrations of H_2O_2. After 18 h, MTS was added to the cells and incubated for two hours, the absorbance was recorded at 490 nm with a 96-well plate reader. Measurements were performed three times in triplicates, values are shown as mean +/- SEM.

In order to test the ability of vitamin K_1 to reverse oxidative stress, cells were treated with 50 µM H_2O_2 in combination with warfarin (500 nM) and K_1 (12 µM). The results are shown in Figure 21. The negative control (black bars) displays cells without any treatment and these values were set as a reference (100%). Treatment with 50 µM H_2O_2 is designated as positive control (white bars). The grey bars (in different nuances) show treatment with 50 µM H_2O_2 plus vitamin K_1 alone, vitamin K_1 in combination with warfarin or warfarin alone. In comparison to the negative control, H_2O_2 treatment resulted in reduced viability of the cells, as already shown in Figure 20. Supplementation of K_1 led to partial reversal of H_2O_2 treatment since the cells showed higher values compared to positive control. Inhibition of VKOR by 500 nM warfarin did not reduce cell viability, but quite contrary reverse H_2O_2 treatment in all cell lines but not DKO cells. Combination of K_1 and warfarin treatment appeared to reverse H_2O_2 treatment only little in DKO and WT HEK 293T cells. In *VKORC1* and *VKORC1L1* KO cells K_1 and warfarin showed higher values compared to K_1 supplementation alone.

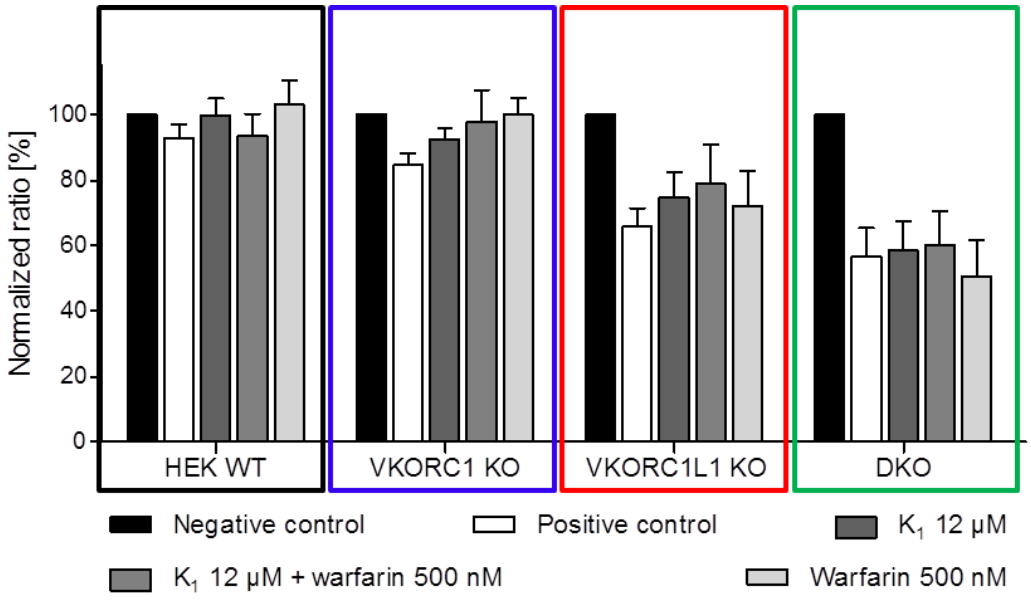

Figure 21: Impact of vitamin K_1 and warfarin on cell viability.
Negative control: without H_2O_2, positive control: 50 µM H_2O_2. The other bars represent cells incubated with 50 µM of H_2O_2 +/- vitamin K_1 (12 µM) and +/- warfarin (500 nM). Measurements were performed three times in triplicates, values are shown as mean +/- SEM.

4.1.4 Inhibition profile of various oral anticoagulants in *VKORC1* and *VKORC1L1* KO cells

To test the susceptibility of either VKORC1 or VKORC1L1 to OACs the *VKORC1L1* KO and *VKORC1* KO cells were exposed to different drugs. The experiments were performed as described in 3.2.2 with K_1 as substrate. The FIX activity assessed in cells incubated without drug was set to 100% and measurements from different drug concentrations were related to the control. The inhibition curves and calculations were made with GraphPad Prism 5.

Coumarin (Figure 22, left graph) showed no ability to reduce FIX activity as normalized FIX activity did not fall below 80%, whereby concentrations up to 1 mM of coumarin were tested. In contrast, 4-hydroxycoumarin (Figure 22, right graph) was capable to inhibit VKORC1 (measured in *VKORC1L1* KO cells) and VKORC1L1 (measured in *VKORC1* KO cells), although a diverse inhibition pattern was observed. VKORC1 showed higher susceptibility to 4-hydroxycoumarin compared to VKORC1L1. However, both enzymes were completely inhibited by 1 mM 4-hydroxycoumarin, i.e. no FIX activity was measured.

Coumarin

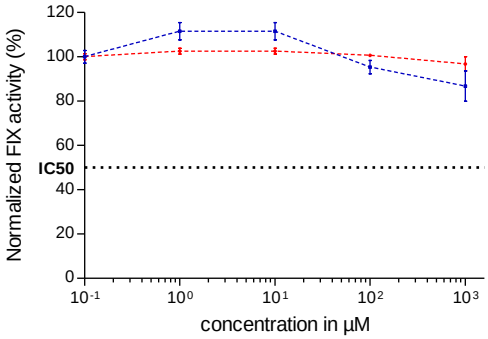

4-hydroxycoumarin

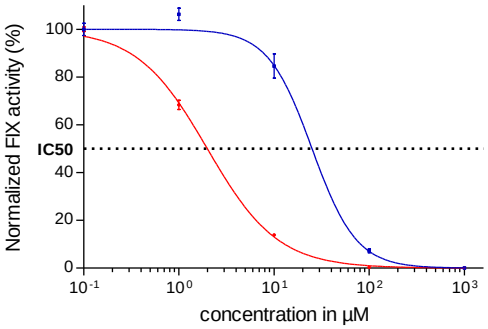

Figure 22: Inhibition curves of coumarin and 4-hydroxycoumarin tested in *VKORC1* KO (blue curves) and *VKORC1L1* KO (red curves) HEK 293T cells.
Measurements were performed in triplicates, values are shown as mean and error bars are represented as SEM.

Next, therapeutically used coumarins were investigated (Figure 23), namely dicoumarol, warfarin, phenprocoumon, and acenocoumarol.

Dicoumarol

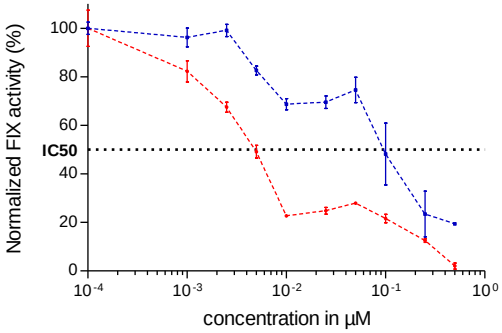

Warfarin

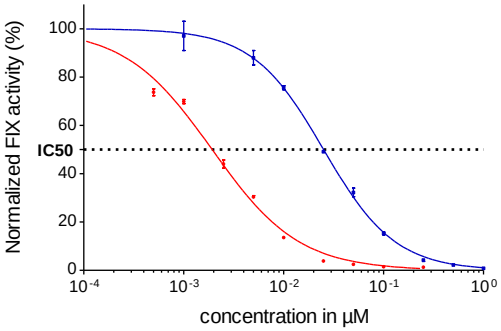

Phenprocoumon

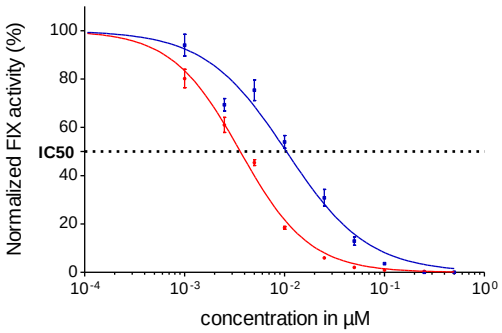

Acenocoumarol

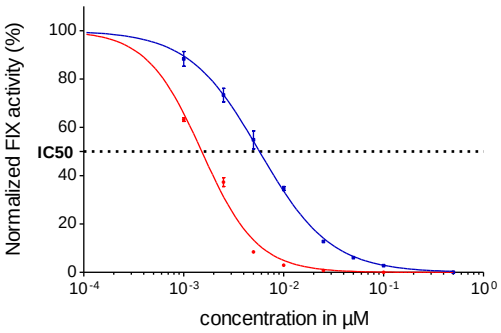

Figure 23: Inhibition curves of OACs with 4-hydroxycoumarin backbone tested in *VKORC1* KO (blue curves) and *VKORC1L1* KO (red curves) HEK 293T cells.
Measurements were performed in triplicates, values are shown as mean and error bars are represented as SEM.

This group of coumarins showed the same inhibition pattern as obtained for 4-hydroxycoumarin, with VKORC1 being more sensitive than VKORC1L1. However, the difference in sensitivity for dicoumarol and warfarin was greater than for phenprocoumon and acenocoumarol since the curves showed higher divergence for VKORC1 and its paralog. A remark concerns the inhibition pattern of dicoumarol. It was not possible to fit the 4-parameter logistic curve for dicoumarol data, because it appeared to be biphasic. Therefore, direct measurements were used to estimate the half maximal inhibitory concentration (VKORC1 49.1% at 5 nM, VKORC1L1 48.2% at 100 nM of mean normalized activities with respect to control).

The other group of OACs, the synthetic indandione derivatives, was investigated as well. Phenindione and fluindione (Figure 24) both showed high enzyme specificity since VKORC1 was inhibited at markedly lower concentrations than VKORC1L1.

Phenindione Fluindione

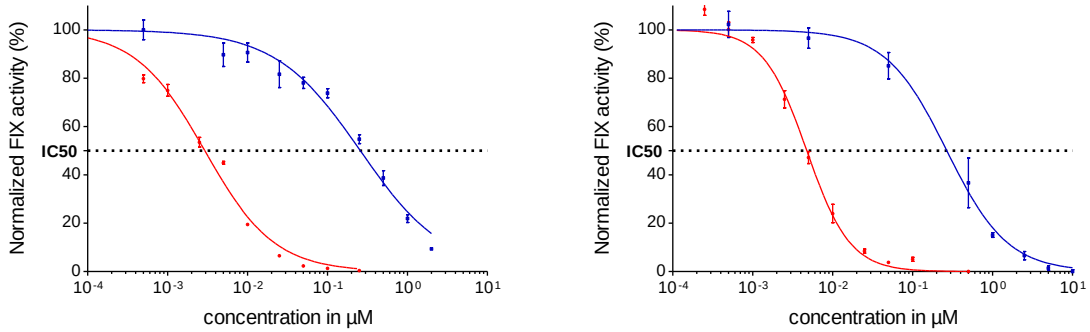

Figure 24: Inhibition curves of OACs with 1,3-indandione backbone (phenindione and fluindione) tested in *VKORC1* KO (blue curves) and *VKORC1L1* KO (red curves) HEK 293T cells. Measurements were performed in triplicates, values are shown as mean and error bars are represented as SEM.

Synthetic coumarins were originally intended for rodent control. Coumatetralyl and coumachlor belong to the group of rodenticides of the first generation, whereby bromadiolone and brodifacoum were developed later and are referred to second generation of rodenticides. Dose-response curves of the before mentioned rodenticides are shown in Figure 25.

Coumatetralyl

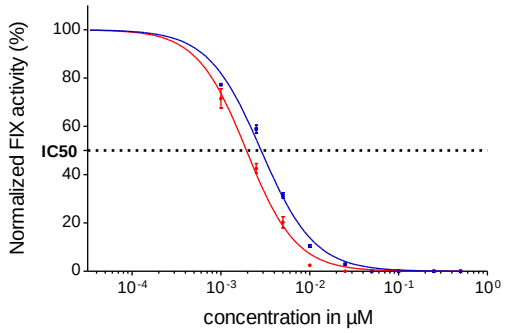

Coumachlor

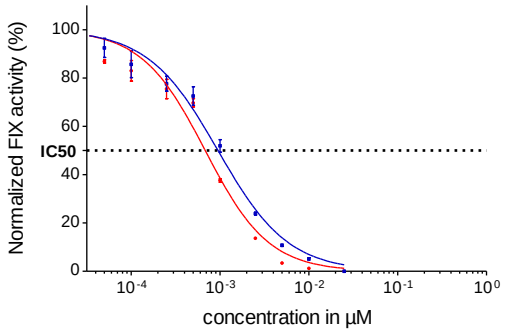

Bromadiolone

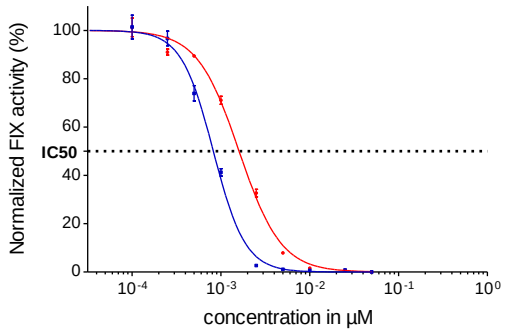

Brodifacoum

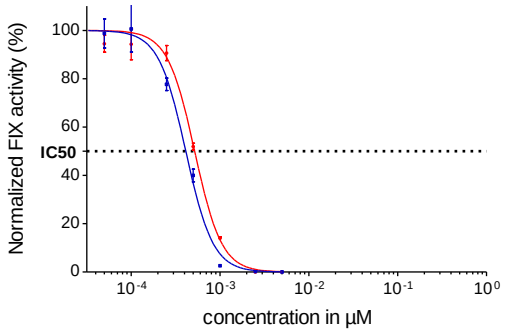

Figure 25: Inhibition curves of rodenticides belonging to the first (coumatetralyl and coumachlor) and the second generation (bromadiolone and brodifacoum).
Compounds were tested in *VKORC1* KO (blue curves) and *VKORC1L1* KO (red curves) HEK 293T cells. Measurements were performed in triplicates, values are shown as mean and error bars are represented as SEM.

Coumatetralyl and coumachlor showed less enzyme specificity compared to OACs since inhibition curves do not differ markedly. Indeed, those two rodenticides are slightly more effective to inhibit VKORC1. In contrast, bromadiolone and brodifacoum had a higher impact on VKORC1L1 compared to VKORC1, although the effect is not as prominent as seen for other anticoagulants (e.g. warfarin or fluindione).

Ferulenol, a natural occurring 4-hydroxycoumarin, was tested in *VKORC1* KO and *VKORC1L1* KO cells (Figure 26). The inhibition pattern of VKORC1 and VKORC1L1 differed as VKORC1 showed a higher susceptibility to ferulenol treatment than VKORC1L1.

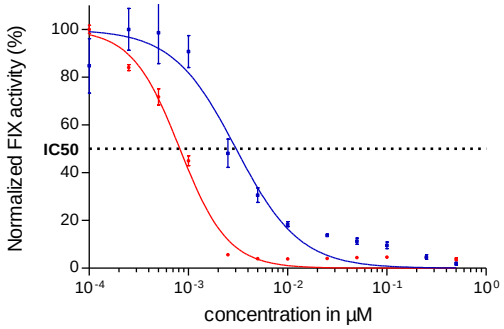

Figure 26: Inhibition curves of ferulenol tested in *VKORC1* KO (blue curves) and *VKORC1L1* KO (red curves) HEK 293T cells.
Measurements were performed in triplicates, values are shown as mean and error bars are represented as SEM.

Half-maximum inhibitory concentration (IC_{50}) was calculated as described by Fregin *et al.* by solving the 4-parameter logistic equation representing dose-response curve fits for the independent variable (drug concentration), as a function of the dependent variable (normalized activity), and substituting a dependent variable value of 50 since FIX mean activities were normalized to a maximum value of 100% in the absence of a drug (e.g. warfarin) [30]. Calculations were performed using GraphPad Prism 5 and the results are summarized in Table 2.

Table 2: Overview of OACs and rodenticides with K_1 supplementation.
The compound class as well as half maximum inhibitory concentrations (IC_{50}) assessed in *VKORC1L1* KO and *VKORC1* KO HEK 293T cells are shown. Measurements were performed in triplicates. Enzyme activities assessed up to 1 mM coumarin;**Biphasic dose-response not fittable with logistic curve; values from n=3 direct measurements (VKORC1 49.1%, VKORC1L1 48.2% mean normalized activities with respect to 0 nM dicoumarol); NA - not applicable, 4HC – 4-hydroxycoumarin, C1 – VKORC1, L1 – VKORC1L1.

Compound	**Compound class**	**VKORC1 IC_{50} (nM)**	**VKORC1L1 IC_{50} (nM)**	**Ratio L1/C1**
Coumarin	Inactive backbone	Not inhibitory*	Not inhibitory*	NA
4-Hydroxycoumarin	Active 4HC backbone	1978	25110	12.7
Dicoumarol	Naturally occurring and therapeutic 4HC	5.0**	100.0**	20.0
Warfarin	Human therapeutic 4HC and rodenticide	1.9	25.2	13.4
Acenocoumarol	Human therapeutic 4HC	1.5	5.8	3.9
Phenprocoumon	Human therapeutic 4HC	3.6	10.5	2.9
Phenindione	Human therapeutic indandione	2.9	258.0	89.0
Fluindione	Human therapeutic indandione	4.8	268.5	55.9
Coumatetralyl	1st generation rodenticide	1.9	2.8	1.5
Coumachlor	1st generation rodenticide	0.7	1.0	1.4
Bromadiolone	2nd generation rodenticide	1.6	0.8	0.5
Brodifacoum	2nd generation rodenticide	0.5	0.4	0.8
Ferulenol	Naturally occurring 4HC	0.8	3.0	3.8

In addition, VKOR activity was assessed in *VKORC1L1* and *VKORC1* KO cells. In Figure 27 the inhibition curves are shown for warfarin, fluindione and coumachlor representing the three most important categories of OACs tested. In comparison to K_1, the inhibition curves do not differ markedly when K_1>O was used. One exception was observed when *VKORC1L1* KO cells were tested with fluindione as represented with higher dose requirements for inhibition.

Warfarin

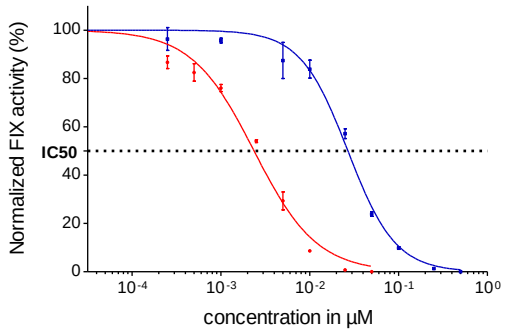

Fluindione

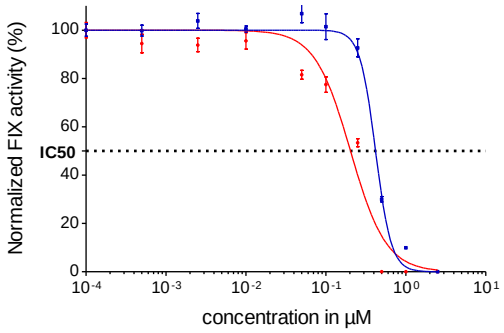

Coumachlor

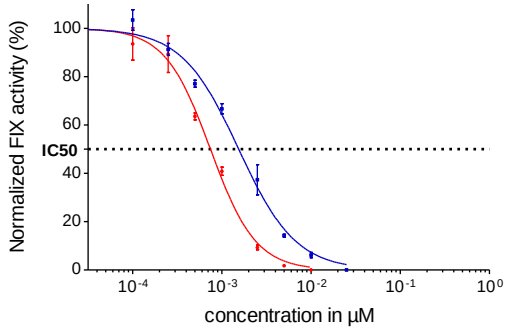

Figure 27: Inhibition curves of warfarin, fluindione and coumachlor tested in *VKORC1* KO (blue curves) and *VKORC1L1* KO (red curves) HEK 293T cells.
In contrast to previous experiments, K_1>O (12 µM) was used. Measurements were performed in triplicates, values are shown as mean and error bars are represented as SEM.

IC_{50} values where calculated for above mentioned compounds using K_1>O as a substrate and are summarized in Table 3.

Table 3: Overview of compounds tested with supplementation of K_1>O.
Half maximum inhibitory concentrations (IC_{50}) were assessed in *VKORC1L1* KO and *VKORC1* KO HEK 293T cells. C1 – VKORC1, L1 – VKORC1L1

Compound	**VKORC1 IC_{50} (nM)**	**VKORC1L1 IC_{50} (nM)**	**Ratio L1/C1**
Warfarin	2.4	27.0	11.3
Fluindione	203.8	419.6	2.1
Coumachlor	0.7	1.5	2.1

4.1.5 Investigation of antibiotics suspected to interfere with coagulation

The group of β-lactam antibiotics, to which penicillins and cephalosporins belong to, has become widely used antimicrobials because of their broad antibacterial spectrum and excellent safety profile. Cephalosporins containing a methyltetrazole-thiol (MTT) group (Figure 28, lower panel) can cause hypoprothrombinemia, a bleeding disorder whereby prothrombin deficiency leads to impaired blood clotting [91].

General structure of cephalosporins[1]

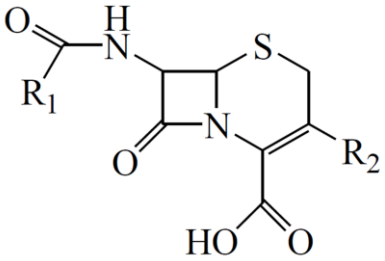

Cephalosporin C[2]

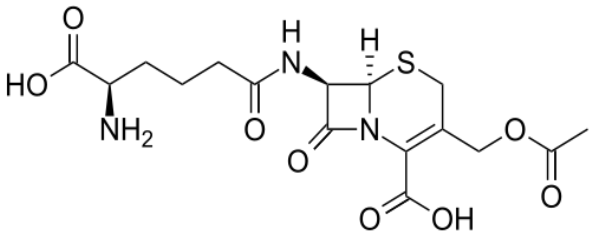

Moxalactam[2]

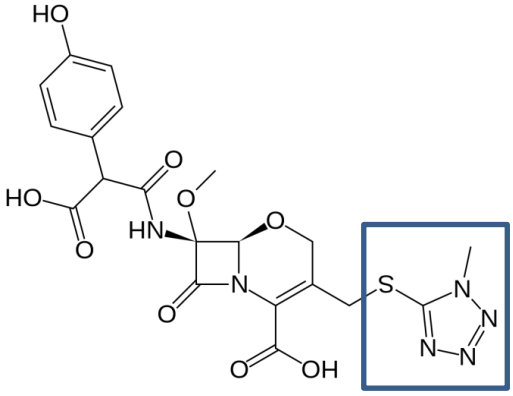

Cefamandole[2]

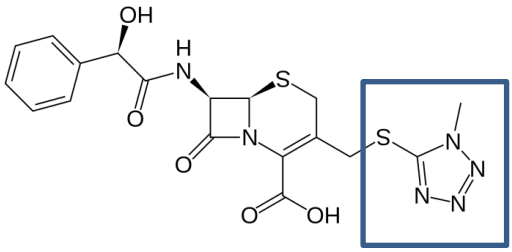

Figure 28: Chemical structures of cephalosporins.
Moxalactam and cefamandole are antibiotics containing a methyltetrazole-thiol (MTT) side chain (blue box).

The results for three antibiotics of cephalosporin family are shown in Figure 29. Cephalosporin C was able to inhibit VKORC1 and VKORC1L1 only at high concentration (125 µM). In contrast to the coumarins, VKORC1L1 showed higher susceptibility compared to VKORC1. Moxalactam did not have properties to inhibit VKOR, since normalized FIX activities did not fall below 80% irrespective of the enzyme investigated. Cefamandole showed similar inhibition profile like cephalosporin C, however the highest concentration (125 µM) was toxic to the cells (cells detached after incubation time).

[1] http://whitesscience.com/product/qsar-modeling-of-beta-lactam-antibiotic-cephalosporin-against-transpeptidase-using-mlr-method/, visited on 19-May-2018

[2] https://en.wikipedia.org/wiki/, visited on 19-May-2018

Cephalosporin C

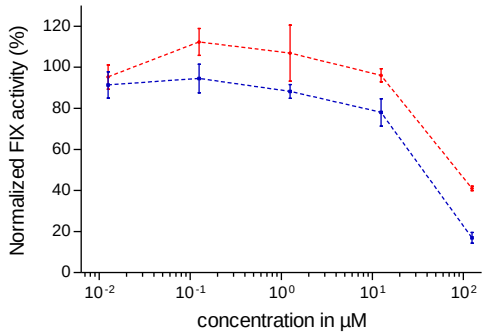

Moxalactam

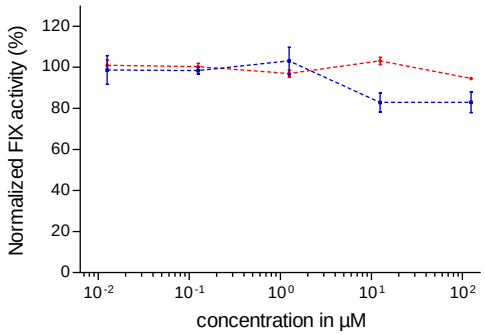

Cefamandole

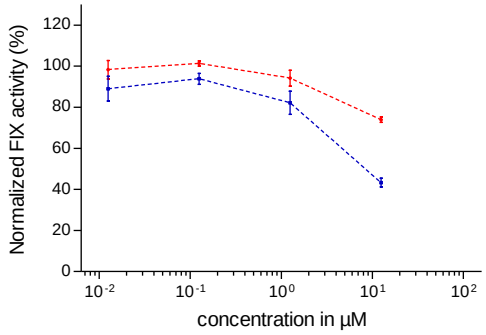

Figure 29: Inhibition curves of selected antibiotics suspected to interfere with anticoagulation therapy.
Cephalosporin C, moxalactam and cefamandole were tested in *VKORC1* KO (blue curves) and *VKORC1L1* KO (red curves) HEK 293T cells. Measurements were performed in triplicates, values are shown as mean and error bars are represented as SEM.

To investigate the cumulative effect of warfarin and antibiotics, *VKORC1* KO and *VKORC1L1* KO HEK 293T cells were incubated with warfarin concentration specific for each cell line to reach half-maximal inhibition. *VKORC1* KO cells were incubated with 25 nM warfarin and different concentrations of cephalosporins, whereby *VKORC1L1* KO cells were treated with 2.5 nM warfarin. The values were normalized to the control representing cells incubated without any drug. The results are shown in Figure 30. Treatment of warfarin yielded about 40% normalized FIX activity related to control. The addition of moxalactam, cefamandole or cephalosporin C did not result in further reduction of FIX activity. Only cefamandole at the lowest concentration (125 nM) resulted in reduced values, however increasing concentrations of that antibiotic gave results comparable to that of warfarin treatment alone.

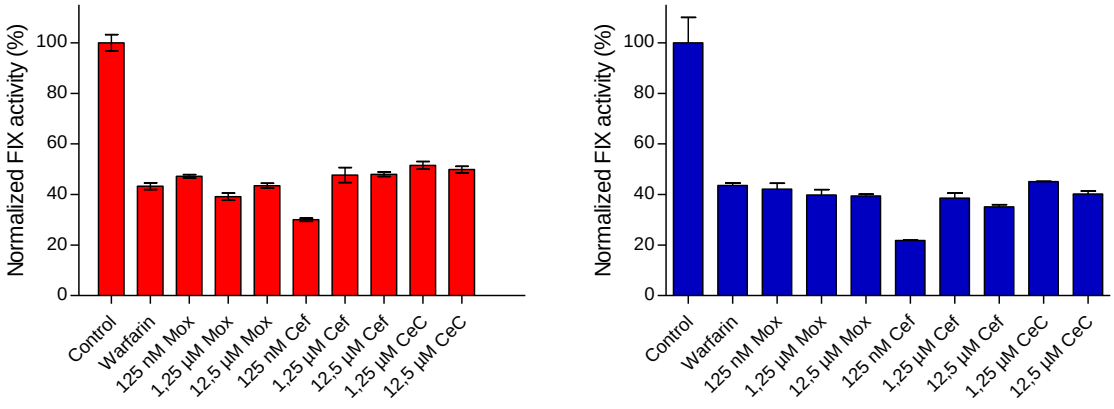

Figure 30: Effect of warfarin and antibiotic combination on FIX carboxylation.
VKORC1 KO shown in blue columns, whereas *VKORC1L1* KO is shown in red. Control represents incubation without warfarin, whereby the second column shows warfarin incubation to yield half-maximal inhibition of endogenous VKOR (*VKORC1* KO: 25 nM, *VKORC1L1* KO: 2.5 nM warfarin). Subsequent columns show treatment of the cells with different antibiotic (moxalactam, Mox; cefamandole, Cef; cephalosporin C, CeC) and warfarin. Measurements were performed in triplicates, values are shown as mean and error bars are represented as SEM.

4.1.6 Characterization of inhibitor binding sites on VKOR enzymes in double knockout cells

DKO cells were generated to abolish endogenous VKOR activity and were proven to be unable to activate FIX at a given vitamin K concentration (4.1.1). To study the effect of mutant VKORC1 or VKORC1L1, the bicistronic vector pIRES was used which allows the simultaneous expression of two proteins separately but from the same mRNA transcript. The cDNA of *F9* was cloned into multiple cloning site A (MCS A), whereby MCS B harbors cDNA of *VKORC1* or *VKORC1L1* and the respective variants. Cloning was performed as described in sections 3.1.1 and 3.1.2.

For warfarin and fluindione, OACs representing the two groups of investigated compounds, dose-response curves were generated for overexpression of VKORC1 and VKORC1L1. In addition, loop swap variants were made. The alignment of loop regions of both enzymes showed 48 % identity (as indicated by asterisk in Figure 31) and 62 % similarity (as indicated by bold letters). The VKORC1 loop swap comprised amino acids Lys30 to Ser79 changed to Glu37 to Pro86 of VKORC1L1 and *vice versa* (Figure 31).

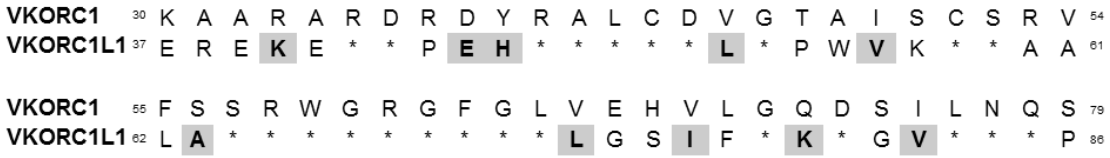

Figure 31: Alignment of loop region of VKORC1 and VKORC1L1.
Human VKORC1 (NP_076869.1) protein sequence was aligned with sequence of VKORC1L1 (NP_775788.2) using NCBI blast tool. Amino acids 30 to 79 of VKORC1 aligned to amino acids 37 to 86 of VKORC1L1. Stars indicate identical amino acids, bold letters (grey background) represent amino acids with similar chemical properties.

Endogenous VKORC1 showed higher susceptibility to warfarin and fluindione compared to VKORC1L1. In DKO HEK 293T cells, overexpression of VKORC1 presented highest susceptibility to warfarin and fluindione and VKORC1L1 required higher concentration for half-maximal inhibition (Figure 32). Calculations of IC_{50} values are given in Table 4. Thus, VKORC1 was about 27-fold more sensitive to warfarin treatment compared to VKORC1L1. Fluindione showed 6-fold higher potency to inhibit VKORC1. VKORC1 loop swap gave similar curves like those of VKORC1L1 WT for both compounds investigated which is also represented by similar IC_{50} values (e.g. VKORC1L1 WT: 474 nM and VKORC1 loop swap: 215 nM for warfarin). When VKORC1 loop was swapped into VKORC1L1 similar results were obtained, i.e. VKORC1L1 loop swap acted like VKORC1 WT with respect to warfarin and fluindione.

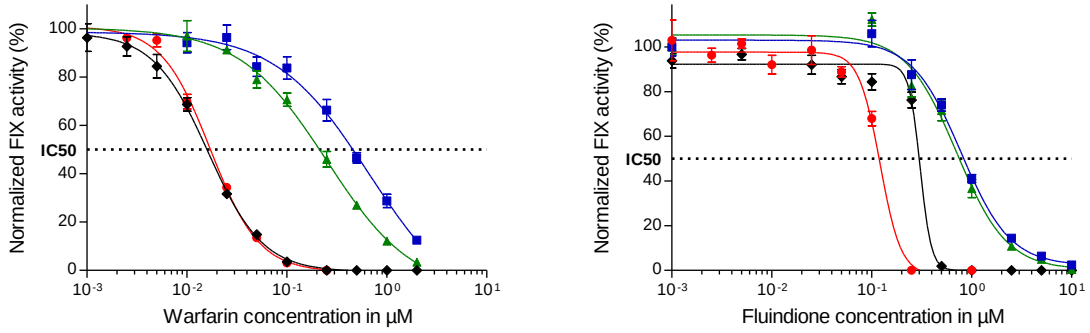

Figure 32: Inhibition curves for warfarin and fluindione assessed in DKO cells.
Activity of VKORC1 (red) and VKORC1 loop swap (black), VKORC1L1 (blue) and VKORC1 loop swap (green) determined in DKO cells by overexpression of different constructs. Measurements were performed in triplicates, values are shown as mean and error bars are represented as SEM.

Table 4: IC_{50} values of warfarin and fluindione.
DKO HEK 293T cells transfected with VKORC1 and VKORC1L1 and its respective loop swaps were supplemented with 12 µM K_1 and warfarin to assess IC_{50} values by means of FIX cell-based assay.

VKOR variant	IC_{50} (nM)	
	Warfarin	Fluindione
VKORC1 WT	16.8	121
VKORC1 loop swap	251	572
VKORC1L1 WT	589	738
VKORC1L1 loop swap	16.8	309

The previous experiment showed that the loop is important at least in warfarin and fluindione binding. To further limit the drug binding site, different modifications in VKORC1 and VKORC1L1 were tested. First, it was proven that Phe55 in VKORC1 is essential in warfarin binding [21]. Therefore, phenylalanine 55 was substituted by alanine (Phe55Ala). As presented in Figure 33, this variant was resistant to warfarin treatment as concentrations up to 5 µM resulted only in ~40% reduction of normalized FIX activity.

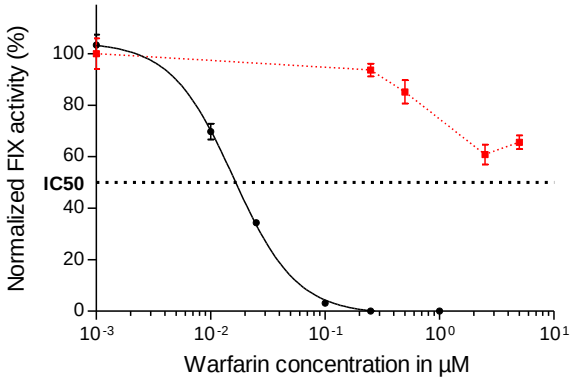

Figure 33: Dose-response for warfarin of VKORC1 Phe55Ala (red curve) assessed in DKO cells. For comparison, VKORC1 WT is included (black curve). Measurements were performed in triplicates, values are shown as mean and error bars are represented as SEM.

By sequence alignment the corresponding amino acid of VKORC1 Phe55 in VKORC1L1 was identified (Figure 34). To test the hypothesis that by introducing the “same” amino acid responsible for warfarin binding in VKORC1 would lead to a more sensitive enzyme, a mutant of VKORC1L1 at Leu62 was generated (Leu62Phe). Furthermore, the amino acids 60 to 62 of VKORC1L1 were changed to corresponding amino acids 53 to 55 of VKORC1 (Ala60Arg, Ala61Val, Leu62Phe, see Figure 34), which represent the putative contact surface II of VKORC1 identified by previously published *in silico* analysis [21].

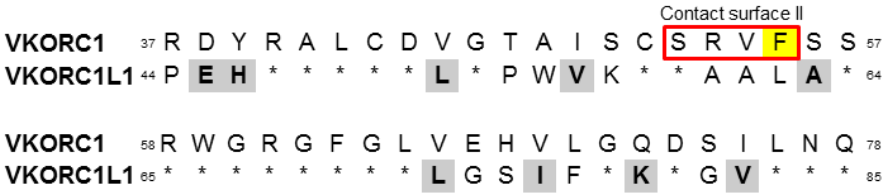

Figure 34: Alignment of loop region of VKORC1 with VKORC1L1.
Amino acids 37 to 78 of VKORC1 aligned to amino acids 44 to 85 of VKORC1L1. Star indicates identical amino acids, bold letters represent amino acids with similar chemical properties. Red box shows contact surface II in VKORC1 identified by *in silico* analysis as published by 21. VKORC1 Phe55 is highlighted in yellow.

The inhibition curves for VKORC1L1 Leu62Phe and the triple mutant comprising amino acids 60 to 62 are shown in Figure 35. Single and/or triple variant of VKORC1L1 was anticipated to move IC_{50} towards VKORC1, since more sensitive enzyme inhibition was expected. On the contrary, both constructs showed shift of dose-response curves to higher warfarin concentration. VKORC1L1 Leu62Phe required 3-fold higher warfarin for half-maximal inhibition compared to VKORC1L1 WT (Table 5). Moreover, the VKORC1L1 triple variant needed almost 4 times higher warfarin concentration for inhibition compared to VKORC1L1 WT.

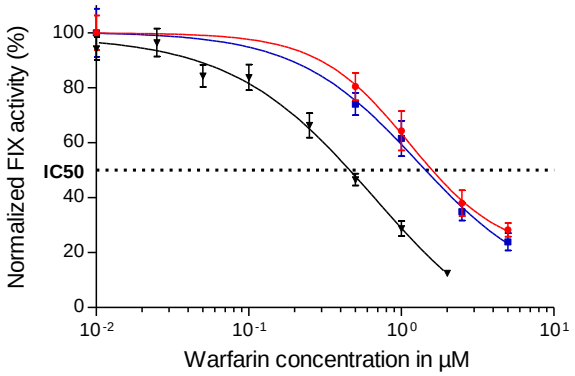

Figure 35: Inhibition curves for warfarin of VKORC1L1 variants assessed in DKO cells.
Normalized FIX activity is shown for VKORC1L1 Leu62Phe (blue) and Ala60Arg+Ala61Val+Leu62Phe (red). For comparison, VKORC1L1 WT is included (black curve) Measurements were performed in triplicates and values are shown as mean +/- SEM.

Table 5: IC_{50} values of warfarin for different VKORC1L1 variants.
DKO HEK 293T cells transfected with VKORC1L1 variants were supplemented with 12 µM K_1 and warfarin to assess IC_{50} values by means of FIX cell-based assay.

VKORC1L1 variants	**IC_{50} (nM)**
WT	474
Leu62Phe	1543
Ala60Arg+Ala61Val+Leu62Phe	1789

The analysis of different OACs revealed different susceptibilities of the two enzymes investigated. By alignment of protein sequence and further *in vitro* analysis it was obvious that to some extent the loop plays an important role in drug binding. Furthermore, these results suggest that warfarin binding site of VKORC1L1 is different from VKORC1. On this occasion *in silico* analysis was performed to identify regions or single amino acids being responsible for different drug binding. Details of *in silico* analysis and subsequent *in vitro* experiments are described in the next section.

4.1.7 *In silico* modeling of hVKORC1 and hVKORC1L1

4.1.7.1 hVKORC1 *in silico* model

In accordance with the template structure, the homology-based hVKORC1 model comprises similar secondary structural elements and overall protein fold i.e. four transmembrane domains and a long flexible/disordered ER luminal loop (Figure 36). An obvious similarity with the bacterial homologue is the presence of a highly conserved serine rich loose helix like region (Ser52-Ser57) in hVKORC1. The Trp59 (in bacteria Trp64) which has been suggested to be the anchor for this helix is in a similar position in our model. The TYA-motif (threonine, tyrosine, alanine) implicated in warfarin binding in previous studies was observed to be part of the fourth transmembrane helix and deep seated within the inner membrane (lipid part of the membrane). The critical cysteine disulfides (Cys43-Cys51 and Cys132-Cys135) are present in the ER lumenal loop and the fourth transmembrane domain.

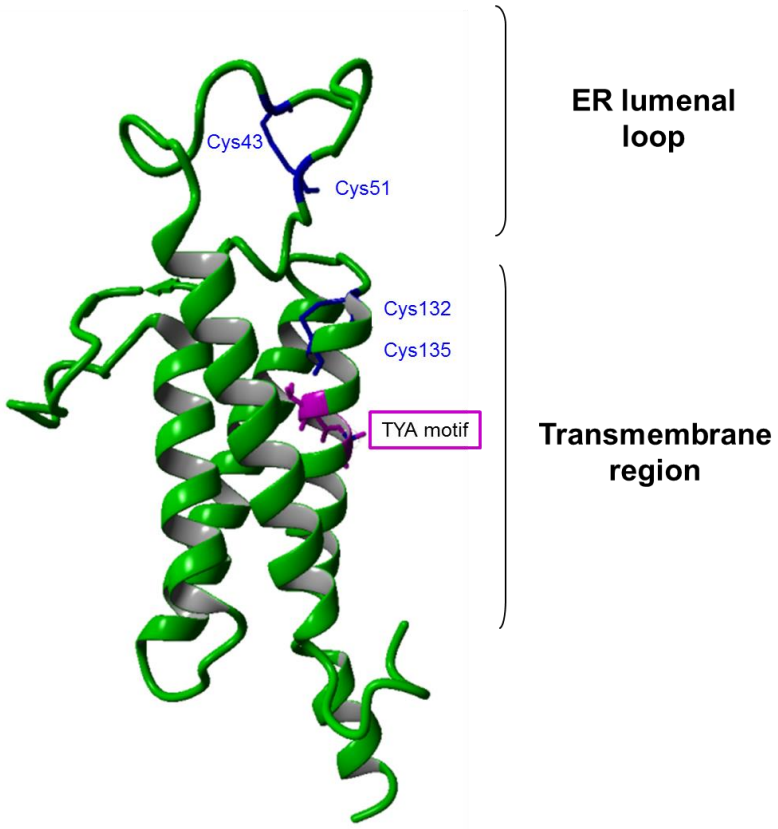

Figure 36: *In silico* model of hVKORC1.
Three dimensional structure shows four transmembrane domains and the ER luminal loop. The cysteines at amino acid positions 43, 51, 132 and 135 are depicted in blue, the TYA motif is shown in purple stick format.

4.1.7.2 hVKORC1L1 *in silico* model

The highest scored model from ITASSER for hVKORC1L1 showed a four transmembrane structure similar to that observed for the homology model of hVKORC1 (Figure 36). Furthermore, the stereochemical parameters agree favorably when compared with the crystal structure represented by 3KP9. Structural alignment with 3KP9 showed a strong similarity of RMSD <1Å (i.e. 0.86 Å) over 110 aligned residues. Similarly alignment of the hVKORC1 and hVKORC1L1 model also showed strong structural similarity i.e. 0.96 Å over 146 aligned residues. Therefore the two models were more similar to each other across their entire length in comparison to the template 3KP9 especially in the region of the ER luminal loop. The ER luminal loops of both appear similar in structure but differed in the thioredoxin-like domain on 3KP9.

The TYV-motif (threonine, tyrosine, valine), similar to TYA-motif in VKORC1, was observed to be part of the fourth transmembrane helix. The critical cysteine disulfides (Cys50-Cys58 and Cys139-Cys142) are present in the ER lumenal loop and the fourth transmembrane domain.

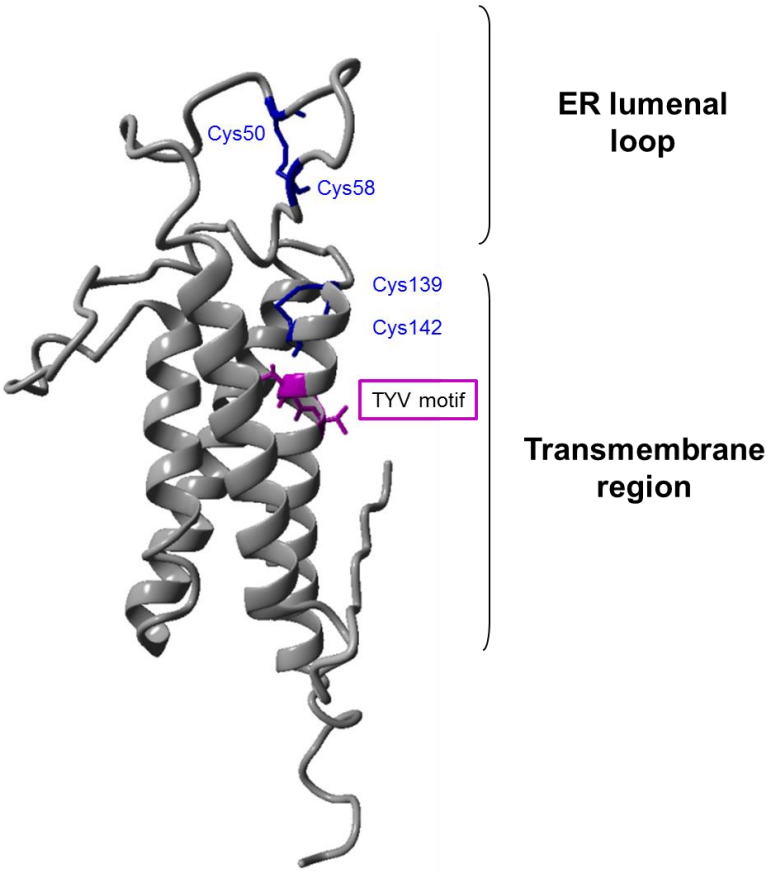

Figure 37: *In silico* model of hVKORC1L1.
Three dimensional structure shows four transmembrane domains and the ER luminal loop. The cysteines at amino acid positions 50, 58, 139 and 142 are depicted in blue, the TYV motif is shown in purple stick format.

4.1.7.3 Docking of OACs on hVKORC1

An initial coarse-grained rolling ball docking search using the deprotonated, open side-chain form of S-warfarin yielded 14 interaction pair geometries. Visual inspection of the docked structures revealed one particular dock which was energetically most favorable (i.e. showed highest *in silico* binding energy) and was proximal to the loop cysteines and the CXXC motif. Docking of warfarin on VKORC1 model showed the concentration of a large number of high scoring docking poses within a hydrophobic pocket which is proximal to both disulfide bonds (Cys43-Cys51 and Cys132-Cys135). Simulation of one of these warfarin docked poses suggests that apart from strong hydrophobic interactions mediating this binding with several residues within this pocket, there are other types of interactions that come into play: A) cation-pi interaction of the warfarin rings with Phe55, B) charge stabilization of the anionic warfarin rings with proximal positively charged arginine residues (Arg33, Arg40 and Arg53), and C) a strong backbone hydrogen bond formed between an oxygen atom of warfarin and nitrogen backbone of Val134. When docking was performed on VKORC1 for the other OACs, they also showed favorable

docking poses (with high binding affinity) that were similar to the warfarin docking pose mentioned above indicating that this is the most likely binding site for OACs on VKORC1 (Figure 38).

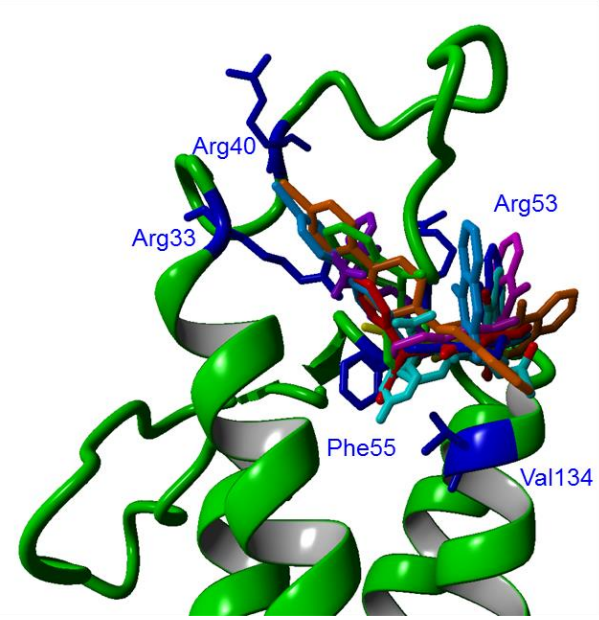

Figure 38: Docking of several anticoagulants on hVKORC1.
The backbone is depicted in green ribbon format while all docked coumarins are depicted in stick forms with different colors (warfarin: element; phenprocoumon: red; phenindione: green; fluindione: yellow; dicoumarol: magenta; coumatetralyl: blue; coumachlor: cyan; brodifacoum: orange; bromadiolone: light blue, acenocoumarol: purple). The principle interacting residues in this binding pocket are depicted in blue stick format.

4.1.7.4 Docking of OACs on hVKORC1L1

The docking of warfarin as well as other OACs to hVKORC1L1 turned up a different site than the hydrophobic binding pocket observed on hVKORC1. This particular site on hVKORC1L1 also resides on the ER luminal loop, but actually lies diametrically opposite to it. The structural alignment of the hVKORC1L1 and hVKORC1 ER luminal loops shows that while they are very much similar in structure, they differ greatly in the amino acid composition, especially the distribution of charge stabilizing arginine residues.

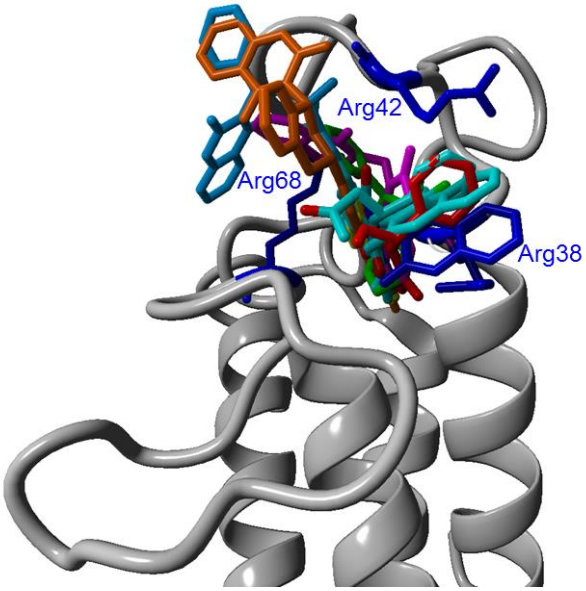

Figure 39: Docking of several anticoagulants on hVKORC1L1.
The backbone is depicted in grey ribbon format while all docked coumarins are depicted in stick forms with different colors (warfarin: element; phenprocoumon: red; phenindione: green; fluindione: yellow; dicoumarol: magenta; coumatetralyl: blue; coumachlor: cyan; brodifacoum: orange; bromadiolone: light blue, acenocoumarol: purple). The principle interacting arginine residues in this binding pocket are depicted in blue stick format.

4.1.8 Confirmation of *in silico* data by *in vitro* experiments

Molecular modeling of warfarin to hVKORC1 revealed three putative arginines at positions 33, 40 and 53. To proof *in silico* data, the arginine residues were changed to glutamic acid, which leads to reversal of polarity (from positively charged arginine to negatively charged glutamic acid). The results are summarized in Figure 40 and the calculated IC_{50} values are given in Table 6. Compared to VKORC1 WT, all variants showed lower susceptibility to warfarin, the order of single mutants was Arg53Glu<Arg40Glu<Arg33Glu. Double mutants showed higher IC_{50} values, whereas Arg33Glu+Arg53Glu required about 80-fold more warfarin for half-maximal inhibition compared to VKORC1 WT.

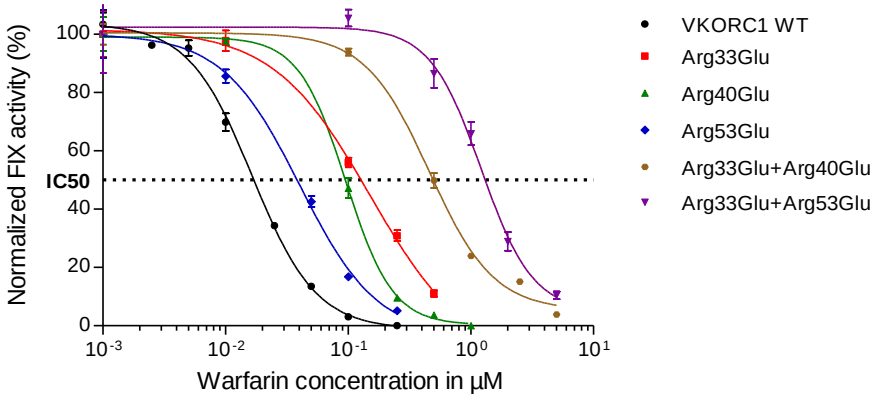

Figure 40: Inhibition curves for warfarin of arginine variants of VKORC1 assessed in DKO cells. Arginine residues at amino acid positions 33, 40 and 53 were substituted by glutamic acid residues. Single as well as double mutants were tested with regard to their warfarin inhibition profile. For comparison, VKORC1 WT is included to the graph. Measurements were performed in triplicates and values are shown as mean +/- SEM.

Table 6: IC_{50} values of warfarin for different VKORC1 arginine variants.
DKO HEK 293T cells transfected with VKORC1 variants were supplemented with 12 µM K_1 and warfarin to assess IC_{50} values by means of FIX cell-based assay.

VKORC1 variants	**IC_{50} (nM)**
WT	17.3
Arg33Glu	129
Arg40Glu	96
Arg53Glu	39
Arg33Glu+Arg40Glu	497
Arg33Glu+Arg53Glu	1326

In silico modeling of VKORC1L1 revealed putative binding sites with positively charged arginines stabilizing warfarin binding at positions Arg38, Arg42 and Arg68, which were mutated to glutamate (Figure 41 and Table 7). Single arginine mutants Arg38Glu and Arg42Glu showed almost indistinguishable inhibition pattern when compared to VKORC1L1 WT. The combination of Arg38Glu+Arg42Glu revealed an eight-fold higher requirement of warfarin compared to VKORC1L1 WT. The variants comprising Arg68 or a combination of all three residues were resistant to warfarin treatment, because concentration up to 5 µM showed maximum 20% reduction of normalized FIX activity (Arg68Glu) or even no effect (Arg38Glu+Arg42Glu+Arg68Glu).

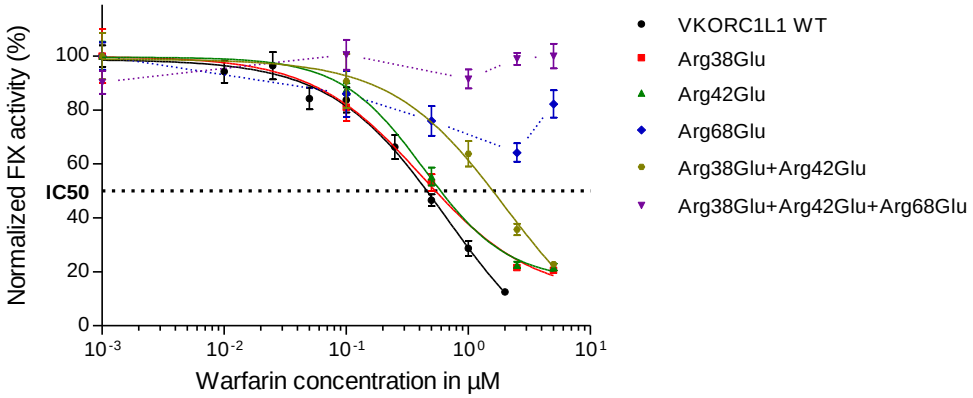

Figure 41: Inhibition curves for warfarin of arginine variants of VKORC1L1 assessed in DKO cells.
Arginine residues at amino acid positions 38, 42 and 68 were substituted by glutamic acid residues. Single, double and triple mutants were tested with regard to their warfarin inhibition profile. For comparison, VKORC1L1 WT is included to the graph. Measurements were performed in triplicates and values are shown as mean +/- SEM.

Table 7: IC_{50} values of warfarin for different VKORC1L1 arginine variants.
DKO HEK 293T cells transfected with VKORC1L1 variants were supplemented with 12 µM K_1 and warfarin to assess IC_{50} values by means of FIX cell-based assay.

VKORC1L1 variants	**IC_{50} (nM)**
WT	474
Arg38Glu	548
Arg42Glu	602
Arg68Glu	Resistant*
Arg38Glu+Arg42Glu	1624
Arg38Glu+Arg42Glu+Arg68Glu	Resistant*

Of note, triple mutant showed reduced activity values, yielding about 15% FIX activity compared to 25% of double mutant and 44% of VKORC1L1 WT.

For quantification of overexpressed VKOR variants HEK 293T cells were transfected with myc-tagged VKOR variants. 48 hours post-transfection, cells were harvested. Expression was detected by Western Blot using an anti-c-myc- antibody including a loading control (ERGIC-53). In Figure 42 VKORC1, VKORC1L1 and its loop swap variants were tested for their protein expression level. VKORC1L1 and its arginine variants were blotted as depicted in Figure 43.

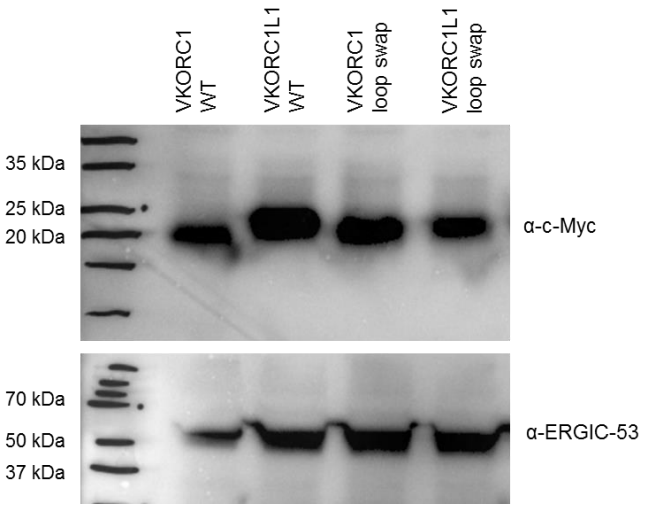

Figure 42: Western blot of VKOR variants analyzed for protein expression level with anti-c-myc-HRP antibody.
As loading control blot was stripped and tested for anti-ERGIC-53 expression. Mock – untransfected cells

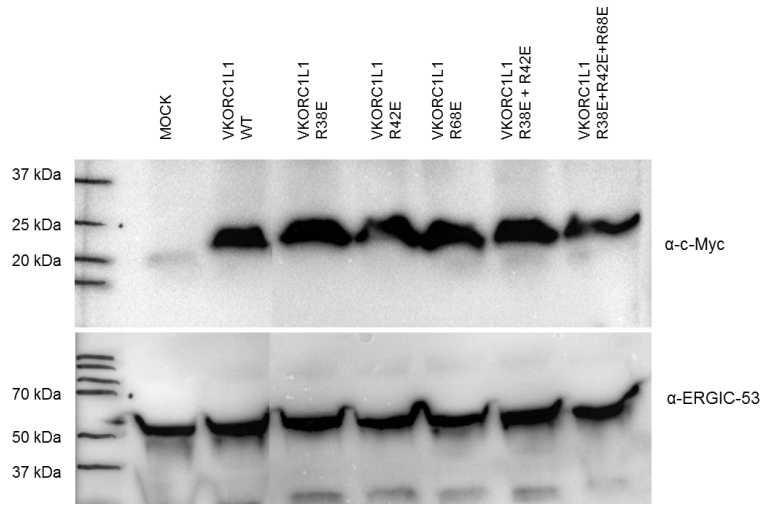

Figure 43: Western blot of VKORC1L1 variants analyzed for protein expression level with anti-c-myc-HRP antibody.
As loading control blot was stripped and tested for anti-ERGIC-53 expression. Mock – untransfected cells

4.2 Generation of *VKORC1L1* KO mice

In order to verify the biological function of VKORC1L1 *in vivo* a mouse model was used. Therefore, genetically modified mice were generated by means of CRISPR/Cas9 gene editing technique. SgRNAs were designed to introduce loxP sites flanking exon 2. Therefore, ssDNA oligonucleotides comprised of loxP sites and a restriction site were designed.

4.2.1 Results from microinjection

The results from multiple rounds of microinjections are shown in Table 8. Out of ten runs, 83 pups were born with equal sex distribution. In total six mice showed a deletion, whereby in four of them exon 2 was deleted. In addition, two mice showed an insertion, but sequencing revealed that nucleotides other than loxP sites were integrated.

Table 8: Summary of pups resulted from microinjection of components of CRISPR/Cas9. The last row presents the mouse numbers which showed a deletion band in genotyping VKORC1L1. ° male * female

Nr	Microinjection	Birth date	Total	Female	Male	Deletion of exon 2
1	F518.1, F518.2xFragment1	14.04.2015	12	6	6	
2	F518.3, F518.4xFragment2	14.04.2015	10	4	6	#17°, #22°
3	542.3xMix25.8.15	13.09.2015	11	6	5	
4	542.1, 542.2xMix26.8.15	14.09.2015	8	4	4	#55*
5	F561.2xMix17.11.15	08.12.2015	8	4	4	
6	F561.1xMix17.11.15	06.12.2015	9	5	4	
7	593.1,593.2xVKORC1/1	25.03.2016	11	5	6	#226°
8	594.1,594.2xVKORC1/1	08.03.2016	4	2	2	
9	598xVKORC1/1	14.03.2016	8	4	4	
10	599xVKORC1/1	15.03.2016	2	1	1	
Total			**83**	**41**	**42**	**4**

To verify the deletion, PCR products amplified with RFLP primers were loaded on a gel and the lower band was excised and sequenced. A summary of the genotypes is shown in Table 9, the sequences of the breakpoints are shown in Figure 44.

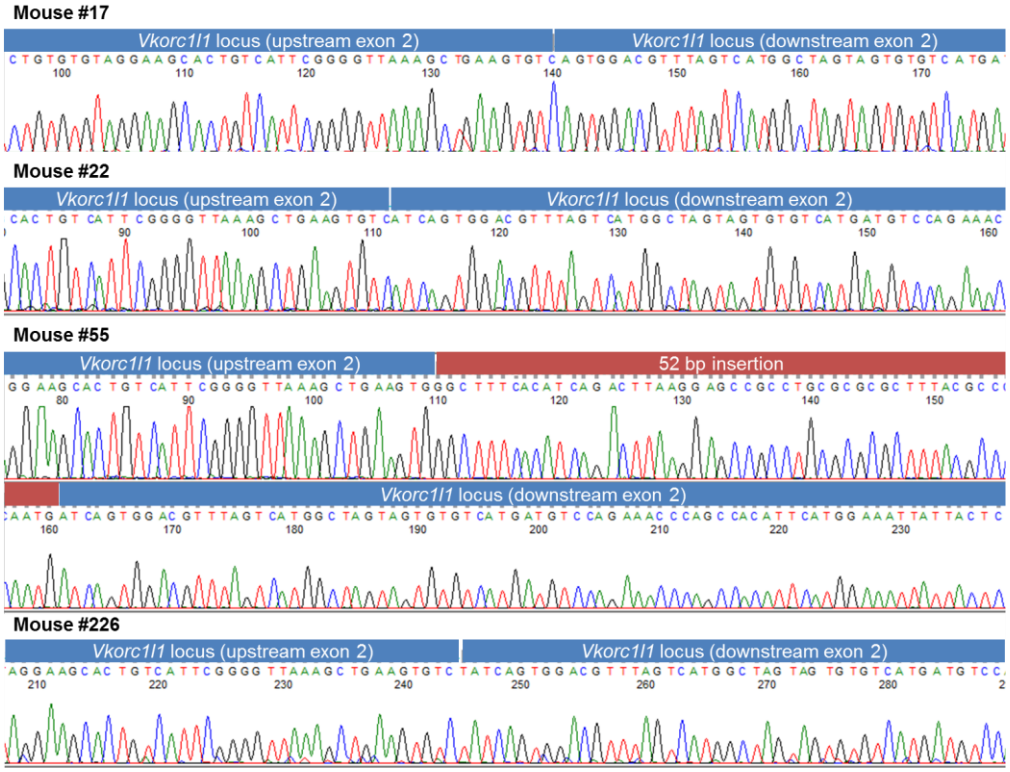

Figure 44: Sequence of *Vkorc1l1* locus upstream and downstream of exon 2 for founder mice. Using RFLP primers for amplification, the lower band showing a deletion was excised and sequenced. Mouse #55 showed a deletion of 1210 bp, additionally an insertion of 52 bp was observed.

In case of mouse #55, 1210 bp were deleted (c.195-940 to c.304+162), this genomic region includes exon 2 of *Vkorc1l1*. In addition, sequencing revealed a 52 bp insertion at the breakpoints. When this sequence was blasted, no significant similarity was found when the mouse genome and transcriptome was used.

Table 9: Detailed description of transgenic founder mice.
All mice showed a deletion of exon 2 of the *Vkorc1l1* locus (NC_000071.6).

Nr	Founder mouse	Description of deletion	Size of deleterious allele
1	17	c.195-938 to c.304+162	1210
2	22	c.195-938 to c.304+162	1210
3	55	c.195-940 to c.304+162, ins52bp	1262
4	226	c.195-938 to c.304+158	1206

4.2.2 Genotyping of transgenic mice

For determination of the genotype, a piece of tail was lysed and analyzed by PCR. In Figure 45, an exemplary result of genotyping PCR is shown. In panel A, L1_KO primers were used, resulting in fragments of ~500 bp for the WT allele and ~400 bp for the KO allele. In addition, RFLP primers (panel B) were used giving fragments of 2.4 kb (for WT) and ~1 kb (for KO), respectively. Thus, mice 153 and 154 were WT, 148, 149, 151, and 152 were heterozygous KO and 150 was homozygous KO.

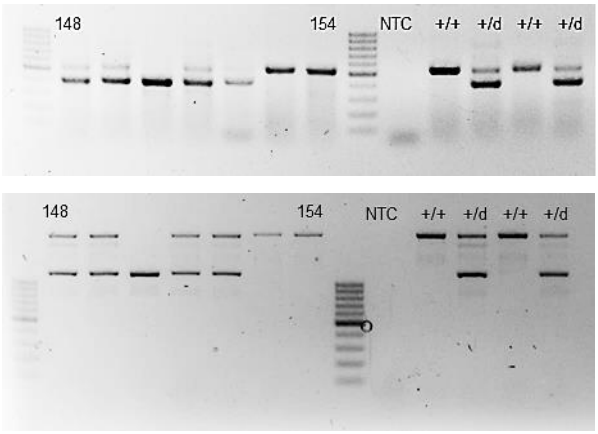

Figure 45: Genotyping *Vkorc1l1* locus of genomic DNA from mouse tails. A: L1_KO primers were used or genotyping. B: RFLP primers were used. For size comparison, the 100 bp ladder was loaded. In this example, mice 148 to 154 were analyzed with regard to their VKORC1L1 genotype. As controls, a non-template control (NTC), WT (+/+) and heterozygous KO (+/d) samples were included.

To check whether the introduced mutation is giving germ line, the founder mice were mated with C57BL/6 (BL6) WT mice. A brief summary of those matings is given in Table 10. Founder mouse #17 and #55 transfer their deleterious allele to the offspring, whereas mating of founder #22 gave siblings with WT genotype.

Table 10: Summary of pups after mating different founder mice (#17, #22, #55, and #226) with BL6.
+/+ WT, +/d heterozygous KO

	Founder mice which showed a deletion			
	#17	**#22**	**#55**	**#226**
Total	40	39	16	9
Female	16	24	9	5
Male	24	15	7	4
Genotyping				
+/+	14	39	9	4
+/d	24	0	7	5

When mating heterozygous KO mice, according to Mendelian law, one would expect half of the mice to be heterozygous. The other half should be in equal parts WT and homozygous KO. When mice from founder #17 were mated, only two out of 16 siblings showed the homozygous deletion of exon 2 in the *Vkorc1l1* gene (Figure 46 A). However, the mice did not show any abnormality or different behavior compared to their littermates.

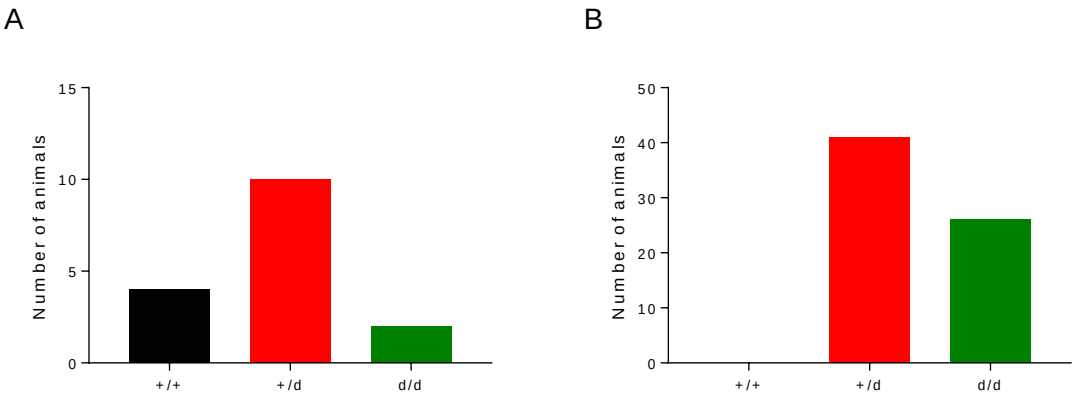

Figure 46: Distribution of genotypes of founder mouse #17.
A: Mating of heterozygous KO mice; B:Mating heterozygous with homozygous KO mice; +/+ WT, +/d heterozygous KO, d/d homozygous KO

The next question which should be answered is does the homozygous KO has any impact on fertility. Therefore, the homozygous KO was mated with heterozygous KO. In Figure 46 B the genotypes of the siblings are summarized. In this mating, no WT mice are expected. The ratio of homozygous to heterozygous mice was expected to be 1:1 and was actually 2:3.

4.2.3 Verification of *Vkorc1l1* knockout on RNA level

In order to verify the KO on mRNA level, total RNA was isolated from tail biopsy. The qPCR was conducted with either RNA or cDNA (Figure 47) to exclude assay-associated bias. For amplification of *Vkorc1l1* mRNA the primers bind in exon 1 and 2, respectively. The probe was designed to cover the exon1-2 boundary in order to avoid amplification of PCR products from genomic DNA. The results for both assays were similar with respect to expression level of *Vkorc1l1* mRNA throughout the different genotypes. After normalization to the house keeping gene *Hprt* the ratio between WT and heterozygous/homozygous KO was calculated. Surprisingly, the homozygous KO gave reliable melting curves with both assays. The presence of a “real” PCR product was proven by gel electrophoresis. However, homozygous KO showed markedly reduction of C_T values and in relation to the WT only 5% remained.

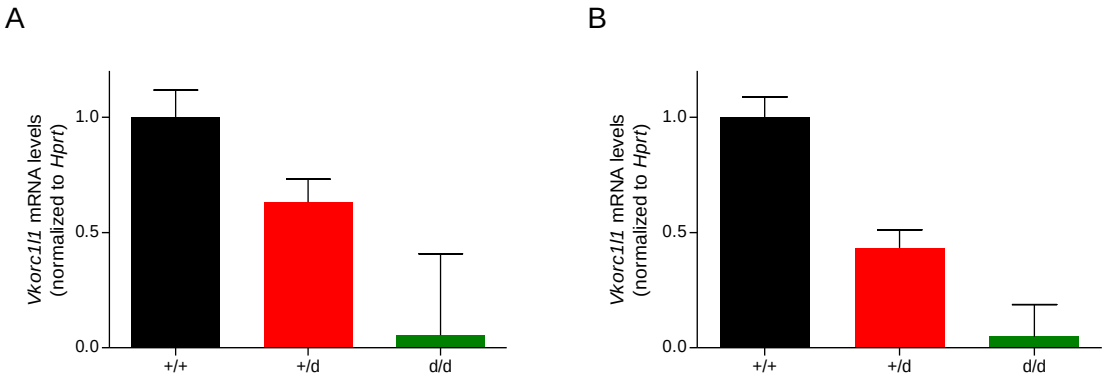

Figure 47: Results of qPCR using TaqMan assay.
RNA isolated from mouse tails were analyzed either directly (A) or after cDNA synthesis (B) by qPCR. The graphs show the ratio of VKORC1L1 expression in relation to WT after normalization to housekeeping gene *Hprt*. +/+ WT, +/d heterozygous KO, d/d homozygous KO

By alignment using BLAST, a processed pseudogene was located at chromosome 15. To verify this finding, primers which bind at start and stop codon of *Vkorc1l1* cDNA were used for amplification of genomic DNA. Those primers would give a product of 40.1 kb, which is unlikely to be amplified during PCR. Elongation time of one min preferably amplifies products of 1 kb or smaller. As shown in Figure 48 A, the samples 148 to 154 as well as the controls (WT and heterozygous KO) showed a clear band at approximately 500 bp which corresponds to the size of the *Vkorc1l1* cDNA (531 bp). Accordingly, when using the primer set for qPCR, the amplicons were about 100 bp in size, which corresponds to an amplicon generated with cDNA (108 bp).

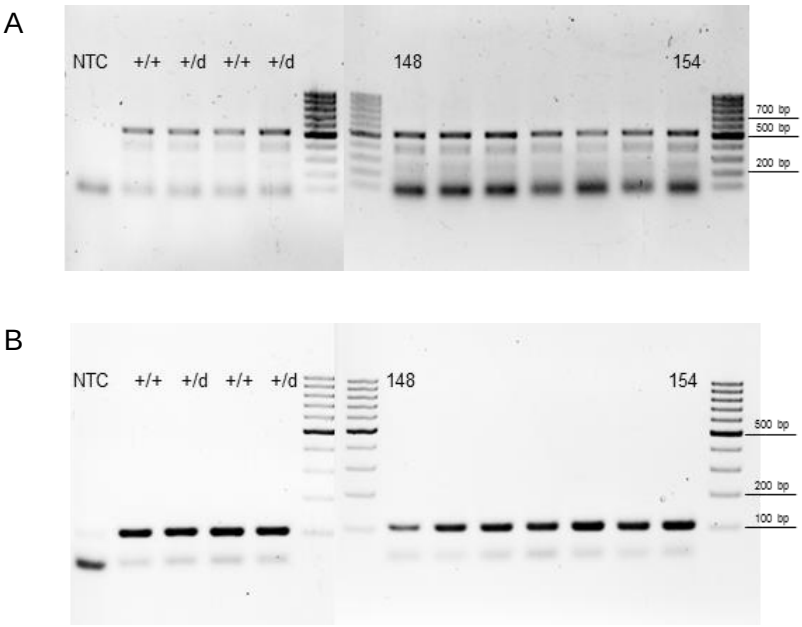

Figure 48: PCR products after amplification of genomic DNA.
A: Primers were used that bind at start and stop of *Vkorc1l1* mRNA. B: *Vkorc1l1* primers for qPCR were used.

Sequencing of before mentioned PCR products as shown in Figure 48 A revealed a nucleotide exchange at c.468T>C (Figure 49). For validation, PCR products of cDNA using the same primers were sequenced and revealed the WT sequence (c.468T).

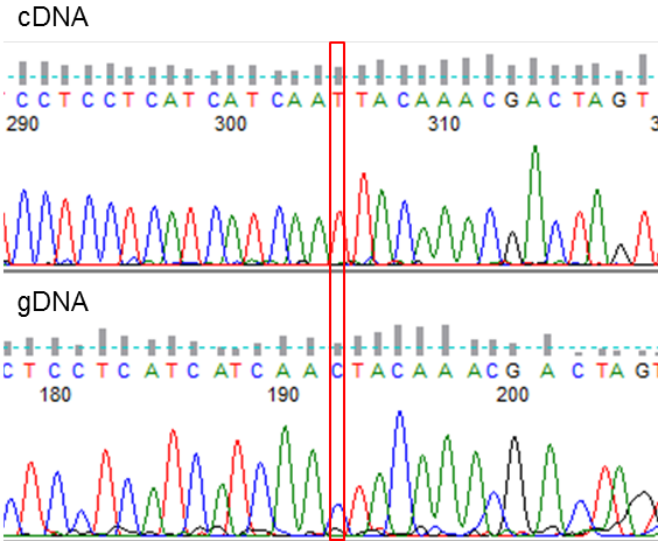

Figure 49: Sequence of processed pseudogene.
PCR products using primers binding at start and stop sequence, respectively, were generated using cDNA and genomic DNA (gDNA). The respective position c.468T is marked with a red box and shows T>C substitution.

4.2.4 German Mouse Clinic - Phenotyping report

In total 61 mice were selected for phenotyping, of which 30 were *Vkorc1l1*$^{-/-}$ (15 animals per sex) and 31 were *Vkorc1l1*$^{+/+}$ (15 females and 16 males). A total of three animals died before end of screening, two were mutant and one was control mouse.

At the age of seven weeks mice were transferred to Munich, two weeks later analysis was started in a highly ordered manner (Figure 17). About 500 parameters belonging to 14 different disease areas were measured during the primary screening. By using this highthroughput screen new hypotheses for the impact of Vkorc1l1 can be generated.

A p-value <0.05 has been used as level of significance; which might be a hint for a new phenotype. However, depending on the effect size also statistically not significant differences might be biologically relevant.

Figures and tables in this section were taken from the “Phenotyping report: Mouse line Vkorc1l1” with permission of the GMC.

Over a time course of 12 weeks the weight of all mice were monitored. Interestingly, weight of *Vkorc1l1*$^{-/-}$ differed significantly in both sexes (Figure 50 and Figure 51).

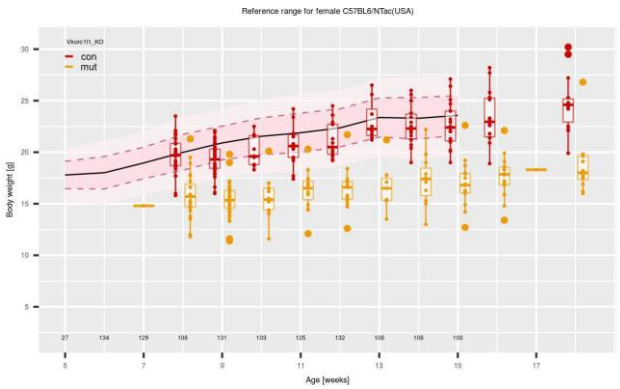

Figure 50: Weight comparison of female *Vkorcl1l1*$^{+/+}$ and *Vkorc1l1*$^{-/-}$ mice.
Red line represents *Vkorcl1l1*$^{+/+}$, yellow line shows *Vkorc1l1*$^{-/-}$. Weight was assessed from week seven to 19.

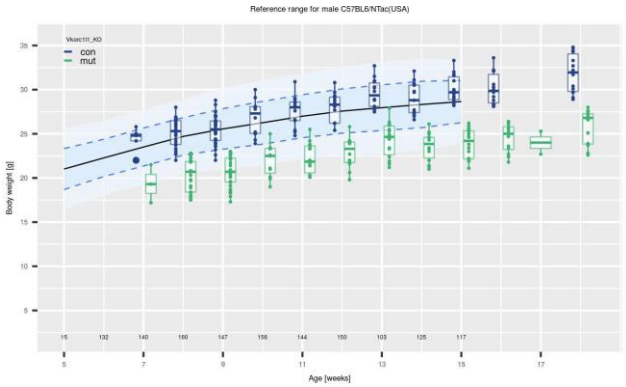

Figure 51: Weight comparison of male *Vkorcl1l1*$^{+/+}$ and *Vkorc1l1*$^{-/-}$ mice.
Blue line represents *Vkorcl1l1*$^{+/+}$, green line shows *Vkorc1l1*$^{-/-}$. Weight was assessed from week seven to 19.

The open field test provides the opportunity to systematically assess novel environment exploration, general locomotor activity, and provide an initial screen for anxiety-related behavior in rodents [92]. The chamber design is a large square chamber with a size of 45.5 x 45.5 cm. Chamber wall is 39.5 cm high, walls and floor use transparent Plexiglas. The open fleld arena is divided into a grid of equally sized areas by infrared photocell beams and beam breaks are recorded as one unit of exploratory activity. Mice will typically spend a significantly greater amount of time exploring the periphery of the arena, usually in contact with the walls, than the unprotected center area. Mutant mice showed a higher horizontal locomotion, the total distance travelled in the open field was significantly increased ($p = 0.014$) compared to wild type littermates (Figure 52A). Vertical locomotion, measured as rearing, was not different in mutant and wild type mice (Figure 52B). Anxiety-related behavior was determined as time spent in center (unprotected area). Mutant mice spent significantly less time in center ($p=0.03$) than wild type mice (Figure 52C). Thus *Vkorc1l1*$^{-/-}$ showed increased locomotor activity and increased anxiety-related behavior.

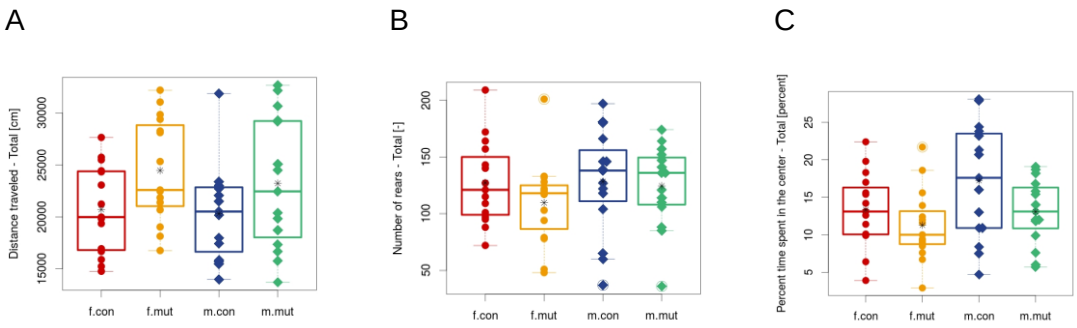

Figure 52: Results of open field test.
A: distance travelled; B: rearing activity; C: time spent in center. Red: female *Vkorcl1l1*$^{+/+}$, yellow: female *Vkorcl1l1*$^{-/-}$, blue: male *Vkorc1l1*$^{+/+}$, green: male *Vkorc1l1*$^{-/-}$

Measurement of acoustic startle responses can provide general information regarding sensorimotor processing. Prepulse inhibition (PPI) is a neurological phenomenon in which a weaker prestimulus (prepulse) inhibits the reaction of an organism to a subsequent strong startling stimulus (pulse) [93]. The extent of the adaptation affects numerous systems, but muscular reactions are measured, which are normally diminished as a result of the nervous inhibition (Figure 53). Deficits of prepulse inhibition manifest in the inability to filter out the unnecessary information. Abnormalities of sensorimotor gating have been linked to schizophrenia and Alzheimer's disease.

Vkorc1l1$^{-/-}$ mice showed decreased acoustic startle reactivity (p=0.016) and decreased prepulse inhibition (p<0.001) compared to their wild type littermates.

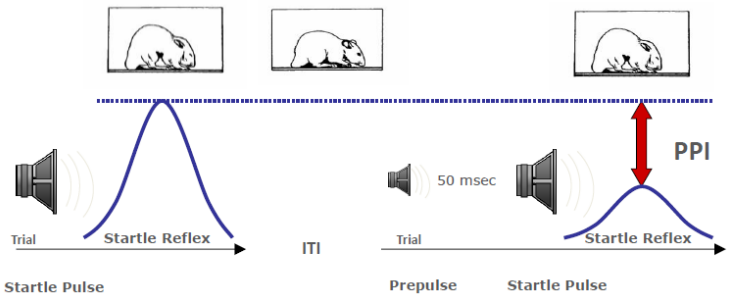

Figure 53: Acoustic startle response and prepulse inhibition.
For PPI the observable and measured response is based on the motor output (startle) following a loud acoustic stimulus. Inhibition of the response to this stimulus is observed if the stimulus is preceded very shortly by a prepulse stimulus to which the organism normally does not respond. PPI is defined as reduction of a response to a stimulus [93].

Thus *Vkorc1l1*$^{-/-}$ mice showed a clear sensorimotor gating deficit as well as altered spontaneous locomotor activity and anxiety-related behavior.

The measurement of grip strength of fore limbs and combined fore and hind limbs was used to assess the muscle function. *Vkorc1l1*$^{-/-}$ mice showed decreased grip strength for two and four paws (Figure 54). The decreased grip strength correlated well with the reduced body mass.

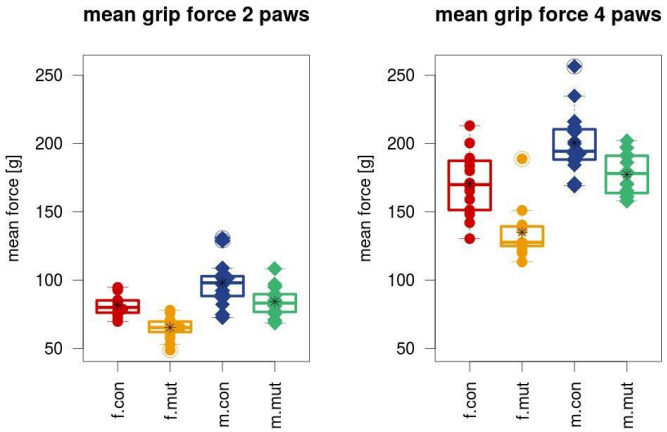

Figure 54: Measurment of grip strength of fore limbs (left panel) and combined fore and hind limbs (right panel).
Red: female *Vkorcl1l1*$^{+/+}$, yellow: female *Vkorcl1l1*$^{-/-}$, blue: male *Vkorc1l1*$^{+/+}$, green: male *Vkorc1l1*$^{-/-}$

For the assessment of coordination and balance, the accelerating rotarod was used. The accelerating speed was 4-40 rpm in 300 s. The experiment was repeated three times with 15 minutes intertrial intervals. *Vkorc1l1*$^{-/-}$ mice showed no difference at rotarod latencies (Figure 55), however slightly more passive rotations of female mutants were observed.

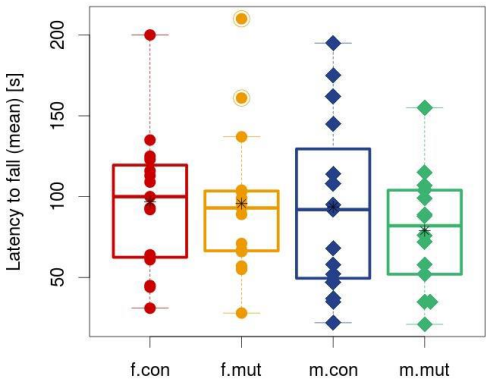

Figure 55: Results of accelerating rotarod measuring the latency to fall.
Red: female *Vkorcl1l1*$^{+/+}$, yellow: female *Vkorcl1l1*$^{-/-}$, blue: male *Vkorc1l1*$^{+/+}$, green: male *Vkorc1l1*$^{-/-}$

For the assessment of nociception, the hot plate test was used. In the test, the mouse is placed on the hot plate (52°C) and the latency to the first contact avoidance response was registered. *Vkorc1l1*$^{-/-}$ mice did not show any significant difference for types of reaction (lifting or licking of the feet or jumping) as well as none for latencies compared to *Vkorc1l1*$^{+/+}$ mice (Figure 56).

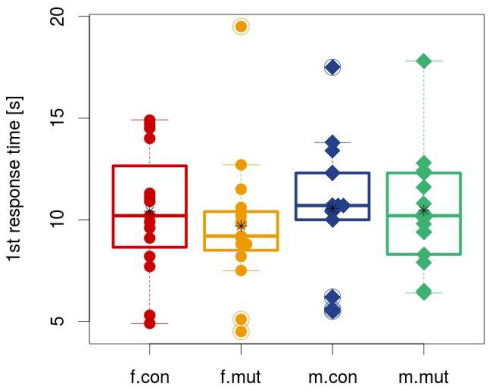

Figure 56: Hot plate test results measuring the first reponse time.
Red: female *Vkorcl1l1*$^{+/+}$, yellow: female *Vkorcl1l1*$^{-/-}$, blue: male *Vkorc1l1*$^{+/+}$, green: male *Vkorc1l1*$^{-/-}$

Auditory evoked potentials were measured to determine hearing sensitivity in a subset of animals (10 animals per sex and genotype). The sound pressure threshold for neural activity was determined to a broadband click tone. Additionally, five different pure tone frequencies (6, 12, 18, 24, and 30 kHz) were measured. No genotype effects on hearing sensitivity were observed (Figure 57).

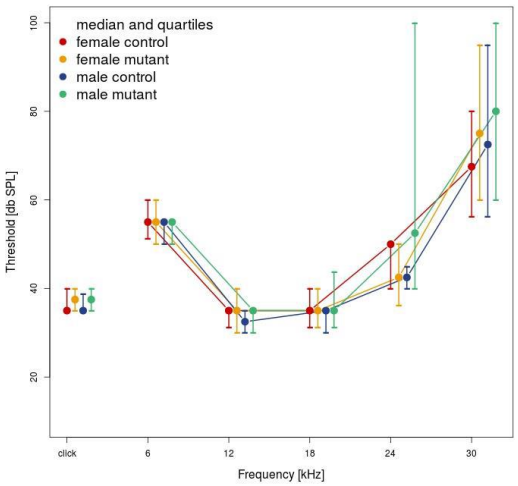

Figure 57: Measurement of auditory evoked potentials.
Red: female *Vkorcl1l1*$^{+/+}$, yellow: female *Vkorcl1l1*$^{-/-}$, blue: male *Vkorc1l1*$^{+/+}$, green: male *Vkorc1l1*$^{-/-}$

For the assessment of body composition parameters like bone mineral content and bone mineral density as well as fat and lean composition were determined using DEXA (Dual-Energy X-Ray Absorptiometry) scan. The major read outs are summarized in Table 11.

Table 11: Dual-Energy X-Ray Absorptiometry (DEXA): major read outs.
Mice were tested with an age of 17 weeks. Values are shown as mean ±SD. Bone mineral content (BMC), Bone mineral density (BMD)

	Female *Vkorc1l1*$^{+/+}$	**Female *Vkorc1l1*$^{-/-}$**	**Male *Vkorc1l1*$^{+/+}$**	**Male *Vkorc1l1*$^{-/-}$**
Number of animals	N=15	N=14	N=14	N=14
Body weight in g	23.4 ± 2.6	17.6 ± 2.1	30.1 ± 1.8	24.3 ± 1.6
Total weight (DEXA) in g	21.5 ± 2.4	16.2 ± 2.1	28.0 ± 1.8	22.7 ± 1.6
Bone area in cm²	8.08 ± 0.42	6.77 ± 0.55	8.66 ± 0.32	7.70 ± 0.57
BMC in mg	486 ± 41	368 ± 48	542 ± 43	456 ± 60
BMD in mg/cm²	60.1 ± 3.1	54.3 ± 3.1	62.6 ± 3.8	59.0 ± 3.4
Lean mass in g	13.8 ± 1.3	10.4 ± 1.3	17.7 ± 2.1	14.9 ± 1.2
Fat mass in g	7.3 ± 1.5	5.4 ± 0.8	9.8 ± 1.7	7.3 ± 0.8

Compared to control mice, mutant mice showed significantly ($p<0.001$) reduced weight, bone area, bone mineral content and density (Table 11). In addition, lean and fat content were significantly ($p<0.001$) decreased in mutant mice (Table 11). All these reductions were more pronounced in females when compared to males.

In mice, both skeleton and body composition are affected by the *Vkorc1l1* mutation.

Blood samples were collected in week 19 by retroorbital puncture under isoflurane anaesthesia. Heparin-plasma samples were used for clinical chemistry, allergology and immunology screen. EDTA samples were used for determination of hematological parameters and FACS analysis. Results are summarized in Table 12 to Table 13.

In addition, blood samples after 6h fasting were tested. Unfortunately only male mice could be tested since female Vkorc1l1$^{-/-}$ weighted less than 18 g (which is the weight limit for the experiment due to local animal experiments committees review). Parameters after fasting are summarized in Table 14.

Table 12: Clinical chemistry – *ad libitum* fed values.
Values were measured in week 19 and are shown as mean ± SD. ALT – alanine aminotransferase, AST – aspartate aminotransferase, LDH – lactate dehydrogenase, ALP – alkaline phosphatase, UIBC – unsaturated iron binding capacity, TIBC – total iron binding capacity

	Female *Vkorc1l1*$^{+/+}$	**Female *Vkorc1l1*$^{-/-}$**	**Male *Vkorc1l1*$^{+/+}$**	**Male *Vkorc1l1*$^{-/-}$**
Number of animals	n=14	n=13	n=14	n=14
Sodium in mM	147 ± 1	149 ± 2	150 ± 2	149 ± 3
Potassium in mM	4.2 ± 0.2	4.5 ± 0.4	4.2 ± 0.3	4.2 ± 0.3
Chloride in mM	111.3 ± 1.5	114.2 ± 2.6	111.2 ± 1.7	111.4 ± 2
Total protein in g/l	50.5 ± 3.2	50.5 ± 2.2	51.8 ± 1.6	51.7 ± 1.4
Albumin in g/l	26.1 ± 1.4	26.4 ± 0.8	25.7 ± 1.1	26.1 ± 1.3
Creatinine in µM	10.73 ± 1.02	10.05 ± 1.16	9.6 ± 1.27	10.26 ± 1.46
Urea in mM	11.46 ± 1.3	13.40 ± 2.24	11.81 ± 1.36	14.10 ± 2.06
Cholesterol in mM	2.193 ± 0.506	1.504 ± 0.666	2.639 ± 0.521	1.791 ± 0.451
Triglyceride in mM	1.838 ± 0.593	1.532 ± 0.627	2.337 ± 0.629	1.578 ± 0.508
ALT in U/l	34 ± 19	43 ± 29	28 ± 7	40 ± 27
AST in U/l	52 ± 12	85 ± 38	43 ± 12	59 ± 19
α-Amylase in U/l	662 ± 111	674 ± 107	745 ± 119	757 ± 84
Glucose in mM	14.33 ± 2.07	12.40 ± 2.35	13.75 ± 2.02	13.10 ± 2.10
LDH in U/l	170 ± 41	219 ± 67	142 ± 20	178 ± 36
Calcium in mM	2.31 ± 0.04	2.26 ± 0.03	2.29 ± 0.04	2.24 ± 0.03
Phosphate in mM	1.94 ± 0.22	1.93 ± 0.34	1.75 ± 0.32	1.68 ± 0.23
ALP in µM	101 ± 18	107 ± 22	70 ± 14	85 ± 17
Iron in µM	24.84 ± 3.17	23.46 ± 2.68	22.62 ± 3.39	21.42 ± 2.51
UIBC [µmol/l]	38.0 ± 6.1	39.8 ± 2.2	41.6 ± 4.8	43.0 ± 3.1
TIBC [µmol/l]	62.8 ± 3.8	63.3 ± 2.4	64.2 ± 2.7	64.4 ± 2.5

Plasma urea levels were increased in *Vkorc1l1*$^{-/-}$ mice ($p<0.001$), but creatinine levels did not reflect this observation. Interestingly, plasma levels of sodium, potassium and chloride were significantly increased in female *Vkorc1l1*$^{-/-}$ mice compared to female control mice ($p=0.011$, $p=0.002$ and $p=0.002$, respectively). Plasma lipids cholesterol and triglycerides were significantly decreased ($p<0.001$ and $p=0.002$, respectively), plasma glucose levels were lower in mutant animals ($p=0.03$). Liver parameters AST and LDH were increased in *Vkorc1l1*$^{-/-}$ mice ($p<0.001$ and $p=0.001$, respectively), but ALT did not differ significantly. Marked decrease in plasma calcium levels were observed in mutant

mice (p<0.001) whereas plasma protein levels were not affected. ALP activity was slightly elevated only in males (p=0.031).

Table 13: Hematological parameters assessed in week 19.
Values are shown as mean ± SD. WBC - White blood cell count; RBC - Red blood cell count; HCT - Hematocrit; HGB - Hemoglobin; MCV - Mean corpuscular volume; MCH - Mean corpuscular hemoglobin; MCHC - Mean corpuscular hemoglobin concentration; RDW - Red blood cell distribution width; PLT - Platelet count; MPV - Mean platelet volume; PDW - platelet distribution width

	Female *Vkorc1l1*$^{+/+}$	**Female *Vkorc1l1*$^{-/-}$**	**Male *Vkorc1l1*$^{+/+}$**	**Male *Vkorc1l1*$^{-/-}$**
Number of animals	n=14	n=14	n=14	n=14
RBC in million/mm³	10.59 ± 0.38	9.92 ± 0.31	10.82 ± 0.73	10.6 ± 0.61
WBC in 10³/mm³	8.69 ± 2.33	5.78 ± 2.14	6.16 ± 1.87	5.9 ± 1.64
PLT in 10³/mm³	917.7 ± 140.7	945.0 ± 116.9	1314.1 ± 191.4	1250.5 ± 164.4
HGB in g/dl	16.44 ± 0.92	15.73 ± 0.6	16.68 ± 1.06	16.6 ± 0.88
HCT in %	50.89 ± 1.88	48.29 ± 1.71	51.7 ± 3.12	51.21 ± 2.62
MCV in fl	48.21 ± 1.12	48.79 ± 1.25	47.86 ± 0.66	48.36 ± 0.74
MCH in pg	15.52 ± 0.51	15.86 ± 0.43	15.41 ± 0.51	15.66 ± 0.28
MCHC in g/dl	32.26 ± 0.86	32.57 ± 0.49	32.27 ± 0.81	32.41 ± 0.55
RDW in %	13.79 ± 0.56	14.04 ± 0.58	15.21 ± 1.1	14.86 ± 0.62
MPV in fl	6.59 ± 0.2	6.44 ± 0.26	6.46 ± 0.16	6.42 ± 0.21
PDW in fl	6.02 ± 0.32	5.77 ± 0.34	5.85 ± 0.28	5.74 ± 0.28

Genotype-related differences in peripheral blood cell counts were predominantly a decrease in red and white blood cell counts (p<0.001 and p=0.002, respectively) but not platelets in female *Vkorc1l1*$^{-/-}$ mice, while effects on erythrocyte indices were rather subtle. In females KO mice decreased red and white cell count, hemoglobin and hematocrit was associated with subtle differences in red cell and platelet distribution width as well as MCV and MCH.

Table 14: Clinical chemistry – after 6h fasting.
In week 11 food was removed for 6h and blood was collected afterwards. Only male mice were examined due to restricted weight of female mice. HDL-cholesterol – High density lipoprotein-cholesterol; NEFA - Non-esterified Free Fatty Acid

	Male *Vkorc1l1*$^{+/+}$	**Male *Vkorc1l1*$^{-/-}$**	**T-test**
Number of animals	n=14	n=14	
Glucose in mM	8.28	10.22	p<0.01
Cholesterol in mM	2.730	1.696	p<0.001
HDL-cholesterol in mM	2.075	1.450	p<0.001
Non-HDL-cholesterol in mM	0.655	0.246	p<0.001
Triglyceride in mM	1.397	0.725	p<0.001
Glycerol in mM	0.305	0.207	p<0.01
NEFA in mM	1.229	0.653	p<0.001

As already mentioned, mutants showed compared to controls decreased body mass. Weight loss during 6h-fasting was high especially in male mutants compared to controls. *Vkorc1l1*$^{-/-}$ mice showed increased fasting glucose and decreased fasting blood lipid values.

For baseline immune status the integrity of immune cell composition in the peripheral blood of mutant mice was evaluated (Figure 58 and Figure 59).

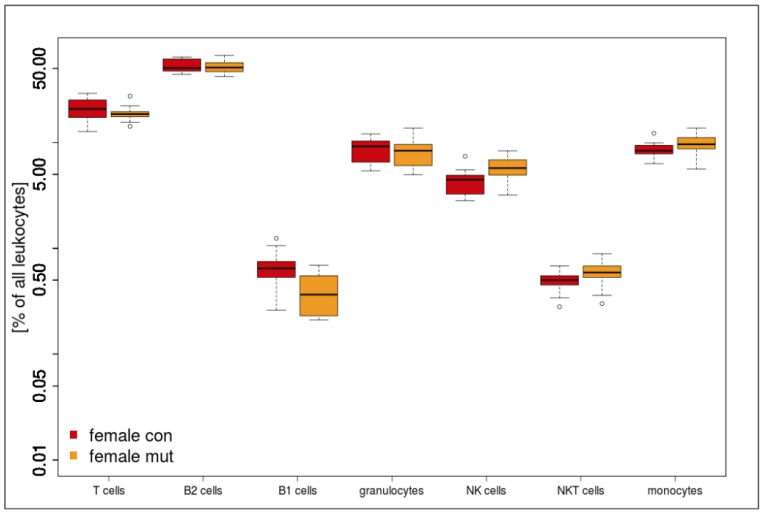

Figure 58: Flow cytometric analysis of peripheral blood of female mice.
Red: female *Vkorcl1l1*$^{+/+}$, yellow: female *Vkorcl1l1*$^{-/-}$

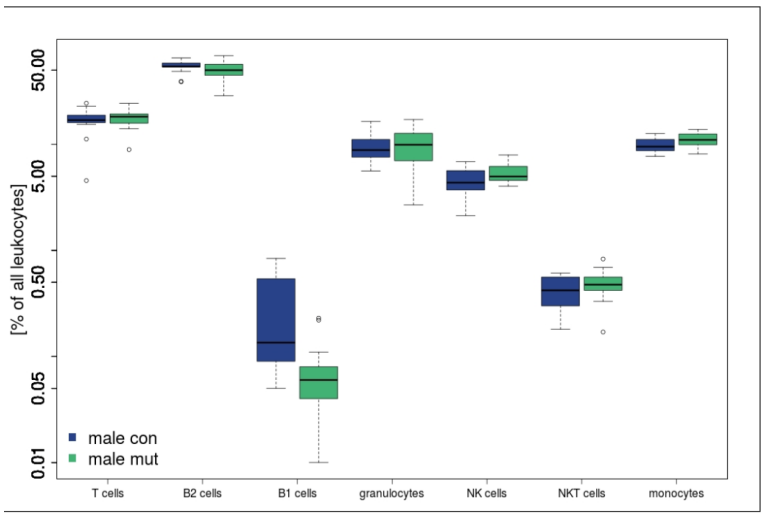

Figure 59: Flow cytometric analysis of peripheral blood of male mice.
Blue: male *Vkorc1l1*$^{+/+}$, green: male *Vkorc1l1*$^{-/-}$

FACS analysis revealed lower production of B1 cells and slightly increased frequency of NK cells as well as monocyte in *Vkorc1l1*$^{-/-}$ mice compared to *Vkorc1l1*$^{+/+}$ mice. Furthermore, these cells remain favorably in inactivated stage.

Cardiovascular screening including ECG and echocardiography did not reveal significant differences. In echocardiography an increased heart rate, mainly in females, was detected (p=0.016). No signs of tachycardia could be seen during echocardiography. Scatter plot analysis showed a strong impact of the body weight on heart parameters, thus explaining more pronounced impact of heart rate in female mice. During ECG analysis mainly male mice showed increased heart rate. However, no pathological phenotype was observed thus relevance of the findings is unclear.

During pathological screen mice were examined macroscopically and microscopically. For that purpose five mice with an age of 18-19 weeks of each sex and genotype were analysed. The results are summarized in Table 15.

Table 15: Body, heart, liver and spleen weights.
Medians, first and third quartile are shown for five mice for each sex and genotype.

	Female *Vkorc1l1*$^{+/+}$	**Female *Vkorc1l1*$^{-/-}$**	**Male *Vkorc1l1*$^{+/+}$**	**Male *Vkorc1l1*$^{-/-}$**
Age of mice in d	129 [126 , 129]	129 [129 , 131]	127 [127 , 127]	130 [125 , 130]
Body weight in g	24.2 [22.1 , 24.7]	17.7 [16.9 , 19.8]	31.7 [30.4 , 32.7]	26.6 [25.3 , 27]
Heart weight in mg	129 [128 , 132]	87 [87 , 107]	159 [145 , 167]	140 [135 , 143]
Tibia length in mm	17.97 [17.44 , 18.01]	16.16 [16.08 , 16.21]	18.02 [17.59 , 18.17]	17.35 [17.3 , 17.77]
Liver weight in g	1.237 [1.091 , 1.295]	1.012 [0.944 , 1.379]	1.794 [1.619 , 1.885]	1.776 [1.69 , 1.79]
Spleen weight in g	0.11 [0.082 , 0.124]	0.059 [0.057 , 0.072]	0.087 [0.083 , 0.087]	0.077 [0.069 , 0.08]

Weight of spleen for female mice differed significantly between genotypes (p=0.032). Other parameters determined did not show statistical significant differences. When calculating the ratio between liver weight and body weight both male and female mice showed a significant difference (each p=0.016) when comparing wild type and mutant *Vkorc1l1* mice. During histological analysis no genotype-related changes of mutant mice had been detected. Tissues investigated included skin, brain, kidney, liver, heart, lung, thymus, spleen, adrenals, organs of the gastrointestinal system and reproductive system.

In week 18/19 the body weight was assessed and confirmed earlier findings. Data is summarized in Figure 60.

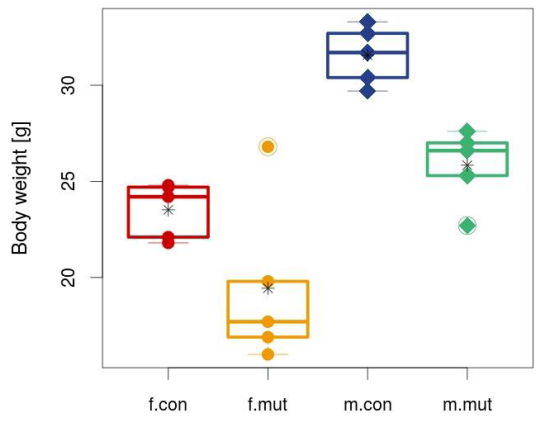

Figure 60: Body weight assessed in week 18/19.
Red: female *Vkorcl1l1*$^{+/+}$ (f.con), yellow: female *Vkorcl1l1*$^{-/-}$ (f.mut), blue: male *Vkorc1l1*$^{+/+}$ (m.con), green: male *Vkorc1l1*$^{-/-}$ (m.mut)

5 Discussion

Vitamin K hydroquinone is an indispensable co-factor in post-translational activation of VKD proteins. *In vitro*, both VKOR enzymes, VKORC1 and VKORC1L1, are able to supply GGCX with KH_2. Warfarin and other 4-hydroxycoumarin derivatives exert their effect by inhibition of VKORC1 [17, 59]. However, only little is known about the inhibitory effect of coumarins on VKORC1L1.

In the first part of this thesis VKOR enzymes were tested with regard to their susceptibility to various coumarins and indandiones. HEK 293T *VKOR* KO cell lines were generated to allow the discrimination of endogenously expressed enzymes. The results led over to *in silico* analysis, which revealed distinct warfarin binding sites in VKORC1 and VKORC1L1. By means of *VKORC1* and *VKORC1L1* double knockout cells *in silico* data were verified by *in vitro* experiments. Results of overexpressed VKORC1 and VKORC1L1 and its respective variants confirmed distinct warfarin binding pattern and conceivably explained different inhibition pattern of OACs.

In the second part of the thesis the generation of *Vkorc1l1* knockout mice is described. The transgenic mice were created by means of CRISPR/Cas9 gene editing technique. In a first analysis the mice showed no lethal phenotype in contrast to *Vkorc1* knockout mice but several diverse phenotypes have been observed which can be linked to neurological diseases, diabetes and fat metabolism. Detailed information regarding the function of *Vkorc1l1* will be collected and may answer the question if Vkorc1l1 plays a role in γ-carboxylation of VKD proteins *in vivo*.

5.1 Characterization of VKORC1 and VKORC1L1 *in vitro*

VKORC1 and *VKORC1L1* KO HEK 293T cell lines

In vivo, VKORC1 was proven to be the essential enzyme to drive the vitamin K cycle since *Vkorc1*$^{-/-}$ mice die due to intracranial bleeding [31]. However, *in vitro*, VKORC1 and VKORC1L1 supply GGCX with KH_2, the essential co-factor for γ-carboxylation [9, 33].

GGCX, VKORC1 and VKORC1L1 are endogenously expressed in HEK 293T cells. These enzymes are required for driving the vitamin K cycle and post-translational modification of vitamin K dependent proteins [9]. To discriminate between VKOR isozymes HEK 293T cell lines were generated in which one or both enzymes were knocked out. The endogenous activity of VKORC1 or VKORC1L1 was assessed by means of the cell-based FIX reporter assay [30]. The single *VKORC1* and *VKORC1L1* KO HEK 293T cells showed FIX activities (Figure 19) comparable to that of WT cells proving that both enzymes independently recycle vitamin K and thus provide GGCX with the co-factor KH_2. In contrast, DKO cells (in which both VKORC1 and VKORC1L1 were knocked out) showed no FIX activity when supplemented with 12 µM K_1.

Further characterization of KO cell lines was difficult because elucidation of VKORC1 and VKORC1L1 knockout on mRNA and protein level were not feasible due to different reasons. mRNA expression profile was not conclusive since primer and probe design for qPCR cannot omit small changes in target sequence. In case of *VKORC1* KO cells NGS revealed a large deletion and subsequently mRNA was not detectable (Table 1). Other clones showed only small changes in genomic DNA (e.g. two nucleotides deletion/ one nucleotide insertion in *VKORC1L1* KO cells, Figure 18) and thus mRNA expression was detected (Table 1). However, copy number was markedly lower as determined in WT HEK 293T cells. Since all genomic alterations led to shift of reading frame, manipulation in *VKORC1* and *VKORC1L1* genes were considered to result in absent protein expression.

Furthermore, detection of endogenous protein expression of VKORC1 and VKORC1L1 in HEK 293T cells proved impossible due to absent suitable antibodies. Different antibodies (from various companies) were tested and none of them showed reliable results.

Susceptibility to oxidative stress of HEK 293T knockout cell lines

The harmful effect of free ROS can be due to either an excessive production of ROS and/or a deficiency of antioxidants. ROS include superoxide radical ($O_2^{\cdot}$), hydroxyl radical ($HO^{\cdot}$) and nonradical molecules like hydrogen peroxide (H_2O_2), generated as a by-product of normal aerobic metabolism, but increases under stress. Human antioxidant system consist of low-molecular-weight antioxidants such as reduced glutathione (GSH) and vitamins C and E as well as noncatalytic antioxidant proteins and ROS-metabolizing enzymes [94]. In addition, KH_2 was shown to be an effective antioxidant [95] but is rapidly oxidized [96].

KO HEK 293T cells were characterized with respect to their antioxidative properties. In a previous *in vitro* study, Westhofen and colleagues postulated that VKORC1L1 plays an ubiquitous and fundamental role in intracellular antioxidation [10]. Indeed, *VKORC1L1* KO cells were greatest affected by H_2O_2 treatment (Figure 20) underlining the putative antioxidative role of VKORC1L1 in scavenging ROS. Moreover, *VKORC1* KO also exhibit a reduced ability to compensate H_2O_2-induced cell death compared to WT HEK 293T cells.

Li and colleagues investigated the role of vitamin K in terms of oxidative injury in oligodendrocyte precursor cells [97]. The induction of oxidative stress by H_2O_2 (800 µM) could not be prevented by K_1 administration (100 µM). In contrast to this study, we could reverse the effect of H_2O_2 treatment (50 µM) with 12 µM K_1 in WT, *VKORC1* KO and *VKORC1L1* KO HEK 293T cells (Figure 21). The controversial results may be due to highly divergent H_2O_2 concentrations. In addition, high concentrations of vitamin K (higher than 50 µM) can be assumed to be toxic. In our assay H_2O_2 concentration of 100 µM led to markedly reduced cell survival although vitamin K was present (Figure 20). Furthermore, endogenous expression level of VKOR enzymes as well as other proteins which may have an impact on antioxidative properties of distinct cell types could explain the debated results. Interestingly, warfarin showed antioxidative properties when WT and single KO HEK 293T cells were treated with H_2O_2. Indeed, Monti and colleagues did not see a negative effect of warfarin (up to 10 µM) on cell proliferation in HEK 293 cells [63].

Vervoort and colleagues investigated the antioxidant properties of vitamin K in rat liver microsomes by means of lipid peroxidation which is initiated by ROS [95]. Vitamin K (without a reducing equivalent) did not contribute to the antioxidant properties. The addition of vitamin K epoxide prevented lipid peroxidation (inversely correlated with the formation of TBARS (thiobarbituric acid reactive substances)) whereas co-incubation with warfarin abolished inhibitory properties of K>O. Furthermore they concluded that KH_2 is

the antioxidant species of vitamin K (Figure 61). At time of this publication the enzymes responsible for vitamin K reduction have not been identified. Furthermore, the function of VKORC1L1 could not be clearified since rat liver samples were used for analysis and in this tissue *VKORC1* is about 50 times higher expressed than *VKORC1L1* [12].

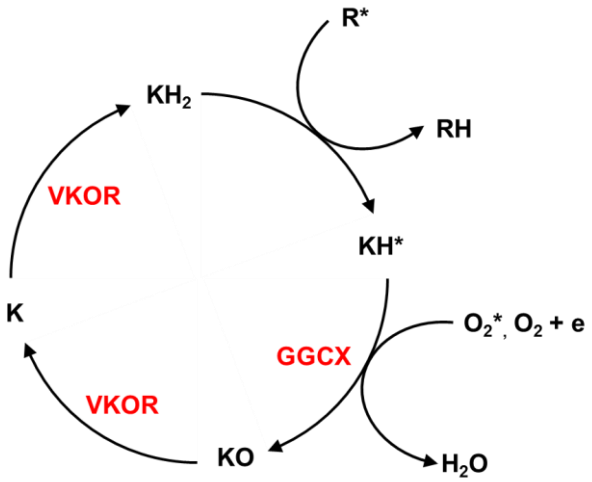

Figure 61: Proposed reaction routes for the antioxidant action of vitamin K. KH_2, KH_2*, KO, and K represent different redox states of vitamin K, R* is a radical species. [95]

Beside the well-known feature of being the exclusive co-factor for γ-carboxylation, KH_2 was recognized to have antioxidant properties. Both VKOR enzymes may provide KH_2 for antioxidation, thus reduced levels of KH_2 due to reduced vitamin K recycling in VKORC1 and VKORC1L1 KO cells may explain these results.

Determination of enzymatic activity of VKOR enzymes

Both VKOR enzymes can utilize K as well as K>O to drive the vitamin K cycle, and catalytic features are designated as VKR (vitamin K reductase) and VKOR (vitamin K 2,3-epoxide reductase) activity, respectively. Previous studies have used two distinct types of assays to examine the capability of VKORC1 and VKORC1L1 to reduce K or K>O *in vitro*.

The DTT-driven VKOR assay (i.e. conversion of K>O to K) was established in the late 1970s [98, 99]. More recently, a modification of the DTT-driven assay was described whereby the conversion of K to KH_2 (i.e. VKR activity) can be monitored using a sealed vial assay [96]. In general, microsomes or cell lysates are incubated with buffer, DTT and $CaCl_2$. A defined concentration of substrate (i.e. K>O to assess VKOR activity or K for VKR activity) is incubated for 60 min at 30°C to allow substrate conversion. The reaction is stopped by isopropanol/hexan and an internal standard is added. The hydrophobic vitamin K derivatives accumulate in the hexan phase, which is vaporized. Finally, the products are dissolved in isopropanol and analyzed by HPLC. The amount of K/KH_2 is

calculated by means of internal standard and peak area of K vitamers. With this assay enzymatic parameters like v_{MAX} and k_M can be determined giving a more precise look into the reaction characteristics. Furthermore, VKOR/VKR activity can be assessed from tissues or cells reflecting endogenous or overexpressed protein levels, but discrimination between VKORC1 and VKORC1L1 is the major disadvantage of this assay because both enzymes catalyze the reduction of K and K>O. Furthermore, the use of the non-physiological reductant DTT together with substrate could drive carboxyation of VKD proteins by non-catalytic active VKOR variants *in vitro* leading to artificial results [17, 98, 99]. Another issue relates to the purification of VKOR enzymes. This is difficult because solubilization renders the enzyme inactive. Thus, microsomes instead of pure enzyme are isolated using CHAPS as detergent leading to native VKOR enzyme [26, 59, 100]. In general, DTT-driven VKOR/VKR assay is very sensitive to small changes of assay components. As shown by Bevans and colleagues minor changes in DTT and K_1>O concentration led to variability of IC_{50} of warfarin ranging from 2.9 µM to 23.7 µM. In addition, pH plays an important role for reproducability and comparability of different studies [101].

The cell-based assay used for determination of VKOR activity was first described in 2011 [102]. In principle, this assay relies on the expression (either stable or transient) of a reporter protein which requires γ-carboxylation for biological activity. Supplementation of K or K>O determines the enzyme activity to be measured, i.e. VKR or VKOR activity, respectively. In our group, FIX is used as a marker for VKOR/VKR enzyme activity, other groups utilize chimeric proteins, e.g. fusion protein of FIX and protein C; FIXgla-PC [9, 102]. In contrast to the DTT-driven VKOR/VKR assay, the reporter protein is activated under physiological conditions, i.e.no DTT is required which is thought to reduce VKOR enzymes and lead to artificial results [21, 103]. One disadvantage may be the disability to determine enzymatic parameters as described above.

The cell-based assay used in this study makes use of WT hFIX, which comprises 12 glutamic acid residues in its Gla domain. Like other VKD proteins, FIX is post-translationally modified by a process described as comprehensive and processive carboxylation [104]. During this process VKD proteins are bound via its propeptide to GGCX and Gla domain undergoes intramolecular movement to reposition Glu's for enzymological modification [104]. Plasma derived FIX is fully carboxylated whereas recombinant protein is not. However, recombinant FIX which is carboxylated at least at 10 Glu residues can be assumed as biologically active as BeneFIX (recombinant FIX concentrate for treatment of hemophilia B) is also not fully carboxylated [105]. If KH_2 availability is decreased VKD proteins dissociate from the carboxylase leading to release of under- or uncarboxylated proteins [106]. In case of FIX the protein is secreted inde-

pendent of carboxylation status [107]. In contrast, protein C is degraded intracellularly if poorly carboxylated [108]. Hence, measurement of extracellular FIX protein based on its activity is more accurate than measurement based on protein itself (i.e. antigen level). Tie *et al*. uses chimeric FIXgla-PC reporter to measure antigen level of protein C as an outcome which should also be feasible due to intracellular degradation of undercarboxylated protein [102].

Specific inhibition of VKORC1 and VKORC1L1 by OACs

The aim of this study was to determine the inhibition profile of VKORC1 and VKORC1L1 with respect to various coumarins and indandiones. Thus, *VKORC1* and *VKORC1L1* KO cells were generated to assess the endogenous inhibitory potential of compounds with 4-hydroxycoumarin and 1,3-indandione backbone in the previously published FIX cell-based assay. Of note, drug inhibition is not influenced by metabolic activity since cytochrome P450 monooxygenases known to be involved in metabolism of K and warfarin are not expressed in HEK 293 cells [109]. Therefore, compounds stay at their initial concentration and metabolic degradation does not have an impact on experimental data.

The naturally occurring coumarin showed no anticoagulatory effect *in vitro*, as concentrations up to 1 mM did not result in reduced FIX activity for both VKOR enzymes (Table 2). *In vivo*, coumarin itself does not show an effect on coagulation, too [65]. In contrast, VKORC1 and VKORC1L1 were inhibited by 4-hydroxycoumarin at micromolar concentrations, indicating that the hydroxyl group at C4-atom is essential for inhibition of both enzymes. Furthermore, dicoumarol, the causative agent in sweet clover disease [64] and the first OAC drug, inhibited VKORC1 and VKORC1L1 with about three orders of magnitude higher efficacy than 4-hydroxycoumarin. However, data of dicoumarol appeared to be biphasic and might explain the poor controllability in therapy of thrombotic events [64].

Warfarin, a synthetic 4-hydroxycoumarin, was more potent than compounds mentioned above and revealed values of 1.9 nM for VKORC1 and 25.4 nM for VKORC1L1, representing about 13-fold higher efficacy for VKORC1 inhibition compared to VKORC1L1. The same tendency was observed with regard to acenocoumarol and phenprocoumon. Interestingly, those OACs revealed greater potential on VKORC1L1 inhibition compared to warfarin. Hence, warfarin might be the better choise to inhibit VKOR actvity in terms of liver-specific VKORC1 enzyme activity.

The increased size and hydrophobicity of the variable 3-position side chains of 4-hydroxycoumarins correlated with decreased IC_{50} values, best seen for 4-hydroxycoumarin (VKORC1 IC_{50} 2000 nM) and acenocoumarol (VKORC1 IC_{50} 1.6 nM).

All synthetic coumarins tested in this study were more potent than dicoumarol irrespective of enzyme investigated.

IC_{50} values for indandiones (phenindione and fluindione) were higher than those for most of 4-hydroxycoumarin drugs investigated. Fluindione exhibited higher IC_{50} values than phenindione, which was apparently due to the fluorine atom attached to the phenyl ring of phenindione. Furthermore, VKORC1L1 inhibition needed much higher concentrations compared to coumarin-based compounds. This effect may be explained by the different chemical structures of the compounds, but further investigation is required.

VKOR enzyme comparison

Although VKOR isozymes are more than 50% identical in their amino acid composition, VKORC1 was more sensitive to therapeutically used 4-hydroxycoumarin derivatives compared to VKORC1L1. Some million years ago, gene duplication occurred resulting in VKORC1 and VKORC1L1 paralogues [110, 111] and both genes were maintained throughout evolution of vertebrates. Thus it is likely that VKOR paralogues carry out different functions, implying tissue rather than substrate specificity.

The majority of published studies were not suitable to discriminate enzyme activities of VKORC1 and VKORC1L1 [9, 10, 30, 33, 101, 102, 109, 112, 113]. In addition, most of the studies focused on warfarin, the most prominent OAC. To date, a systematic overview on clinically applied OACs is lacking. In Table 16 results on VKOR enzyme inhibition with special regard to warfarin are summarized.

Published data on the inhibitory potential of warfarin varied (Table 16) presenting IC_{50} values from 2.2 µM [112] to 25 nM [30]. Differences in IC_{50} or K_i (inhibitory constant) values arise from the type of assay used (DTT vs. cell-based), the substrate (K_1 vs. K_1>O) and its concentration, the amount (endogenous vs. overexpressed) and source of protein (kidney- vs. liver-derived) tested. All these studies have in common that they were not able to discriminate between endogenous VKORC1 and VKORC1L1. Conclusions from previous studies can only be made with regard to distinct inhibition profile of warfarin for both VKOR enzymes. Westhofen and colleagues incubated cell lysates overexpressing VKORC1 or VKORC1L1 with 5 µM warfarin and measured VKOR activity by the DTT-driven assay [10]. At this particular warfarin concentration VKORC1 was inhibited by half, whereas VKORC1L1 retained 70% of activity. Hammed *et al.* used human and rat VKORC1 or VKORC1L1 expressed in yeast *Pichia pastoris* and determined enzyme kinetic parameters V_{max} and K_m in DTT-driven assay. Comparison of inhibitory constants revealed 30- to 50-fold higher susceptibility of VKORC1 compared to VKORC1L1 [33]. In the present study, endogenous VKOR activity revealed (only) 13-

fold difference in warfarin sensitivity when comparing VKORC1 with VKORC1L1 (Table 2). In contrast, data of overexpressed VKOR enzymes are in accordance to Hammed *et al.* since warfarin was about 30-fold more effective in VKORC1 inhibition compared to VKORC1L1 (Figure 32, Table 4). Hence the results imply that expression level account for different results of inhibition pattern. In WT HEK 293T cells, *VKORC1* mRNA was present in about 10-fold excess compared to *VKORC1L1* mRNA, whereas in cells using overexpression mRNA level can be considered as equal. Thus results from endogenous vs. overexpressed protein cannot be compared directly, but comparison of overexpressed VKORC1 and VKORC1L1 might reflect the protein's characteristics *in vitro,* because same expression level can be assumed. In liver and in HEK 293T cells, *VKORC1* mRNA expression is higher than *VKORC1L1* and results from endogenous studies may reflect *in vivo* situation well, especially with regard to coagulation.

Table 16: Overview of published assays to determine VKORC1 and/or VKORC1L1 inhibition.
NA- not applicable, K_1>O - vitamin K_1 epoxide, K_1 – vitamin K_1, K_i – inhibitory constant, C1 – VKORC1, L1 – VKORC1L1, KO – knockout, DKO – double knockout.

	Gebauer 2007 [112]	**Tie *et al.*, 2011** [102]	**Westhofen *et al.*, 2007** [10]	**Tie *et al.*, 2013** [9]	**Fregin *et al.*, 2013** [30]	**Hammed *et al.*, 2013** [33]	**Haque *et al.*, 2014** [109]	**Matagrin *et al.*, 2016** [113]	**This thesis**	**This thesis**	**This thesis**
Expression system/ Cell line	Rat liver microsomes	HEK 293	HEK 293T	HEK 293 WT and C1 KO	HEK 293T	*Pichia pastoris*	HEK 293-C3	*Pichia pastoris*	C1 KO and L1 KO HEK 293T	C1 KO and L1 KO HEK 293T	DKO HEK 293T
VKOR expression	Endogenous	Endogenous	VKOR over-expression	Endogenous	VKOR over-expression	VKOR over-expression	Endogenous	VKOR over-expression	Endogenous	Endogenous	VKOR over-expression
Type of measurement	Direct	Indirect	Direct	Indirect	Indirect	Direct	Indirect	Direct	Indirect	Indirect	Indirect
Activity measurement	K>O conversion	FIXgla-PC	K>O conversion	FIXgla-PC	FIX	K>O conversion	F9CH	K>O conversion	FIX	FIX	FIX
Reporter expression	NA	Stable	NA	Stable	Transient	NA	Inducible, stable	NA	Transient	Transient	Transient
Substrate	25 mM K_1>O	5 µM K_1>O	50 µM K_1>O	5 µM K_1>O	10 µM K_1	Up to 0.2 mM K_1>O	50 nM K_1	Up to 0.2 mM K_1>O	12 µM K_1	12 µM K_1>O	12 µM K_1
Type of assay	DTT assay	ELISA	DTT assay	ELISA	Clotting assay	DTT assay	FACS	DTT assay	Clotting assay	Clotting assay	Clotting assay
Discrimination between C1 and L1	No	No	Yes (but remaining endogenous activity)	Yes (in KO cells)	Yes (but remaining endogenous activity)	Yes	No	Yes	Yes	Yes	Yes
Warfarin inhibition	IC_{50} 2200 nM	IC_{50} 100 nM	At 5 µM: C1: 53% inhibition L1: 29 % inhibition	IC_{50} < 50 nM	IC_{50} 25 nM	K_i values: hL1/hC1: 29x rL1/rC1: 54x	IC_{50} 125 nM	K_i values: hC1: 1.65 µM hL1: 52 µM	IC_{50}**:** C1: 2 nM L1: 25 nM	IC_{50}**:** C1: 2.4 nM L1: 27 nM	IC_{50}**:** C1: 17.3 nM L1: 474 nM

Comparative data for warfarin and other compounds are sparsely available [103, 112, 113] and all published data were generated by means of DTT-driven VKOR assay (Table 17). Gebauer tested different 4-hydroxycoumarins, whereby acenocoumarol was the most potent drug [112]. Hodroge and colleagues used microsomal preparation of *P. pastoris* overexpressing VKORC1. The inhibitory constant for warfarin was equal to previously published values (1.65 µM), acenocoumarol and fluindione were more effective by a factor of 5 and 7, respectively [103]. Recently, the same group published results for various 4-hydroxycoumarins with respect to both VKOR enzymes [113]. VKORC1L1 was shown to be less affected by OAC treatment whereby warfarin and fluindione were the compounds with the most distinct inhibition pattern yielding 30- and 80-fold difference on both VKOR enzymes. Although obtained with different types of assays the results showed the same overall tendency proving the quality of the data presented in this study. However, IC_{50} values of the present study are much lower indicating that the cell-based assay used here represents a more sensitive method.

Table 17: Overview of published data for warfarin and other OACs.
ND- not determined, K_1>O - vitamin K_1 epoxide, K_1 – vitamin K_1, Ki – inhibitory constant

	Gebauer 2007 [112]	**Hodroge *et al.*, 2011** [103]	**Matagrin *et al.*, 2016** [113]	**This thesis**	**This thesis**
Expression system/ Cell line	Rat liver microsomes	*Pichia pastoris*	*Pichia pastoris*	*VKORC1L1* KO HEK 293T	*VKORC1L1* KO HEK 293T
VKOR expression	Endogenous	VKORC1 overexpression	VKORC1 overexpression	Endogenous	Endogenous
Type of measurement	Direct	Direct	Direct	Indirect	Indirect
Activity measurement	K>O conversion	K>O conversion	K>O conversion	FIX	FIX
Reporter expression	NA	NA	NA	Transient	Transient
Substrate	25 mM K_1>O	Up to 0.2 µM K_1>O	Up to 0.2 µM K_1>O	12 µM K_1	12 µM K_1>O
Type of assay	DTT assay	DTT assay	DTT assay	Clotting assay	Clotting assay
Warfarin	IC_{50}: 2.2 µM	K_i: 1.65 µM	K_i: 1.65 µM	IC_{50}: 1.9 nM	IC_{50}: 2.4 nM
Acenocoumarol	IC_{50}: 0.8 µM	K_i: 0.33 µM	K_i: 0.33 µM	IC_{50}: 1.5 nM	ND
Phenprocoumon	IC_{50}: 1.8 µM	ND	K_i: 0.72 µM	IC_{50}: 3.6 nM	ND
Fluindione	ND	K_i: 0.25 µM	K_i: 0.25 µM	IC_{50}: 4.8 nM	IC_{50}: 204 nM

Inhibitory data rely mostly on VKR activity, but data presented here were generated using K_1 as a substrate, i.e.VKOR activity was assessed. To complete the picture of VKOR enzyme inhibition, VKR activity was evaluated using warfarin and fluindinione (usage of K>O as substrate). In the cell-based assay, endogenous VKOR and VKR

activity of VKORC1 in *VKORC1L1* KO cells was equally inhibited by warfarin. However, fluindione showed heterogeneous results. Firstly, controversial to published data, fluindione was less potent on VKORC1 inhibition, regardless of K vitamer supplementation [103]. Secondly, IC_{50} values for VKR and VKOR activity differed by a factor of 40. On this issue only speculations can be made. It could be that the interaction between K>O and fluindione may lead to distinct inhibition profile. Or fluindione has different binding characteristics in the presence of K>O. Another possibility is that K>O accumulates in the ER membrane. However, no data is available to strengthen one of the aforementioned aspects. These data potentially explain the difficulty in stable treatment of patients with fluindione compared to coumarin-based drugs.

Clinical impact of VKOR enzyme inhibition

Oral anticoagulants are used to treat and prevent thromboembolic events. Anticoagulation status is measured by INR (international normalized ratio) which reflects the time required for clot formation based on prothrombin time. Patients are adjusted to an INR between 2 and 3, which mirrors about 20% residual activity of all VKD clotting factors that could be reflected by IC_{80} (Table 18). Calculations of this modified inhibitory constant revealed essentially similar ratio of VKORC1L1 to VKORC1 compared to IC_{50} values discussed before. Again, warfarin showed the highest discrepancy regarding 4-hydroxycoumarin derivatives. Indandiones are by far more effective in VKORC1 inhibition compared to VKORC1L1 as already seen in calculation of IC_{50} values.

Table 18: IC_{80} values reflecting patient's INR of 2-3.
Calculations based on inhibition curves generated for assessment of IC_{50} values.

Compound	IC_{80} (nM) for VKORC1	IC_{80} (nM) for VKORC1L1	Ratio VKORC1L1/ VKORC1
Warfarin	7.8	79	10
Acenocoumarol	3.9	21.7	6
Phenprocoumon	11	97	9
Phenindione	12	1187	99
Fluindione	19	1445	76

OACs have been used for more than six decades for long-term anticoagulation. One advantage is the experience of those drugs and its reversibility by vitamin K administration. The major disadvantage is the narrow therapeutic window leading to safety and efficacy issues. In addition, pharmacokinetic and pharmacogenetic factors influence the success of the therapy. Allelic variants of VKORC1 have an impact on dosing of OACs,

but no drug-specific variations have been reported [21, 67, 114]. Cytochrome P450 (CYP) is a group of hepatic microsomal enzymes which incorporates a hydroxyl group into substrate, to which drugs like OACs belong to. Thereby, lipophilic compounds are transformed to more hydrophilic metabolites being ready for elimination and renal excretion. CYP2C9 is the principal metabolzing enzyme of OACs. About 30 variants are known of which CYP2C9*2 and *3 are the most frequent allelic variants in the Caucasian population. Metabolism of warfarin and acenocoumarol by CYP2C9 depends on the enantiomer, drugs are admistered as racemic mixtures constisting of 50% of each enantiomer [69]. In general, S-enantiomers are more potent but are metabolized faster. Elimination of warfarin and acenocoumarol occurs almost completely by metabolism thus allelic variants of CYP450 have a higher effect. CYP2C9 does not play a major role in clearance of phenprocoumon because CYP3A4 is the key catalyst for metabolism and about 40% of this drug is excreted as parent compound [69]. In contrast to VKORC1 and CYP2C9 allelic variants of GGCX are not known to have an impact on coumarin anticoagulant dose finding [67].

Recently, many efforts have been made with regard to variability in *VKORC1* gene leading to distinct warfarin resistance types [21]. Dosing algorithms can predict the correct dose of OAC to omit under- or over-anticoagulation [115]. Of the OACs investigated acenocoumarol displays the shortest half-life of less than 10 hours [67]. Thus anticoagulation states below and above desired INR are frequently present with increased risk of bleeding and thrombosis during therapy. Data on IC_{50} values for VKORC1 revealed potency of acenocoumarol being as effective as warfarin. Warfarin and fluindione have medium-ranged half-lives of more than one day [67, 70]. The longest-acting clinically used agent is phenprocoumon with a half-life of more than 5 days. Those compounds showed IC_{50} for VKORC1 inhibition in low nanomolar range making them more favorable than acenocoumarol due to more predictable and stable anticoagulation.

Another enzyme of the vitamin K cycle

In the past few years, it became apparent that a third - yet unknown - enzyme can provide GGCX with KH_2 [102]. This enzyme catalyzes the reduction of K but not K>O (i.e. only VKR activity) which was shown independently by different groups [102, 116]. In the presence of 11 µM K_1, Tie and colleagues detected their γ-carboxylated reporter protein (fusion protein of FIX and protein C; FIXgla-PC) even in the presence of very high warfarin concentrations (up to 15 µM). This is in contrast to our results, because at 12 µM K_1 we obtained no measurable FIX activity in DKO cells (Figure 19). Only at

higher K_1 concentrations activity of the third enzyme was observed (e.g. 50 µM K_1) [116]. The existence of another enzyme with VKR activity is in complete agreement throughout the literature [102, 116]. The divergent results concerning K concentration needed to bypass the vitamin K cycle may arise from the different cell lines. Although cell lines used by Tie and our group have the same origin (human embryonic kidney cells), HEK 293T cells express a SV-40 antigen - to yield higher expression levels - whereas HEK 293 do not [90]. Multiple independent passages could have an impact on the genome structure and thus may influence the expression level of the third enzyme. Moreover, Tie and colleagues' measurement was based on γ-carboxylation meaning that even not fully carboxylated reporter protein was detected, too. In contrast, the assay used in this thesis the reporter protein (i.e. FIX) was measured only if the protein was fully carboxylated which might explain the different results, too.

To proof the impact of the third enzyme warfarin and fluindione were tested in *VKORC1* and *VKORC1L1* KO HEK 293T cells using K_1>O instead of K_1. Treatment with warfarin and 12 µM K_1>O showed similar IC_{50} values when compared with 12 µM K_1 supplementation. Non-compliant data were generated for fluindione when VKOR activity was assessed. Especially VKORC1 characteristics resulted in 40-fold higher fluindione requirement for inhibition, VKORC1L1's increased by a factor of 2. A clear explanation for these results cannot be provided, interaction of K_1>O and fluindione may be one.

Overall, activity of third enzyme can be excluded in the assay setup used. When assessing VKR activity (most of the data on endogenous VKOR activity were generated using K_1) the third enzyme may impact results on IC_{50} values giving higher values due to its coumarin insensitivity. By determination of VKOR activity, activity of third enzyme is absent and inhibition characteristics can solely be attributed to VKORC1 or VKORC1L1. Thus, if IC_{50} values were affected by the third enzyme during K_1 supplementation, values should be lower when assessing VKOR activity which was not the case for both compounds tested. Therefore, data on endogenous VKORC1 and VKORC1L1 inhibition can be specifically attributed to the enzyme investigated because the third enzyme was proven not to be active in the experimental setting used.

Impact of VKORC1L1 inhibition

Results from mouse studies highlighted the importance of *Vkorc1* in terms of blood coagulation. A constitutive knockout of *Vkorc1* led to postpartal death due to predominantely intrachranial hemorrhage and mice died two weeks after birth [31]. In addition, mice harboring one or two deleterious alleles showed significant reduction in the length of long bones [31]. Thus, Vkorc1 supplies Ggcx with co-factor in hepatic and extra-

hepatic cells. For further examination of Vkorc1 function in extrahepatic cells a mouse model will be helpful which lacks Vkorc1 expression in all cells beside liver. This can be accomplished by knocking in *Vkorc1* in liver cells (on top of constitutive *Vkorc1* knockout) or by using a liver-specific promoter which allows expression of *Vkorc1* in liver but no other cells. With this special approach mice should survive to adulthood and consequences of gene deletion in extrahepatic tissues can be observed. Data from constitutive Vkorc1 knockout already indicated an involvement in bone metabolism, which is plausible since osteocalcin and MGP are well known vitamin K dependent proteins with function in mineralization of bone.

The impact of VKORC1L1 inhibition *in vivo* is not known yet since it is still unclear if VKORC1L1 supports KH_2 generation for γ-carboxylation by GGCX *in vivo*. Results from mouse studies indicate that VKORC1L1 is not able to compensate lack of VKORC1 activity since bleeding phenotype in constitutive *Vkorc1*$^{-/-}$ was not rescued [31]. In liver, were coagulation factors are synthesized, *Vkorc1l1* expression is very low and not up-regulated in *Vkorc1*$^{-/-}$ mice [12, 33]. Assessment of VKOR activity in *Vkorc1*$^{-/-}$ liver microsomes showed markedly reduced activity (by 97%) compared to control [33]. Furthermore, *Vkorc1l1*$^{-/-}$ in osteoblasts revealed no difference in OCN levels compared to control mice [32]. Knockout of *Vkorc1l1* in murine osteoblasts did not have an effect on γ-carboxylation of OCN suggesting a minor role of Vkorc1l1 in this special cell type. Further studies are needed to elucidate the effect of *Vkorc1l1*$^{-/-}$ in other cells than liver and osteoblasts. In the second part of this section this issue will be discussed in more detail.

Inhibition of VKORC1 and VKORC1L1 by rodenticides and ferulenol

In the US more than 13,000 exposures to rodenticides (warfarin and related compounds) have been reported in 1996. The vast majority was unintended, however a small number (4%) was due to suicidal attempts.[3] In cases of clinically relevant poisoning, high dose maintenance K_1 therapy was needed to prevent fatal bleedings [71].

Rodenticides are long lasting coumarin derivatives and the second generation of rodenticides emerged due to cross-resistance to warfarin and other compounds of the first generation. The substitution of methyl group by long, phenyl side-chains yielded tremendous increase in potency and duration of action [74]. Data on half-life of rodenticides are sparsely available. It can be assumed that elimination is very slow (compared

[3] https://edis.ifas.ufl.edu/pi113, visited on 10-Feb-2018

to therapeutically used OACs) and half-life ranges between several weeks up to several months [117].

In contrast to rodenticides, ferulenol is naturally occurring with a much higher potency than coumarin (also naturally occurring). Ferulenol is plant-derived and found in Mediterranean area. The prenylated 4-hydroxycoumarin was reported to cause hemorrhagic symptoms (ferulosis) in mammals [118]. Intoxication can occur in cattle, sheep, pig and horse, in men ferulosis have been reported only sporadically [119].

Conclusive data on inhibitory potential of rodenticides with regard to VKOR enzymes are rare since most of the studies analyzed microsomes using the DTT-driven VKR/VKOR assay. Data presented here revealed that rodenticides appear to have high affinity for both VKORC1 and VKORC1L1, which is reflected by low discrepant measurement of both enzymes. In contrast, ferulenol showed enzyme specificity comparable to coumarin-based OACs, with VKORC1L1 being less sensitive to ferulenol treatment than VKORC1.

In previous studies different parameters (i.e. inhibitory constant k_i, half maximal inhibitory constant IC_{50}) were assessed (Table 19) [63, 112, 118, 120].

Table 19: Overview of published studies on VKOR inhibition of rodenticides and ferulenol. ND - not determined, k_i - inhibitory constant

	Monti *et al.*, 2007 [63]	**Gebauer 2007** [112]	**Hodroge *et al.*, 2011** [120]		**Louvet *et al.*, 2015** [118]
Expression system	BHK cells with stable FX expression	Rat liver microsomes	Rat liver microsomes	VKORC1 in *Pichia pastoris*	Rat liver microsomes
Warfarin	5 µM: 59 %	IC_{50}: 2.2 µM	k_i: 0.72 µM	k_i: 0.50 µM	k_i: 0.50 µM
Bromadiolone	ND	ND	k_i: 0.13 µM	k_i: 0.07 µM	ND
Brodifacoum	ND	IC_{50}: 0.15 µM	k_i: 0.04 µM	k_i: 0.03 µM	ND
Ferulenol	10 nM: 67 %	IC_{50}: 0.098 µM	ND	ND	k_i: 0.03 µM

The inhibitory constant K_i reflects the binding affinity, whereby half maximal inhibition constant IC_{50} mirrors the functional strength of the inhibitory drug. In the cell-based assay VKR/VKOR activity is measured indirectly which makes enzyme kinetic studies not suitable. In contrast, the DTT-driven VKOR assay allows determination of those parameters. Therefore, direct comparison is not applicable due to type of assay and biological material used. But values from warfarin can be related to other compounds and thus provide a basis for comparison of published results and data presented here.

Gebauer investigated brodifacoum and ferulenol, as well as warfarin in rat liver microsomes. In comparison to warfarin, brodifacoum was about 15-fold more potent [112]. Hodroge and colleagues tested warfarin, bromadiolone and brodifacoum in microsomes prepared from rat liver and *P. pastoris* after overexpresssion of VKORC1 [120]. Thereby, brodifacoum and bromadiolone were found to be more potent than warfarin when comparing the K_i values (~18 times vs. ~6 times, respectively). Data generated by Gebauer and Hodroge were similar with respect to brodifacoum yielding almost the same ratio to warfarin. In rat liver, VKORC1 is expected to be solely responsible for K recycling [33]. Therefore, inhibition values should be attributed to VKORC1, which would allow the comparison of the present data on VKORC1. In our assay, inhibition of endogenous VKORC1 revealed higher potential of brodifacoum (4-fold for VKORC1), but bromadiolone showed same inhibitory potential compared to warfarin (1.2-fold for VKORC1). With respect to VKORC1L1 inhibition, bromadiolone and brodifacoum had a 30 to 60-fold higher potency, which is not reflected by previous studies.

A French group described a 17- to 60-fold higher effect (depend on the species tested) on VKOR inhibition of ferulenol compared to warfarin [118]. Gebauer's data revealed a 22-higher potential of ferulenol to inhibit VKOR in the experimental setting. In the cell-based assay, VKORC1 required 2.5-fold less ferulenol compared to warfarin for half maximal inhibition. In contrast, VKORC1L1 needed only one eighth of warfarin concentration.

Monti and colleagues compared warfarin and ferulenol treatment by means of FX stable expressing baby hamster kidney (BHK) cells. They state that ferulenol was much more effective compared to warfarin (three orders of magnitude) [63]. However, since BHK and HEK 293T cell originate from kidney, the results are doubtful. They have shown that by warfarin treatment (5 µM) resulted in only 40% less FX carboxylation. In contrast, in HEK 293T cells FIX levels were reduced by more than 90% when treated with 1 µM warfarin. Values can vary between cell lines and experiment, but the range should be consistent.

Impact of antibiotics on coagulation

Since many years, antibiotics are used to treat bacterial infections. Drug-drug interactions influencing effectiveness are well known for oral contraceptives and alcohol and others. β-lactam antibiotics with MTT side chain are suspected to cause hypoprothrombinemia and platelet dysfunction [121]. Patients under antibiotic therapy showed prolongation of prothrombin time (PT) [122], however administration of cefamandole or moxalactam in healthy volunteers did not result in hypoprothrombinemia [123]. Antibiot-

ics can destruct the intestinal flora which was supposed to lead to hypoprothrombinemia because a source of vitamin K disappeared. In animals like rats or mice antbiotic treatment can influence vitamin K status due to coprophagy and vitamin K_2 produced by bacteria in gut may represent a dietary source. However, when rats were fed with vitamin K deficient diet they developed hypoprothrombinemia despite intact intestinal flora when coprophagy was prevented [124]. Thus vitamin K_2 produced by intestinal flora is not sufficiently absorbed and does not contribute to vitamin K status without a second gut passage [125]. Data from animal studies cannot be transferred to human beings due to absent coprophagy, an important dietary source of vitamin K in animals [126]. Therefore, predisposition to antibiotic-associated hypoprothrombinemia can be assumed as malnutrition, malabsorption, total parenteral feeding and decreased renal function [123, 126].

Therefore, a selection of antibiotics suspected to cause bleeding phenotype was tested in the cell-based FIX assay to determine the effect on VKOR enzymes by means of single KO cell lines. Cephalosporin C represents a β-lactam antibiotic without MTT side chain, whereby cefamandole and moxalactam belong to the same group of antibiotics containing MTT side chain. In the assay, antibiotic concentrations up to 125 µM were tested reflecting the maximum solubility of the compounds. Antibiotic containing MTT side chain was more effective on inhibition of γ-carboxylation of FIX when comparing cephalosporin C and cefamandole. But moxalactam (β-lactam antibiotic with MTT side chain) did not affect γ-carboxylation. Mitchell and colleagues studied rat liver microsomes and showed that neither moxalactam nor cefamandole inhibited carboxylation greater than 20%, whereby concentrations up to 2.5 mM were tested [127]. Thus, *in vitro* the bleeding phenotype of those antibiotics cannot be proven. It is assumed that MTT-containing cephalosporins are weak inhibitors of VKOR leading to the accumulation of K>O in plasma which is also seen in patients under warfarin therapy [123]. *In vivo*, hypoprothrombinemia is favored by low vitamin K status caused by malnutrition or decreased renal function [126]. In contrast, data presented here were generated with saturated concentration of vitamin K. MTT-containing antibiotics are proposed to be weak inhibitors for VKOR enzymes and vitamin K status *in vitro* may superimpose with inhibitory effect of antibiotic [123]. MTT is released from parent compound and this moiety (or its metabolite) was found to inhibit γ-carboxylation of glutamic acid with an IC_{50} value of 1 mM, but MTT levels in human are considerably lower (0.03 mM) [128].

Thus, the different levels of K *in vivo* and *in vitro* might explain the contrary results. Moreover, systemic effects like vitamin K status cannot be mirrored in cell culture.

In another experiment, the additive effect of β-lactam antibiotics and anticoagulation therapy was tested. Angaran and colleagues proved that cefamandole can have an

additive effect to warfarin leading to hypoprothrombinemia, whereby cefazolin's (cephalosporin without MTT side chain) potential is intermediate, and vancomycin (glycopeptide antibiotic) does not influence the risk at all [129]. Contrary data were published in 2005 when Holbrook *et al.* concluded that it is unlikely that cefamandole potentiate warfarin therapy, whereby ciprofloxacin, a fluoroquinolone antibiotic, is highly probable to affect warfarin treatment [130]. A more recent study found out that different classes of antibiotics can significantly increase INR when administered concomitant with warfarin [131]. *In vitro*, co-incubation of warfarin and different concentrations of cephalosporin C, cefamandole and moxalactam did not result in an additive effect. However, metabolism of warfarin and antibiotics is different *in vivo* since it is known that monooxygenases relevant for metabolism of warfarin and vitamin K are not expressed in HEK 293 cells [109]. MTT may be metabolized by Flavin-containing monooxygenase but expression level of this enzyme is not known in HEK cells [132]. In addition, the complexity of *in vivo* warfarin and antibiotic metabolism, their interaction among each other and potential reuptake of the metabolites by the gastrointestinal system cannot be modeled in this *in vitro* study. Thus, conclusions from *in vitro* data presented here can only be drawn with regard to direct inhibition of VKOR enzymes. Antibiotics tested in this experimental setting (with saturated K concentration) did not have any direct inhibitory effect on VKORC1 or VKORC1L1 since FIX activity was not reduced.

Identification of warfarin binding sites in VKORC1 and VKORC1L1

Investigation of different OACs in *VKORC1* KO and *VKORC1L1* KO HEK 293T cells revealed for most compounds different inhibition pattern whereby VKORC1 was more sensitive than VKORC1L1. To elucidate the molecular basis we had a closer look on the amino acid composition of both enzymes. For VKORC1 a 4TM structure is considered, however a 3TM structure is also under investigation (Figure 4) [21, 22, 133]. In contrast, the 4TM structure of VKORC1L1 is not subject of discussion (Figure 5) [10, 22, 34]. Overall, VKORC1 and VKORC1L1 are identical to 44% and similar to 68% with respect to amino acid composition (Figure 62) and this alignment provided the basis for further experiments.

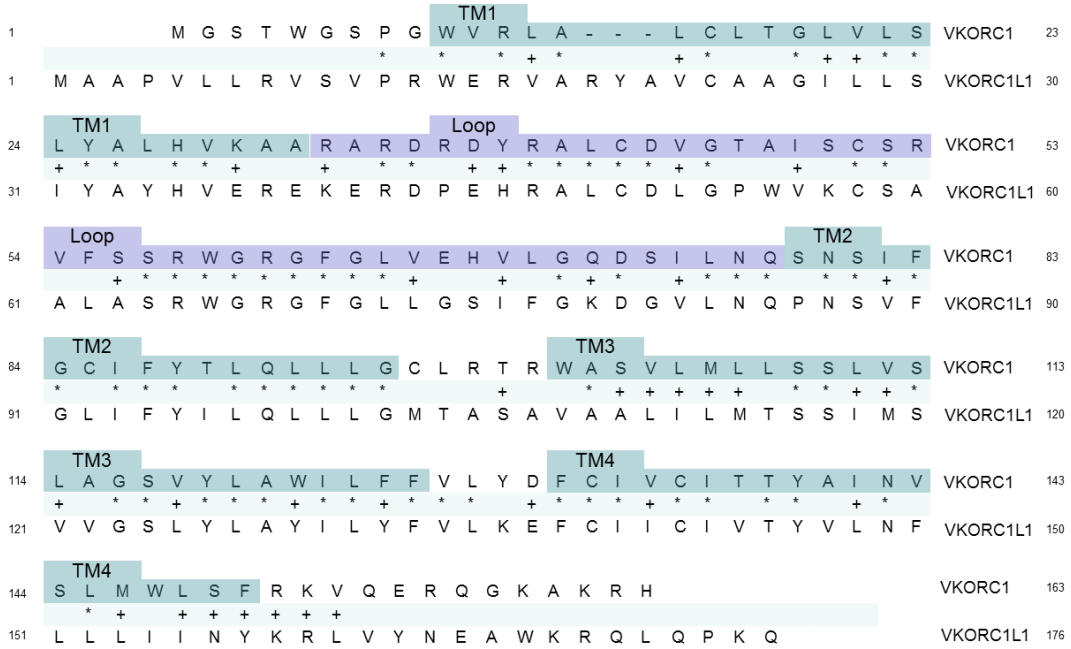

Figure 62: Human VKORC1 (NP_076869.1) protein sequence was aligned with sequence of human VKORC1L1 (NP_775788.2) using NCBI blast tool.
The transmembrane domains (TM1 to TM4) and the loop region of VKORC1 are marked. Asterisks indicate identical amino acids, plus sign represents amino acids with similar chemical properties.

In a first approach the loop of VKORC1L1 was swapped in *VKORC1* cDNA and *vice versa*. For warfarin and fluindione loop swap showed almost similar inhibition curves as their WT counterparts. This suggests that the loop is important (at least partially)and indicate that those amino acids are involved in drug binding. This is sustained by previously published *in silico* data on VKORC1, where three molecular surfaces for warfarin binding had been identified. Thereby, amino acids Ser52 to Phe55 located in the loop of VKORC1 belong to one of three contact surfaces with Phe55 forming hydrophobic interactions with warfarin (contact surface II) [21]. By sequence alignment, the amino acids Ser59 to Leu62 of VKORC1L1 correspond to the contact surface of VKORC1 (Ser52 to Phe55). Neither single mutation (VKORC1L1 Leu62Phe) nor complete swap of the four amino acids (Ser59 to Phe62) of VKORC1 contact surface II showed lower susceptibility to warfarin, which indicates that warfarin binding sites of VKORC1 and VKORC1L1 are different. By swapping particular amino acids of VKORC1 identified to be involved in warfarin binding in VKORC1L1, we expected to approximate VKORC1L1 variant to VKORC1 WT inhibition pattern, but the opposite was the case.

In silico analysis of both enzymes revealed three distinct arginine residues to stabilize warfarin binding by their positive charge but do not necessarily align to the same amino acid of the counterpart (Figure 63). However, for none of the predicted arginine resi-

dues in VKORC1 the corresponding amino in VKORC1L1 acid was predicted to be involved in warfarin binding.

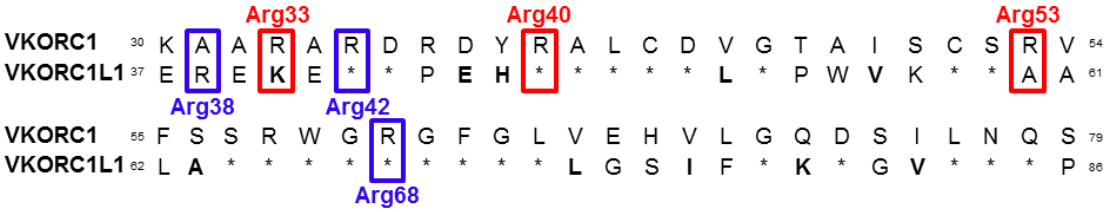

Figure 63: Alignment of VKORC1 (amino acids 30 to 79) with VKORC1L1 (amino acids 37 to 86).
Star indicates identical amino acids, bold letters represent amino acids with similar chemical properties. Red box indicate arginines in VKORC1 expected to be involved in warfarin binding; blue box represents arginines in VKORC1L1.

Mutation of selected amino acids (Phe55, Arg33, Arg40 and Arg53) proved the *in silico* model of VKORC1. Whereby Phe55Ala showed a complete resistance, mutated arginine residues shifted warfarin dose-responses to higher requirement for half-maximal inhibition.

In silico analysis of VKORC1L1 revealed three putative arginines at amino acid positions 38, 42 and 68 to be involved in warfarin binding. Substitution of two arginines (*VKORC1L1* R38E+R42E) yielded eight-fold higher IC_{50} value of warfarin compared to *VKORC1L1* WT. The triple mutant *VKORC1L1* R38E+R42E+R68E showed even complete resistance to warfarin, whereby concentrations up to 5 µM were used. Therefore, *in silico* docking analysis was confirmed by inhibition data revealing resistance for the potential amino acids being involved in warfarin binding on VKORC1L1.

Thus warfarin binding takes place in different regions of the loop in VKORC1 and VKORC1L1 and therefore might explain the different affinities of OACs on VKORC1 and VKORC1L1 enzyme (Figure 64). Since almost all OACs bear a negative charge, this is of great consequence for their comparative binding. While in VKORC1 these arginines cluster around the hydrophobic pocket close to a short helix formed in the cytoplasmic loop (residues Arg33, Arg40 and Arg53 in VKORC1 as mentioned above), in the case of VKORC1L1 they occur around a region which is on the opposite site of this short helix (Arg38, Arg42 and Arg68).

Moreover, in VKORC1L1 no amino acids were identified to form hydrogen bonds or phi-phi interactions to warfarin as shown for VKORC1 (Phe55) which might explain the reduced sensitivity of VKORC1L1 towards OACs compared to VKORC1.

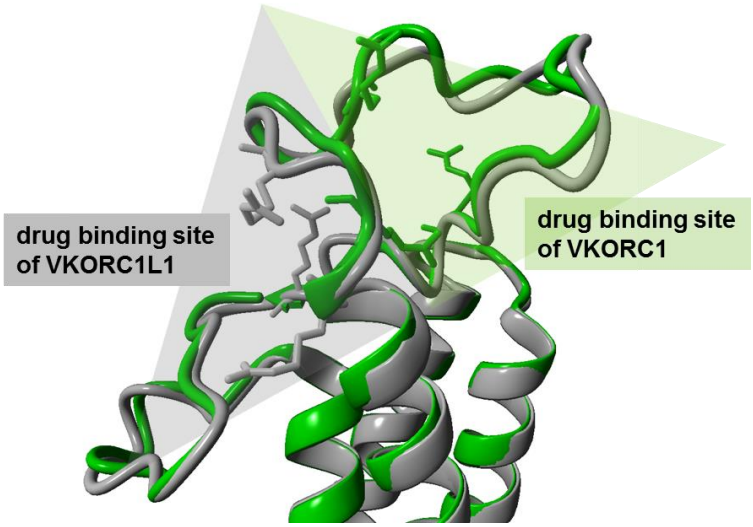

Figure 64: Comparative binding poses for warfarin on VKORC1 and VKORC1L1.
The structural alignment of the hVKORC1 and hVKORC1L1 models is shown. The backbone of hVKORC1 and hVKORC1L1 are depicted in green and blue colored ribbon format, respectively. The arginine residues clustered around the favored warfarin binding site of each model are depicted in stick format.

Future perspectives of these results

For many decades, warfarin has been the drug of choice for prevention and long-term treatment of arterial and venous thromboembolism [60]. OAC treatment is safe, cheap and effective when the patient is stable anticoagulized (i.e. a high time in therapeutic range is achieved). INR adjustment is challenging in the context of drug and food interactions and liver disease, resulting in either undertreatment (with an increased risk of thromboembolism) or overtreatment (leading to bleeding). In the past few years, new drugs for oral anticoagulation - known as direct oral anticoagulants (DOACs) - had been approved for antithrombotic therapy. These DOACs (direct thrombin inhibitors (e.g. dabigatran) or direct factor Xa inhibitors (e.g. rivaroxaban)) produce a more predictable, less labile anticoagulant effect and have been shown to be at least as safe and effective as warfarin in stroke prevention in atrial fibrillation [134]. However, disadvantages for DOAC treatment are present especially in terms of reversing anticoagulation therapy in emergency cases (antidot is available only for one drug) and special precaution should be taken for patients with renal impairment [134].

OAC treatment reduces the risk of recurring arterial and venous thrombosis by affecting carboxylation of VKD coagulation factors. A major side effect of long term OAC treatment is vascular calcification, a thightly regulated process in which vascular cells and VKD proteins are involved [135]. Vascular calcification is associated with an increased risk of cardiovascular disease [136]. MGP is the most potent inhibitor of vascu-

lar calcification which is highlighted by animal studies. $MGP^{-/-}$ mice died some 8 weeks after birth due to calcification and subsequent rupture of medium and large arterial vessels [48]. OAC treatment thus leads to reduced γ-carboxylated (undercarboxylated) MGP levels. Another vitamin K dependent protein with regultatory properties is GRP which has, like MGP, calcium-binding properties and thus is assumed to be an inhibitor of vascular calcification [49]. However, knockout studies in mice revealed no pathological effect suggesting a minor importance than MGP in terms of calcification [137].

Several studies showed an impact on vitamin K status and vascular calcification, whereby K_2 is advantageous over K_1. Tissue specific K_1 accumulation in liver has been shown in rats which were fed with equal amounts of K_1 and MK-4. In contrast, MK-4 accumulated in non-hepatic tissues like arterial vessel wall [138]. To overcome side effects of OAC treatment in extra-hepatic tissues supplementation of K_2 may be of importance. Observational studies have shown an inverse relationship between high vitamin K (mainly menaquinones) intake and coronary calcification or risk of cardiovascular disease [5]. Furthermore, a systematic review and meta-analysis revealed that high pharmacological doses of MK-4 had beneficial effects on bone parameters [139]. However, health benefits of supplementation of vitamin K is still under debate and depend on the cohorts under investigation [140]. Of note, excess intake of vitamin K does not result in thrombosis even when taking supraphysiological doses [141]. Indeed, vitamin K supplementation interferes with OAC treatment, but data suggest that K_2 supplementation should have minor effect on carboxylation of clotting factors with normal carboxylation status of extra-hepatic VKD proteins like MGP or OCN. Furthermore, vitamin K supplementation in healthy people may have a positive effect on bone health and vasculature.

Due to different inhibition pattern of warfarin, acenocumarol, phenprocoumon and fluindione one would expect different extent of treatment on extrahepatic VKD proteins. Based on the assumption – but data to support or withdraw this hypothesis is missing - that VKORC1L1 is capable of providing GGCX with KH_2 *in vivo*, fluindione may be the drug of choice because of the distinct inhibition pattern. Theoretically, at a given dose VKORC1 is inhibited by 50% whereas VKORC1L1 is not affected at all meaning normal carboxylation of (extrahepatic?) VKD proteins. In liver, VKORC1 is the major enzyme responsible for vitamin K recycling, VKORC1L1 does not play a role in this particular tissue. This study also demonstrated that anticoagulation with fluindione might be difficult due to different inhibition pattern using different substrates (K *vs.* K>O). In this light, warfarin might be the “best” OAC to achieve stable anticoagulation irrespective of the substrate and comparably low VKORC1L1 inhibition. However, studies addressing the long term effect of different OACs on extra-hepatic tissues are lacking.

5.2 Generation of *Vkorc1l1* KO mice

Generation of transgenic mice is used intensively in research and allows studying of gene function in a model organism. In a constitutive KO, the gene function is absent in every cell. However, in 15% of KO mice, the severity of the phenotype (i.e. developmental lethality) precludes the analysis of the gene's impact [142]. Therefore, Cre/loxP technology was introduced to generate conditional KO [143, 144].

Cyclization recombination of bacteriophage P1 (abbreviated as Cre) catalyzes the recombination between two loxP (locus of X over P1) sites independent of additional cofactors (Figure 65). The loxP site is a 34 bp nucleotide sequence that can be genetically targeted around an essential exon in a gene [145].

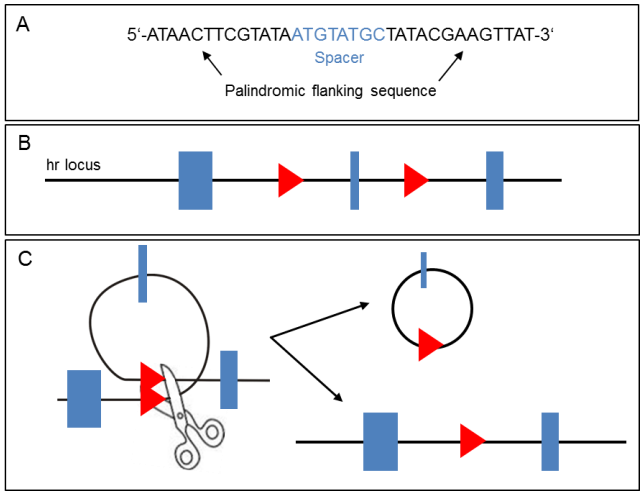

Figure 65: Cre/loxP system to generate constitutional or conditional KO mice.
A: LoxP site is characterized by 13 bp palindromic sequences separated by a 8 bp spacer. B: The homologous recombination (hr) locus is characterized by the integration of two loxP sites flanking exon of the target gene. C: Cre binds to loxP sites and cuts at both loxP sites. During this process, gene fragment flanked by loxP sites is removed and recombination yields deletion of the respective exon. Dependent on the orientation of loxP sites, insertions and translocations can be generated (not shown).

Conventionally, mice are generated by means of homologous recombination using embryonic stem (ES) cells. Thereby, a vector harboring the desired modification including loxP sites is used to manipulate ES cells. Targeted ES cells are then injected into blastocysts and subsequently transferred to the uterus of a recipient mouse which will act as a surrogate mother. Pups are called chimeras characterized by different coat colors (e.g. black and brown). The chimeric pubs are bred with WT mice to check if modified ES cells have contributed to the germline of the chimera. Overall, the procedure is time and lab consuming. Furthermore, additional time is needed due to extensive mating with WT mice for seven to ten generations in order to avoid strain specific bias. This is

due to the requirement of different strains of ES cells and blastocysts to identify chimeric mice.

In contrast, CRISPR/Cas9-mediated genome engineering provides a straight forward technique to generate transgenic mice. Extensive cloning and maintenance of ES cells can be slipped. The components of CRISPR/Cas9 were injected into oocytes at pronucleus state and lab-intensive steps as described above can be omitted. In addition, extensive backcrossing as described above is not required. By means of this technique, constitutive as well as conditional KO can be generated [89, 146]. Our approach was to generate floxed mice in order to allow mouse study in case of lethal phenotype of constitutive KO. As shown in Table 9 a deletion of exon 2 and adjacent region was obtained, but integration of loxP sites failed. Other groups were more successful. Lobocka and colleagues reported the integration of two loxP sites in one allele was successful and 15% of pubs showed floxed target gene in heterozygous state [147]. The reason for failure of integration of loxP sites in *Vkorc1l1* locus may be multi-faceted. One answer may lie in the gene itself. *Vkorc1l1* is a small gene harboring only three exons which restricts selection and design of sgRNAs. Furthermore, the intronic sequence between exon 1 and 2 is large (36 kb) which may have an impact on the success of process. Secondly, the reason may lie in the gRNA, which can be optimized in terms of length. A group from China generated KO mice by targeting exon 2 of FVII with gRNAs which differed in length. They yielded 23% and 54% mutation frequency for normal gRNA (20 nt) and truncated gRNA (17-18 nt), respectively. Even homozygous KO was obtained. The variations they detected included substitutions, deletions (2-167 nt), and insertions (1-13 nt) [148]. However, constitutive *Vkorc1l1* KO was not lethal and the necessity for generation of floxed gene does no longer exist.

During any manipulation on genetic material non-desired, so-called off-target, effects can be generated. Thereby insertion, deletions or substitutions can occur at a site different from target. Fu and colleagues targeted eGFP in U2OS.EGFP cells (human bone osteosarcoma epithelial cell line expressing a fluorescent protein) at three different positions and found out that for optimal effect different amounts of sgRNA-/Cas9-expressing plasmids were required for the three target sites within the same gene. Furthermore, they tested six sgRNAs in four different genes in U2OS.EGFP cells with regard to their off-target effects. Whereas three target genes showed only one or even no off-target, gRNA for vascular endothelial growth factor A revealed multiple off-targets, most of them concerned protein-coding regions [149]. Such dramatic consequences of manipulation are not desired and the occurrence cannot be predicted. Nevertheless, in mice occurred off-targets can be washed out by certain cycles of breeding and backcrossing.

Compared to the conventional approach, mice were generated in much shorter time. As shown in Table 8, generation of *Vkorc1l1* KO mouse was successful in four mice, but one mouse (founder mouse #22) was not transmitting the deleterious allele to germ line. For establishment of *Vkorc1l1* KO stock founder mouse #17 was selected. This mouse showed a deletion of 1.2 kb, expression of *Vkorc1l1* should be completely omitted in homozygous state. To proof this mRNA expression was quantified using real-time PCR. Analysis revealed, irrespective if RNA or cDNA was used as a template, amplification of template even in homozygous *Vkorc1l1* KO. The probe was designed to bind exon 1/2 boundary and should not give any amplification in homozygous *Vkorc1l1* KO. By database search it became apparent that the reason for amplicons in qPCR in homozygous *Vkorc1l1* KO samples may be due to a “processed pseudogene” [150]. Processed pseudogenes arise by integration of transcribed mRNA of the parent gene at a new locus in the genome.

The alignment of the *Vkorc1l1* mRNA (NM_027121.4, 4935 bp) with the murine genome resulted in a match with 99% identity over more than 1 kb including the cDNA sequence of *Vkorc1l1* (i.e. from start to stop codon) (Figure 66). Only at three positions nucleotide exchange was observed, one substitution in the coding region (c.468T>C) and two substitutions in 3‘UTR (c.531+1T>C and c.531+11A>G, respectively).

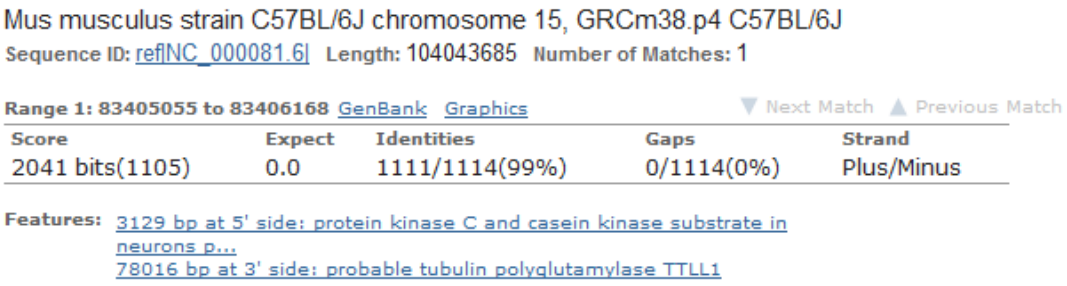

Figure 66: Screenshot of alignment of *Vkorc1l1* mRNA to the murine genomic sequence by using BLAST.
A part of the mRNA (1114 bp) was also found on chromosome 15 (NC_000081.6). Database search was assessed on 07-Jul-2018.

In order to verify the hypothesis of processed pseudogene primers binding at start and stop of *Vkorc1l1* cDNA were used for amplification of gDNA. A product of the expected size was generated, sequencing revealed single base substitution at c.468T>C (Figure 47 and Figure 48). On the basis of these results we concluded that amplification in qPCR in KO samples was due to contamination of RNA sample with gDNA.

Studies on protein level failed due to appropriate antibody against *Vkorc1l1* which would represent the ultimate proof of the absence of Vkorc1l1 protein. Another possibil-

ity to verify *Vkorc1l1* KO could be done on RNA level by means of a Northern Blot. After size separation RNA is blotted on a membrane and incubated with DNA probes which allow detection of RNA-DNA hybrids. However, based on RNA and DNA analysis presented here *Vkorc1l1* KO mice were considered to lack endogenous expression of Vkorc1l1 protein in mice constitutively.

Phenotypic screen of *Vkorc1l1* KO mice

As described before, generation of the KO mice was sucessful and *Vkorc1l1* KO mice did not show lethal phenotype as seen with *Vkorc1* KO [31]. For phenotypic analysis the cohort of founder mouse #17 was expanded. In cooperation with German Mouse Clinic (GMC) *Vkorc1l1* KO phenotype was examined [151]. GMC was founded in 2001 being the first facility worldwide with open access for the scientific community and developed a large scale of comprehensive and standardized phenotypic check-up with more than 550 parameters. The screens are designated to the areas of behavior, bone and cartilage development, neurology, clinical chemistry, eye development, immunology, allergy, steroid metabolism, energy metabolism, lung function, vision and pain perception, molecular phenotyping, cardiovascular analyses and pathology[4]. In December 2016, mating of *Vkorc1l1*$^{+/-}$ mice was started to obtain *Vkorc1l1*$^{-/-}$ mice and respective control animals (*Vkorc1l1*$^{+/+}$ mice). At age of 7 weeks mice were sent to GMC facility, characterization started after two weeks of acclimatization period. An overview and time scale of the screen is depicted in Figure 17.

The first and most impressive result of the screen was that mutant mice weighed less compared to their wild type littermates. This observation was consistent throughout the screen over more than 12 weeks.

Secondly, *Vkorc1l1* KO mice showed differences in behaviour when compared to their WT littermates. In the open field – a measure of spontaneous reactions to a novel environment – *Vkorc1l1*$^{-/-}$ mice showed increased locomotor activity and speed along with decreased time spent in center. These results indicate that the knockout mice are slightly hyperactive when confronted with a mildy stressful situation. In addition, the results point to heightened anxiety. Results from PPI suggested deficits in sensorimotor gating, which is largely regulated by neuronal connections between different brain regions. However, further examination is needed to resolve the impact of Vkorc1l1 in terms of behavioral changes observed during the phenotypic screen. A first hint can be provided when the *Vkorc1l1* expression pattern in different brain regions is elucidated.

[4] https://www.mouseclinic.de/about-gmc/general/index.html, visited on 29-Sep-2017

As mentioned already, antibodies binding specifically to Vkorc1 or Vkorc1l1 proteins are to date not available. However, this issue could be resolved using advanced approaches like *in situ* hybridization, Vkorc1l1-specific aptamers or transgenic mice harboring fluorescence protein N- or C-terminal fused to Vkorc1l1. Information for Vkorc1l1 expression pattern, especially with regards to Vkorc1, could be meaningful in terms of specific enzyme function.

The correlation between vitamin K and sphingolipids was initially demonstrated in bacteria, where it was found to be essential to cell membrane structure synthesis by induction of a specific enzyme (3-ketodihydrosphingosine (3-KDS) synthase) which is involved in the initial step of sphingolipid biosynthesis [152]. Earlier findings were then confirmed in rodents, thus warfarin treatment was associated with decreased 3-KDS synthase activity and significant reductions in brain sulfatides, sphingomyelin and cerebrosides. Warfarin-induced alterations in sphingolipid synthesis could be reversed by subsequent administration of vitamin K [153]. Vitamin K in the brain occurs predominantly as MK-4 (K_2 derivative), anatomically distributed in all brain regions, although concentrations differed according to regions [154]. Sphingolipids are important for cellular events such as proliferation, differentiation, senescence, cell–cell interaction, and transformation. Furthermore, they have been linked to alterations in aging processes and neurodegenerative disorders such as Alzheimer's and Parkinson's disease.

Vkorc1l1 KO mice were different compared to WT mice, thus suggesting that Vkorc1l1 does play a role in brain function. Indeed, in the neurological screen *Vkorc1l1* KO mice showed increased locomotor activity. Increased body tone and hyperactivity could be an indicator of neuronal hyperexcitability. This could be due to either reduced inhibitory or increased excitatory signaling, which is also involved in epilepsy disorders.

Knowledge of *Vkorc1l1* expresion *in vivo* is currently restricted to mRNA expression profile assessed in different tissues [12]. It was shown that *Vkorc1l1* is uniformely expressed with highest level in brain suggesting an important function in this organ. To date, special brain regions of *Vkorc1l1* expression have not been identified and further experiments are needed to clearify the function of Vkorc1l1 (especially in the context of its paralog Vkorc1) in brain. Years ago it was shown that vitamin K intake have an impact on sphingolipid biosynthesis (which is dependent on warfarin treatment) [153]. One explanation is that in brain or more precisely in distinct brain regions yet unknown VKD proteins are involved in sphingolipid metabolism which are dependent on γ-carboxylation for proper function. Another possibility is that enzymes or enzyme complexes are dependent on KH_2 but do not need to be γ-carboxylated.

The analysis of clinical chemistry revealed some deviations compared to control mice. Marked effects on body weight as well as plasma lipid concentrations in both, fasting and the *ad libitum* fed state suggest that the *Vkorc1l1* knockout affects energy metabolism with a predominat effect on lipid metabolism. In addition, glucose metabolism appeared slightly altered as well. *Vkorc1l1*$^{-/-}$ mice showed lowered glucose levels and a reduced body fat mass compared to their *Vkorc1l1*$^{+/+}$ littermates, which might be an indicator of disturbed energy metabolism. In men insufficient supply with carbohydrates leads to low glucose plasma level [155]. Enhanced protein catabolism may also induce lowered body weight, and could also be due to insufficient supply of carbohydrates and thus may induce increased urea concentration in plasma [155, 156]. Morevover, increased liver parameters (i.e. AST and LDH, but not ALT) were detected which could indicate muscle or erythrocyte damage. Elevated levels of sodium and chloride may be due to loss of body fluid balance. Increased concentration of potassium and urea may be an indicator of kidney dysfunction. Indeed, not all parameters were significantly increased thus interpretation is difficult. Furthermore, the morphological screen did not yield any pathological findings during histological examination. Overall, a clear picture of liver dysfunction or renal impairment was not observed. Remarkable is the clear sexual dimorphism observed in many parameters during the phenotypic screen, hence in most cases females were more affected.

Age-related phenotype of *Vkorc1l1*$^{-/-}$ mice

Aging and antioxidative defense mechanisms are closely connected. Aging affects all cells and not one tissue is directly responsible for aging which makes research difficult. Several knockout mouse models have been generated to elucidate the function of a protein in terms of antioxidation and aging. Glutathione peroxidases (GPx) and superoxide dismutases (SOD) are enzymes which scavenge ROS. Manganese superoxide dismutase (MnSOD) is encoded by *Sod-2* and located in the mitochondrial matrix, where it is the only scavenger. Homozygous *Sod-2* KO showed a lethal phenotype and mice died shortly after birth [157]. In heterozygous state enzyme activity was sufficient under normal metabolism, but pathophysiological conditions caused elevated mitochondrial superoxide production [158]. Mice in which *Sod-1*, *Sod-3*, and *GPx1* genes were deleted appeared to be viable. Cupper zinc superoxide dismutase (CuZnSOD), encoded by *Sod-1*, is located in the cytoplasm and mitochondrial intermembrane space. Homozygous *Sod-1* KO mice showed accelerated age-dependent pathologies and a rapid, age-dependent decline in fertility in female [159]. Thus, knockout of a single gene can have a tremendous effect on viability, life span and fertility in mouse model. Phenotypic screen of our *Vkorc1l1*$^{-/-}$ mice did not show any abnormalities in

terms of viability and fertility. Characterization of an age-related phenotype can provide a better understanding of function of Vkorc1l1 *in vivo* in terms of aging.

Future perspectives based on these results

Vkorc1l1 KO mice provide a fundamental basis for further research of Vkorc1l1 protein function *in vivo*. Knowing that *Vkorc1l1* KO is not lethal constitutes a great step forward because it suggests that even if Vkorc1 and Vkorc1l1 are isozymes both enzymes have different tasks most probably due to their tissue distribution. On the basis of mRNA expression studies this suggestion is substantiated having highest *Vkorc1* expression in liver and high mRNA levels of *Vkorc1l1* in whole brain [12]. An important outcome of the phenotypic screen was that *Vkorc1l1* KO mice were lighter than their WT littermates. In addition, *Vkorc1l1* KO mice showed different behaviour and energy metabolism with a predominat effect on lipid metabolism. Further experiements are required to explore the effect of *Vkorc1l1* KO in detail.

In vitro data suggest that Vkorc1l1 is involved in aging processes because it is speculated that the enzyme has a function in scavenging ROS. Indeed, it was shown that *VKORC1L1* mRNA is upregulated when HEK 293T cells were treated with 75 µM H_2O_2 (peak after 40 min), whereby *VKORC1* mRNA stayed constant [10]. Hence, it would be meaningful to screen aged *Vkorc1l1*$^{-/-}$ mice to strengthen this hypothesis.

However, one major issue remains: both VK OR enzymes can reduce K and K>O to provide KH_2 as a potent antioxidant [96]. To investigate the impact of KH_2 in antioxidation and aging processes the source of KH_2 needs to be eliminated thus both enzymes must be silenced (although *Vkorc1l1* mRNA is highest in brain minor *Vkorc1* mRNA expression was detected, too) [12]. But due to the lethal phenotype of *Vkorc1*$^{-/-}$ one would expect that *Vkorc1*/*Vkorc1l1* double KO mice are lethal postpartum or even die *in utero*. By tissue- or cell-specific *Vkorc1*$^{-/-}$ using Cre/loxP system lethal effects of constitutional *Vkorc1*$^{-/-}$ can be omitted. Another possibility is to knock-in *Vkorc1* specifically in liver in a constitutional *Vkorc1*$^{-/-}$ mouse and generate *Vkorc1*/*Vkorc1l1* double KO mice without a bleeding phenotype. This would allow to evaluate the effect of KH_2 absence on antioxidation and aging processes *in vivo*. However, results of these mice studies may be confounded due to the third yet unknown enzyme which can reduce K to KH_2 [102, 116]. Because the enzyme is still unknown one cannot guess for tissue distrubution and expression level especially in brain.

6 References

1. Dam H. Vitamin K, its discovery, biochemistry and application in medicine. J Mt Sinai Hosp N Y. 1946;12:961–70.

2. Dam H. The antihaemorrhagic vitamin of the chick. Biochem J. 1935;29:1273–85.

3. Booth SL. Roles for vitamin K beyond coagulation. Annu Rev Nutr. 2009;29:89–110. doi:10.1146/annurev-nutr-080508-141217.

4. Booth SL. Vitamin K: food composition and dietary intakes. Food Nutr Res 2012. doi:10.3402/fnr.v56i0.5505.

5. Beulens JWJ, Booth SL, van den Heuvel, Ellen G H M, Stoecklin E, Baka A, Vermeer C. The role of menaquinones (vitamin K(2)) in human health. Br J Nutr. 2013;110:1357–68. doi:10.1017/S0007114513001013.

6. Shearer MJ. Vitamin K deficiency bleeding (VKDB) in early infancy. Blood Rev. 2009;23:49–59. doi:10.1016/j.blre.2008.06.001.

7. Nakagawa K, Hirota Y, Sawada N, Yuge N, Watanabe M, Uchino Y, et al. Identification of UBIAD1 as a novel human menaquinone-4 biosynthetic enzyme. Nature. 2010;468:117–21. doi:10.1038/nature09464.

8. Oldenburg J, Bevans CG, Muller CR, Watzka M. Vitamin K epoxide reductase complex subunit 1 (VKORC1): the key protein of the vitamin K cycle. Antioxid Redox Signal. 2006;8:347–53. doi:10.1089/ars.2006.8.347.

9. Tie J-K, Jin D-Y, Tie K, Stafford DW. Evaluation of warfarin resistance using transcription activator-like effector nucleases-mediated vitamin K epoxide reductase knockout HEK293 cells. J Thromb Haemost. 2013;11:1556–64. doi:10.1111/jth.12306.

10. Westhofen P, Watzka M, Marinova M, Hass M, Kirfel G, Muller J, et al. Human vitamin K 2,3-epoxide reductase complex subunit 1-like 1 (VKORC1L1) mediates vitamin K-dependent intracellular antioxidant function. J Biol Chem. 2011;286:15085–94. doi:10.1074/jbc.M110.210971.

11. Gong X, Gutala R, Jaiswal AK. Quinone oxidoreductases and vitamin K metabolism. Vitam Horm. 2008;78:85–101. doi:10.1016/S0083-6729(07)00005-2.

12. Caspers M, Czogalla KJ, Liphardt K, Muller J, Westhofen P, Watzka M, Oldenburg J. Two enzymes catalyze vitamin K 2,3-epoxide reductase activity in mouse: VKORC1 is highly expressed in exocrine tissues while VKORC1L1 is highly expressed in brain. Thromb Res. 2015;135:977–83. doi:10.1016/j.thromres.2015.01.025.

13. Friedman PA, Shia MA, Gallop PM, Griep AE. Vitamin K-dependent gamma-carbon-hydrogen bond cleavage and nonmandatory concurrent carboxylation of peptide-bound glutamic acid residues. Proc Natl Acad Sci U S A. 1979;76:3126–9.

14. Larson AE, Friedman PA, Suttie JW. Vitamin K-dependent carboxylase. Stoichiometry of carboxylation and vitamin K 2,3-epoxide formation. J Biol Chem. 1981;256:11032–5.

15. Stafford DW. The vitamin K cycle. J Thromb Haemost. 2005;3:1873–8. doi:10.1111/j.1538-7836.2005.01419.x.

16. Zhu A, Sun H, Raymond RM, JR, Furie BC, Furie B, Bronstein M, et al. Fatal hemorrhage in mice lacking gamma-glutamyl carboxylase. Blood. 2007;109:5270–5. doi:10.1182/blood-2006-12-064188.

17. Rost S, Fregin A, Ivaskevicius V, Conzelmann E, Hortnagel K, Pelz H-J, et al. Mutations in VKORC1 cause warfarin resistance and multiple coagulation factor deficiency type 2. Nature. 2004;427:537–41. doi:10.1038/nature02214.

18. Li T, Chang C-Y, Jin D-Y, Lin P-J, Khvorova A, Stafford DW. Identification of the gene for vitamin K epoxide reductase. Nature. 2004;427:541–4. doi:10.1038/nature02254.

19. Li W, Schulman S, Dutton RJ, Boyd D, Beckwith J, Rapoport TA. Structure of a bacterial homologue of vitamin K epoxide reductase. Nature. 2010;463:507–12. doi:10.1038/nature08720.

20. Tie J-K, Nicchitta C, Heijne G von, Stafford DW. Membrane topology mapping of vitamin K epoxide reductase by in vitro translation/cotranslocation. J Biol Chem. 2005;280:16410–6. doi:10.1074/jbc.M500765200.

21. Czogalla KJ, Biswas A, Wendeln A-C, Westhofen P, Muller CR, Watzka M, Oldenburg J. Human VKORC1 mutations cause variable degrees of 4-hydroxycoumarin resistance and affect putative warfarin binding interfaces. Blood. 2013;122:2743–50. doi:10.1182/blood-2013-05-501692.

22. Cao Z, van Lith M, Mitchell LJ, Pringle MA, Inaba K, Bulleid NJ. The Membrane Topology of Vitamin K Epoxide Reductase is conserved between Human Isoforms and the Bacterial Enzyme. Biochem J 2016. doi:10.1042/BJ20151223.

23. Czogalla KJ, Watzka M, Oldenburg J. Structural Modeling Insights into Human VKORC1 Phenotypes. Nutrients. 2015;7:6837–51. doi:10.3390/nu7085313.

24. Goodstadt L, Ponting CP. Vitamin K epoxide reductase: homology, active site and catalytic mechanism. Trends Biochem Sci. 2004;29:289–92. doi:10.1016/j.tibs.2004.04.004.

25. Jin D-Y, Tie J-K, Stafford DW. The conversion of vitamin K epoxide to vitamin K quinone and vitamin K quinone to vitamin K hydroquinone uses the same active site cysteines. Biochemistry. 2007;46:7279–83. doi:10.1021/bi700527j.

26. Rishavy MA, Usubalieva A, Hallgren KW, Berkner KL. Novel insight into the mechanism of the vitamin K oxidoreductase (VKOR): electron relay through Cys43 and Cys51 reduces VKOR to allow vitamin K reduction and facilitation of vitamin K-dependent protein carboxylation. J Biol Chem. 2011;286:7267–78. doi:10.1074/jbc.M110.172213.

27. Pelz H-J, Rost S, Hunerberg M, Fregin A, Heiberg A-C, Baert K, et al. The genetic basis of resistance to anticoagulants in rodents. Genetics. 2005;170:1839–47. doi:10.1534/genetics.104.040360.

28. Marinova M, Lutjohann D, Breuer O, Kolsch H, Westhofen P, Watzka M, et al. VKORC1-dependent pharmacokinetics of intravenous and oral phylloquinone (vitamin

K1) mixed micelles formulation. Eur J Clin Pharmacol. 2013;69:467–75. doi:10.1007/s00228-012-1362-y.

29. Watzka M, Geisen C, Bevans CG, Sittinger K, Spohn G, Rost S, et al. Thirteen novel VKORC1 mutations associated with oral anticoagulant resistance: insights into improved patient diagnosis and treatment. J Thromb Haemost. 2011;9:109–18. doi:10.1111/j.1538-7836.2010.04095.x.

30. Fregin A, Czogalla KJ, Gansler J, Rost S, Taverna M, Watzka M, et al. A new cell culture-based assay quantifies vitamin K 2,3-epoxide reductase complex subunit 1 function and reveals warfarin resistance phenotypes not shown by the dithiothreitol-driven VKOR assay. J Thromb Haemost. 2013;11:872–80. doi:10.1111/jth.12185.

31. Spohn G, Kleinridders A, Wunderlich FT, Watzka M, Zaucke F, Blumbach K, et al. VKORC1 deficiency in mice causes early postnatal lethality due to severe bleeding. Thromb Haemost 2009. doi:10.1160/TH09-03-0204.

32. Ferron M, Lacombe J, Germain A, Oury F, Karsenty G. GGCX and VKORC1 inhibit osteocalcin endocrine functions. J Cell Biol. 2015;208:761–76. doi:10.1083/jcb.201409111.

33. Hammed A, Matagrin B, Spohn G, Prouillac C, Benoit E, Lattard V. VKORC1L1, an enzyme rescuing the vitamin K 2,3-epoxide reductase activity in some extrahepatic tissues during anticoagulation therapy. J Biol Chem. 2013;288:28733–42. doi:10.1074/jbc.M113.457119.

34. Tie J-K, Jin D-Y, Stafford DW. Conserved loop cysteines of vitamin K epoxide reductase complex subunit 1-like 1 (VKORC1L1) are involved in its active site regeneration. J Biol Chem. 2014;289:9396–407. doi:10.1074/jbc.M113.534446.

35. Shen G, Cui W, Zhang H, Zhou F, Huang W, Liu Q, et al. Warfarin traps human vitamin K epoxide reductase in an intermediate state during electron transfer. Nat Struct Mol Biol. 2017;24:69–76. doi:10.1038/nsmb.3333.

36. Yin T, Hanada H, Miyashita K, Kokubo Y, Akaiwa Y, Otsubo R, et al. No association between vitamin K epoxide reductase complex subunit 1-like 1 (VKORC1L1) and the variability of warfarin dose requirement in a Japanese patient population. Thromb Res. 2008;122:179–84. doi:10.1016/j.thromres.2007.09.015.

37. Stenflo J, Fernlund P, Egan W, Roepstorff P. Vitamin K dependent modifications of glutamic acid residues in prothrombin. Proc Natl Acad Sci U S A. 1974;71:2730–3.

38. Ferland G. The vitamin K-dependent proteins: an update. Nutr Rev. 1998;56:223–30.

39. Danziger J. Vitamin K-dependent proteins, warfarin, and vascular calcification. Clin J Am Soc Nephrol. 2008;3:1504–10. doi:10.2215/CJN.00770208.

40. Ferland G. Vitamin K and the nervous system: an overview of its actions. Adv Nutr. 2012;3:204–12. doi:10.3945/an.111.001784.

41. Manfioletti G, Brancolini C, Avanzi G, Schneider C. The protein encoded by a growth arrest-specific gene (gas6) is a new member of the vitamin K-dependent proteins related to protein S, a negative coregulator in the blood coagulation cascade. Mol Cell Biol. 1993;13:4976–85.

42. Yanagita M, Ishimoto Y, Arai H, Nagai K, Ito T, Nakano T, et al. Essential role of Gas6 for glomerular injury in nephrotoxic nephritis. J. Clin. Invest. 2002;110:239–46. doi:10.1172/JCI200214861.

43. Shankar SL, O'Guin K, Cammer M, McMorris FA, Stitt TN, Basch RS, et al. The growth arrest-specific gene product Gas6 promotes the survival of human oligodendrocytes via a phosphatidylinositol 3-kinase-dependent pathway. J Neurosci. 2003;23:4208–18.

44. Katagiri M, Hakeda Y, Chikazu D, Ogasawara T, Takato T, Kumegawa M, et al. Mechanism of stimulation of osteoclastic bone resorption through Gas6/Tyro 3, a receptor tyrosine kinase signaling, in mouse osteoclasts. J Biol Chem. 2001;276:7376–82. doi:10.1074/jbc.M007393200.

45. Angelillo-Scherrer A, Frutos P de, Aparicio C, Melis E, Savi P, Lupu F, et al. Deficiency or inhibition of Gas6 causes platelet dysfunction and protects mice against thrombosis. Nat Med. 2001;7:215–21. doi:10.1038/84667.

46. Price PA, Otsuka AA, Poser JW, Kristaponis J, Raman N. Characterization of a gamma-carboxyglutamic acid-containing protein from bone. Proc Natl Acad Sci U S A. 1976;73:1447–51.

47. Fraser JD, Price PA. Lung, heart, and kidney express high levels of mRNA for the vitamin K-dependent matrix Gla protein. Implications for the possible functions of matrix Gla protein and for the tissue distribution of the gamma-carboxylase. J Biol Chem. 1988;263:11033–6.

48. Luo G, Ducy P, McKee MD, Pinero GJ, Loyer E, Behringer RR, Karsenty G. Spontaneous calcification of arteries and cartilage in mice lacking matrix GLA protein. Nature. 1997;386:78–81. doi:10.1038/386078a0.

49. Viegas CSB, Rafael MS, Enriquez JL, Teixeira A, Vitorino R, Luis IM, et al. Gla-rich protein acts as a calcification inhibitor in the human cardiovascular system. Arterioscler Thromb Vasc Biol. 2015;35:399–408. doi:10.1161/ATVBAHA.114.304823.

50. Viegas CSB, Cavaco S, Neves PL, Ferreira A, João A, Williamson MK, et al. Gla-Rich Protein Is a Novel Vitamin K-Dependent Protein Present in Serum That Accumulates at Sites of Pathological Calcifications. The American Journal of Pathology. 2009;175:2288–98. doi:10.2353/ajpath.2009.090474.

51. Rios H, Koushik SV, Wang H, Wang J, Zhou H-M, Lindsley A, et al. periostin null mice exhibit dwarfism, incisor enamel defects, and an early-onset periodontal disease-like phenotype. Mol Cell Biol. 2005;25:11131–44. doi:10.1128/MCB.25.24.11131-11144.2005.

52. Coutu DL, Wu JH, Monette A, Rivard G-E, Blostein MD, Galipeau J. Periostin, a member of a novel family of vitamin K-dependent proteins, is expressed by mesenchymal stromal cells. J Biol Chem. 2008;283:17991–8001. doi:10.1074/jbc.M708029200.

53. Annis DS, Ma H, Balas DM, Kumfer KT, Sandbo N, Potts GK, et al. Absence of Vitamin K-Dependent γ-Carboxylation in Human Periostin Extracted from Fibrotic Lung

or Secreted from a Cell Line Engineered to Optimize γ-Carboxylation. PLoS ONE. 2015;10:e0135374. doi:10.1371/journal.pone.0135374.

54. Kulman JD, Harris JE, Haldeman BA, Davie EW. Primary structure and tissue distribution of two novel proline-rich gamma-carboxyglutamic acid proteins. Proc Natl Acad Sci U S A. 1997;94:9058–62.

55. Kulman JD, Harris JE, Xie L, Davie EW. Identification of two novel transmembrane gamma-carboxyglutamic acid proteins expressed broadly in fetal and adult tissues. Proc Natl Acad Sci U S A. 2001;98:1370–5. doi:10.1073/pnas.98.4.1370.

56. Justice ED, Barnum SJ, Kidd T. The WAGR syndrome gene PRRG4 is a functional homologue of the commissureless axon guidance gene. PLoS Genet. 2017;13:e1006865. doi:10.1371/journal.pgen.1006865.

57. Husain M, Boermans HJ, Karrow NA. Mesenteric lymph node transcriptome profiles in BALB/c mice sensitized to three common food allergens. BMC Genomics. 2011;12:12. doi:10.1186/1471-2164-12-12.

58. Rechenmacher SJ, Fang JC. Bridging Anticoagulation: Primum Non Nocere. J Am Coll Cardiol. 2015;66:1392–403. doi:10.1016/j.jacc.2015.08.002.

59. Chu P-H, Huang T-Y, Williams J, Stafford DW. Purified vitamin K epoxide reductase alone is sufficient for conversion of vitamin K epoxide to vitamin K and vitamin K to vitamin KH2. Proc Natl Acad Sci U S A. 2006;103:19308–13. doi:10.1073/pnas.0609401103.

60. Ansell J, Hirsh J, Hylek E, Jacobson A, Crowther M, Palareti G. Pharmacology and management of the vitamin K antagonists: American College of Chest Physicians Evidence-Based Clinical Practice Guidelines (8th Edition). Chest. 2008;133:160–98. doi:10.1378/chest.08-0670.

61. Harbrecht U. Old and new anticoagulants. Hamostaseologie. 2011;31:21–7. doi:10.5482/ha-1149.

62. Venugopala KN, Rashmi V, Odhav B. Review on natural coumarin lead compounds for their pharmacological activity. Biomed Res Int. 2013;2013:963248. doi:10.1155/2013/963248.

63. Monti M, Pinotti M, Appendino G, Dallocchio F, Bellini T, Antognoni F, et al. Characterization of anti-coagulant properties of prenylated coumarin ferulenol. Biochim Biophys Acta. 2007;1770:1437–40. doi:10.1016/j.bbagen.2007.06.013.

64. Link KP. The discovery of dicumarol and its sequels. Circulation. 1959;19:97–107.

65. Wardrop D, Keeling D. The story of the discovery of heparin and warfarin. Br J Haematol. 2008;141:757–63. doi:10.1111/j.1365-2141.2008.07119.x.

66. Lacut K, Ayme-Dietrich E, Gourhant L, Poulhazan E, Andro M, Becquemont L, et al. Impact of genetic factors (VKORC1, CYP2C9, CYP4F2 and EPHX1) on the anticoagulation response to fluindione. Br J Clin Pharmacol. 2012;73:428–36. doi:10.1111/j.1365-2125.2011.04095.x.

67. Beinema M, Brouwers, Jacobus R B J, Schalekamp T, Wilffert B. Pharmacogenetic differences between warfarin, acenocoumarol and phenprocoumon. Thromb Haemost. 2008;100:1052–7.

68. Verstuyft C, Delavenne X, Rousseau A, Robert A, Tod M, Diquet B, et al. A pharmacokinetic-pharmacodynamic model for predicting the impact of CYP2C9 and VKORC1 polymorphisms on fluindione and acenocoumarol during induction therapy. Clin Pharmacokinet. 2012;51:41–53. doi:10.2165/11595560-000000000-00000.

69. Ufer M. Comparative pharmacokinetics of vitamin K antagonists: warfarin, phenprocoumon and acenocoumarol. Clin Pharmacokinet. 2005;44:1227–46. doi:10.2165/00003088-200544120-00003.

70. Mentre F, Pousset F, Comets E, Plaud B, Diquet B, Montalescot G, et al. Population pharmacokinetic-pharmacodynamic analysis of fluindione in patients. Clin Pharmacol Ther. 1998;63:64–78. doi:10.1016/S0009-9236(98)90122-9.

71. King N, Tran M-H. Long-Acting Anticoagulant Rodenticide (Superwarfarin) Poisoning: A Review of Its Historical Development, Epidemiology, and Clinical Management. Transfus Med Rev. 2015;29:250–8. doi:10.1016/j.tmrv.2015.06.002.

72. Misenheimer TM, Suttie JW. Warfarin resistance in a Chicago strain of rats. Biochem Pharmacol. 1990;40:2079–84.

73. Misenheimer TM, Lund M, Baker EM, Suttie JW. Biochemical basis of warfarin and bromadiolone resistance in the house mouse, Mus musculus domesticus. Biochem Pharmacol. 1994;47:673–8.

74. Hadler MR, Buckle AP, editors. Forty five years of anticoagulant rodenticides — Past, Present and Future Trends. http://digitalcommons.unl.edu/vpc15/36: University of Nebraska - Lincoln; 1992.

75. Hadler MR, Shadbolt RS. Novel 4-hydroxycoumarin anticoagulants active against resistant rats. Nature. 1975;253:275–7. doi:10.1038/253275a0.

76. Mosterd JJ, Thijssen HH. The long-term effects of the rodenticide, brodifacoum, on blood coagulation and vitamin K metabolism in rats. British Journal of Pharmacology. 1991;104:531–5.

77. Olmos V, Lopez CM. Brodifacoum poisoning with toxicokinetic data. Clin Toxicol (Phila). 2007;45:487–9. doi:10.1080/15563650701354093.

78. Krieger E, Vriend G. YASARA View--molecular graphics for all devices--from smartphones to workstations. Bioinformatics. 2014;30:2981–2. doi:10.1093/bioinformatics/btu426.

79. Pettersen EF, Goddard TD, Huang CC, Couch GS, Greenblatt DM, Meng EC, Ferrin TE. UCSF Chimera--a visualization system for exploratory research and analysis. J Comput Chem. 2004;25:1605–12. doi:10.1002/jcc.20084.

80. Ho SN, Hunt HD, Horton RM, Pullen JK, Pease LR. Site-directed mutagenesis by overlap extension using the polymerase chain reaction. Gene. 1989;77:51–9. doi:10.1016/0378-1119(89)90358-2.

81. Unger T, Jacobovitch Y, Dantes A, Bernheim R, Peleg Y. Applications of the Restriction Free (RF) cloning procedure for molecular manipulations and protein expression. J Struct Biol. 2010;172:34–44. doi:10.1016/j.jsb.2010.06.016.

82. Rosenblum B. New dye-labeled terminators for improved DNA sequencing patterns. Nucleic Acids Res. 1997;25:4500–4. doi:10.1093/nar/25.22.4500.

83. Graham FL, Smiley J, Russell WC, Nairn R. Characteristics of a human cell line transformed by DNA from human adenovirus type 5. J Gen Virol. 1977;36:59–74. doi:10.1099/0022-1317-36-1-59.

84. Jinek M, Chylinski K, Fonfara I, Hauer M, Doudna JA, Charpentier E. A programmable dual-RNA-guided DNA endonuclease in adaptive bacterial immunity. Science. 2012;337:816–21. doi:10.1126/science.1225829.

85. Horvath P, Barrangou R. CRISPR/Cas, the immune system of bacteria and archaea. Science. 2010;327:167–70. doi:10.1126/science.1179555.

86. Makarova KS, Haft DH, Barrangou R, Brouns SJJ, Charpentier E, Horvath P, et al. Evolution and classification of the CRISPR-Cas systems. Nat Rev Microbiol. 2011;9:467–77. doi:10.1038/nrmicro2577.

87. Roy A, Kucukural A, Zhang Y. I-TASSER: A unified platform for automated protein structure and function prediction. Nat Protoc. 2010;5:725–38. doi:10.1038/nprot.2010.5.

88. Morris GM, Goodsell DS, Halliday RS, Huey R, Hart WE, Belew RK, Olson AJ. Automated docking using a Lamarckian genetic algorithm and an empirical binding free energy function. J. Comput. Chem. 1998;19:1639–62. doi:10.1002/(SICI)1096-987X(19981115)19:14<1639::AID-JCC10>3.0.CO;2-B.

89. Yang H, Wang H, Jaenisch R. Generating genetically modified mice using CRISPR/Cas-mediated genome engineering. Nat Protoc. 2014;9:1956–68. doi:10.1038/nprot.2014.134.

90. Lin Y-C, Boone M, Meuris L, Lemmens I, van Roy N, Soete A, et al. Genome dynamics of the human embryonic kidney 293 lineage in response to cell biology manipulations. Nat Commun. 2014;5:4767. doi:10.1038/ncomms5767.

91. Sattler FR. Potential for Bleeding with the New Beta-Lactam Antibiotics. Ann Intern Med. 1986;105:924. doi:10.7326/0003-4819-105-6-924.

92. Prut L, Belzung C. The open field as a paradigm to measure the effects of drugs on anxiety-like behaviors: a review. Eur J Pharmacol. 2003;463:3–33.

93. Curzon P, Zhang M, Radek RJ, Fox GB. The Behavioral Assessment of Sensorimotor Processes in the Mouse: Acoustic Startle, Sensory Gating, Locomotor Activity, Rotarod, and Beam Walking. In: Buccafusco JJ, editor. Frontiers in Neuroscience : Methods of Behavior Analysis in Neuroscience. 2nd ed. Boca Raton (FL); 2009.

94. Ma Q. Advances in Mechanisms of Anti-oxidation. Discov Med. 2014;17:121–30.

95. Vervoort LMT, Ronden JE, Thijssen HHW. The potent antioxidant activity of the vitamin K cycle in microsomal lipid peroxidation. Biochem Pharmacol. 1997;54:871–6. doi:10.1016/S0006-2952(97)00254-2.

96. Rishavy MA, Hallgren KW, Wilson LA, Usubalieva A, Runge KW, Berkner KL. The vitamin K oxidoreductase is a multimer that efficiently reduces vitamin K epoxide to hydroquinone to allow vitamin K-dependent protein carboxylation. J Biol Chem. 2013;288:31556–66. doi:10.1074/jbc.M113.497297.

97. Li J, Lin JC, Wang H, Peterson JW, Furie BC, Furie B, et al. Novel role of vitamin k in preventing oxidative injury to developing oligodendrocytes and neurons. J Neurosci. 2003;23:5816–26.

98. Friedman PA, Shia M. Some characteristics of a vitamin K-dependent carboxylating system from rat liver microsomes. Biochemical and Biophysical Research Communications. 1976;70:647–54. doi:10.1016/0006-291X(76)91096-2.

99. Mack DO, Suen ET, Girardot JM, Miller JA, Delaney R, Johnson BC. Soluble enzyme system for vitamin K-dependent carboxylation. J Biol Chem. 1976;251:3269–76.

100. Krettler C, Bevans CG, Reinhart C, Watzka M, Oldenburg J. Tris(3-hydroxypropyl)phosphine is superior to dithiothreitol for in vitro assessment of vitamin K 2,3-epoxide reductase activity. Anal Biochem. 2015;474:89–94. doi:10.1016/j.ab.2014.12.004.

101. Bevans CG, Krettler C, Reinhart C, Tran H, Kossmann K, Watzka M, Oldenburg J. Determination of the warfarin inhibition constant Ki for vitamin K 2,3-epoxide reductase complex subunit-1 (VKORC1) using an in vitro DTT-driven assay. Biochim Biophys Acta. 2013;1830:4202–10. doi:10.1016/j.bbagen.2013.04.018.

102. Tie J-K, Jin D-Y, Straight DL, Stafford DW. Functional study of the vitamin K cycle in mammalian cells. Blood. 2011;117:2967–74. doi:10.1182/blood-2010-08-304303.

103. Hodroge A, Matagrin B, Moreau C, Fourel I, Hammed A, Benoit E, Lattard V. VKORC1 mutations detected in patients resistant to vitamin K antagonists are not all associated with a resistant VKOR activity. Journal of Thrombosis and Haemostasis. 2012;10:2535–43. doi:10.1111/jth.12019.

104. Stenina O, Pudota BN, McNally BA, Hommema EL, Berkner KL. Tethered processivity of the vitamin K-dependent carboxylase: factor IX is efficiently modified in a mechanism which distinguishes Gla's from Glu's and which accounts for comprehensive carboxylation in vivo. Biochemistry. 2001;40:10301–9.

105. Liu J, Jonebring A, Hagstrom J, Nystrom A-C, Lovgren A. Improved expression of recombinant human factor IX by co-expression of GGCX, VKOR and furin. Protein J. 2014;33:174–83. doi:10.1007/s10930-014-9550-5.

106. Malhotra OP. Purification and characterization of dicoumarol-induced prothrombins. III. Alumina pH 4.6 atypical (2-Gla) variant. Thromb Res. 1979;15:449–63.

107. Hallgren KW, Qian W, Yakubenko AV, Runge KW, Berkner KL. r-VKORC1 expression in factor IX BHK cells increases the extent of factor IX carboxylation but is limited by saturation of another carboxylation component or by a shift in the rate-limiting step. Biochemistry. 2006;45:5587–98. doi:10.1021/bi051986y.

108. Tokunaga F, Wakabayashi S, Koide T. Warfarin causes the degradation of protein C precursor in the endoplasmic reticulum. Biochemistry. 1995;34:1163–70.

109. Haque JA, McDonald MG, Kulman JD, Rettie AE. A cellular system for quantitation of vitamin K cycle activity: structure-activity effects on vitamin K antagonism by warfarin metabolites. Blood. 2014;123:582–9. doi:10.1182/blood-2013-05-505123.

110. Bevans CG, Krettler C, Reinhart C, Watzka M, Oldenburg J. Phylogeny of the Vitamin K 2,3-Epoxide Reductase (VKOR) Family and Evolutionary Relationship to the Disulfide Bond Formation Protein B (DsbB) Family. Nutrients. 2015;7:6224–49. doi:10.3390/nu7085281.

111. Oldenburg J, Watzka M, Bevans CG. VKORC1 and VKORC1L1: Why do Vertebrates Have Two Vitamin K 2,3-Epoxide Reductases? Nutrients. 2015;7:6250–80. doi:10.3390/nu7085280.

112. Gebauer M. Synthesis and structure-activity relationships of novel warfarin derivatives. Bioorg Med Chem. 2007;15:2414–20. doi:10.1016/j.bmc.2007.01.014.

113. Matagrin B, Hammed A, Michaux A. Identification of Key Functional Residues in the Active Site of Vitamin K Epoxide Reductase-like Protein (VKORC1L1). Biochem Mol Biol J 2016. doi:10.21767/2471-8084.100024.

114. Geisen C, Watzka M, Sittinger K, Steffens M, Daugela L, Seifried E, et al. VKORC1 haplotypes and their impact on the inter-individual and inter-ethnical variability of oral anticoagulation. Thromb Haemost. 2005;94:773–9. doi:10.1160/TH05-04-0290.

115. Geisen C, Luxembourg B, Watzka M, Toennes SW, Sittinger K, Marinova M, et al. Prediction of phenprocoumon maintenance dose and phenprocoumon plasma concentration by genetic and non-genetic parameters. Eur J Clin Pharmacol. 2011;67:371–81. doi:10.1007/s00228-010-0950-y.

116. Czogalla KJ, Biswas A, Honing K, Hornung V, Liphardt K, Watzka M, Oldenburg J. Warfarin and vitamin K compete for binding to Phe55 in human VKOR. Nat Struct Mol Biol. 2017;24:77–85. doi:10.1038/nsmb.3338.

117. Deng Y, Qiu L. Therapeutic plasma exchange: a second-line treatment for brodifacoum poisoning following an anaphylactoid reaction to vitamin K. Clin Case Rep. 2017;5:35–8. doi:10.1002/ccr3.756.

118. Louvet M-S, Gault G, Lefebvre S, Popowycz F, Boulven M, Besse S, et al. Comparative inhibitory effect of prenylated coumarins, ferulenol and ferprenin, contained in the 'poisonous chemotype' of Ferula communis on mammal liver microsomal VKORC1 activity. Phytochemistry. 2015;118:124–30. doi:10.1016/j.phytochem.2015.08.012.

119. Gault G, Riera M, Berny P, Benoit E, Grancher D, editors. Giant fennel (Ferula communis L.) intoxications in livestock in France. Hohhot (PR China); 2015.

120. Hodroge A, Longin-Sauvageon C, Fourel I, Benoit E, Lattard V. Biochemical characterization of spontaneous mutants of rat VKORC1 involved in the resistance to antivitamin K anticoagulants. Arch Biochem Biophys. 2011;515:14–20. doi:10.1016/j.abb.2011.08.010.

121. Hooper CA, Haney BB, Stone HH. Gastrointestinal bleeding due to vitamin K deficiency in patients on parenteral cefamandole. Lancet. 1980;1:39–40.

122. Andrassy K, Bechthold H, Ritz E. Hvpoprothrombinemia caused by cephalosporins. J Antimicrob Chemother. 1985;15:133–6. doi:10.1093/jac/15.2.133.

123. Shearer MJ, Bechtold H, Andrassy K, Koderisch J, McCarthy PT, Trenk D, et al. Mechanism of cephalosporin-induced hypoprothrombinemia: relation to cephalosporin side chain, vitamin K metabolism, and vitamin K status. J Clin Pharmacol. 1988;28:88–95.

124. Barnes RH, Fiala G. Effects of the prevention of coprophagy in the rat. 6. Vitamin K. Journal of Nutrition. 1959;68:603–14.

125. Uchida K, Nomura Y, Takase H, Harauchi T, Yoshizaki T, Nakao H. Effects of vitamin K-deficient diets and fasting on blood coagulation factors in conventional and germ-free rats. Jpn.J.Pharmacol. 1986;40:115–22. doi:10.1254/jjp.40.115.

126. Lipsky JJ. Antibiotic-associated hypoprothrombinaemia. J Antimicrob Chemother. 1988;21:281–300.

127. Mitchell MC, Mallat A, Lipsky JJ. Cephalosporin-induced alteration in hepatic glutathione redox state. A potential mechanism for inhibition of hepatic reduction of vitamin K1,2,3-epoxide in the rat. J. Clin. Invest. 1990;86:1589–94. doi:10.1172/JCI114879.

128. Aronoff GR, Wolen RL, Obermeyer BD, Black HR. Pharmacokinetics and Protein Binding of Cefamandole and Its 1-Methyl-1 H-Tetrazole-5-Thiol Side Chain in Subjects with Normal and Impaired Renal Function. Journal of Infectious Diseases. 1986;153:1069–74. doi:10.1093/infdis/153.6.1069.

129. Angaran DM, Dias VC, Arom KV, Northrup WF, Kersten TG, Lindsay WG, Nicoloff DM. The comparative influence of prophylactic antibiotics on the prothrombin response to warfarin in the postoperative prosthetic cardiac valve patient. Cefamandole, cefazolin, vancomycin. Ann Surg. 1987;206:155–61.

130. Holbrook AM, Pereira JA, Labiris R, McDonald H, Douketis JD, Crowther M, Wells PS. Systematic overview of warfarin and its drug and food interactions. Arch Intern Med. 2005;165:1095–106. doi:10.1001/archinte.165.10.1095.

131. Ghaswalla PK, Harpe SE, Tassone D, Slattum PW. Warfarin–Antibiotic Interactions in Older Adults of an Outpatient Anticoagulation Clinic. The American Journal of Geriatric Pharmacotherapy. 2012;10:352–60. doi:10.1016/j.amjopharm.2012.09.006.

132. Ziegler DM. Metabolic oxygenation of organic nitrogen and sulfur compounds. 1984.

133. Tie J-K, Jin D-Y, Stafford DW. Human vitamin K epoxide reductase and its bacterial homologue have different membrane topologies and reaction mechanisms. J Biol Chem. 2012;287:33945–55. doi:10.1074/jbc.M112.402941.

134. Sikorska J, Uprichard J. Direct Oral Anticoagulants: A Quick Guide. European Cardiology Review. 2017;12:40. doi:10.15420/ecr.2017:11:2.

135. Chatrou MLL, Winckers K, Hackeng TM, Reutelingsperger CP, Schurgers LJ. Vascular calcification: the price to pay for anticoagulation therapy with vitamin K-antagonists. Blood Rev. 2012;26:155–66. doi:10.1016/j.blre.2012.03.002.

136. van Gorp RH, Schurgers LJ. New Insights into the Pros and Cons of the Clinical Use of Vitamin K Antagonists (VKAs) Versus Direct Oral Anticoagulants (DOACs). Nutrients. 2015;7:9538–57. doi:10.3390/nu7115479.

137. Eitzinger N, Surmann-Schmitt C, Bösl M, Schett G, Engelke K, Hess A, et al. Ucma is not necessary for normal development of the mouse skeleton. Bone. 2012;50:670–80. doi:10.1016/j.bone.2011.11.017.

138. Ronden JE, Thijssen HH, Vermeer C. Tissue distribution of K-vitamers under different nutritional regimens in the rat. Biochim Biophys Acta. 1998;1379:16–22.

139. Cockayne S, Adamson J, Lanham-New S, Shearer MJ, Gilbody S, Torgerson DJ. Vitamin K and the prevention of fractures: systematic review and meta-analysis of randomized controlled trials. Arch Intern Med. 2006;166:1256–61. doi:10.1001/archinte.166.12.1256.

140. Tamura T, Morgan SL, Takimoto H. Vitamin K and the prevention of fractures. Arch Intern Med. 2007;167:94; author reply 94-5. doi:10.1001/archinte.167.1.94-a.

141. Vermeer C. Vitamin K: the effect on health beyond coagulation - an overview. Food Nutr Res 2012. doi:10.3402/fnr.v56i0.5329.

142. Hall B, Limaye A, Kulkarni AB. Overview: Generation of Gene Knockout Mice. Current protocols in cell biology / editorial board, Juan S. Bonifacino … [et al.]. 2009;CHAPTER:19. doi:10.1002/0471143030.cb1912s44.

143. Sternberg N, Hamilton D. Bacteriophage P1 site-specific recombination. I. Recombination between loxP sites. J Mol Biol. 1981;150:467–86.

144. Sauer B, Henderson N. Site-specific DNA recombination in mammalian cells by the Cre recombinase of bacteriophage P1. Proc Natl Acad Sci U S A. 1988;85:5166–70.

145. Gu H, Marth JD, Orban PC, Mossmann H, Rajewsky K. Deletion of a DNA polymerase beta gene segment in T cells using cell type-specific gene targeting. Science. 1994;265:103–6.

146. Yang H, Wang H, Shivalila CS, Cheng AW, Shi L, Jaenisch R. One-step generation of mice carrying reporter and conditional alleles by CRISPR/Cas-mediated genome engineering. Cell. 2013;154:1370–9. doi:10.1016/j.cell.2013.08.022.

147. Lobocka MB, Rose DJ, Plunkett G3, Rusin M, Samojedny A, Lehnherr H, et al. Genome of bacteriophage P1. J Bacteriol. 2004;186:7032–68. doi:10.1128/JB.186.21.7032-7068.2004.

148. An L, Hu Y, Chang S, Zhu X, Ling P, Zhang F, et al. Efficient generation of FVII gene knockout mice using CRISPR/Cas9 nuclease and truncated guided RNAs. Sci Rep. 2016;6:25199. doi:10.1038/srep25199.

149. Fu Y, Foden JA, Khayter C, Maeder ML, Reyon D, Joung JK, Sander JD. High-frequency off-target mutagenesis induced by CRISPR-Cas nucleases in human cells. Nat Biotechnol. 2013;31:822–6. doi:10.1038/nbt.2623.

150. Vanin EF. Processed pseudogenes: characteristics and evolution. Annu Rev Genet. 1985;19:253–72. doi:10.1146/annurev.ge.19.120185.001345.

151. Gailus-Durner V, Fuchs H, Becker L, Bolle I, Brielmeier M, Calzada-Wack J, et al. Introducing the German Mouse Clinic: open access platform for standardized phenotyping. Nature Methods. 2005;2:403 EP -. doi:10.1038/nmeth0605-403.

152. Lev M, Milford AF. The 3-ketodihydrosphingosine synthetase of Bacteroides melaninogenicus: Induction by vitamin K. Arch Biochem Biophys. 1973;157:500–8. doi:10.1016/0003-9861(73)90668-1.

153. Sundaram KS, Lev M. Regulation of sulfotransferase activity by vitamin K in mouse brain. Arch Biochem Biophys. 1990;277:109–13.

154. Carrie I, Portoukalian J, Vicaretti R, Rochford J, Potvin S, Ferland G. Menaquinone-4 concentration is correlated with sphingolipid concentrations in rat brain. J Nutr. 2004;134:167–72.

155. Bisschop PH, Sauerwein HP, Endert E, Romijn JA. Isocaloric carbohydrate deprivation induces protein catabolism despite a low T3-syndrome in healthy men. Clin Endocrinol (Oxf). 2001;54:75–80.

156. Thomas L. Labor und Diagnose: Indikation und Bewertung von Laborbefunden für die medizinische Diagnostik. 8th ed. Frankfurt/Main: Th-Books Verl.-Ges; 2012.

157. Li Y, Huang TT, Carlson EJ, Melov S, Ursell PC, Olson JL, et al. Dilated cardiomyopathy and neonatal lethality in mutant mice lacking manganese superoxide dismutase. Nat Genet. 1995;11:376–81. doi:10.1038/ng1295-376.

158. Williams MD, van Remmen H, Conrad CC, Huang TT, Epstein CJ, Richardson A. Increased oxidative damage is correlated to altered mitochondrial function in heterozygous manganese superoxide dismutase knockout mice. J Biol Chem. 1998;273:28510–5.

159. Reaume AG, Elliott JL, Hoffman EK, Kowall NW, Ferrante RJ, Siwek DF, et al. Motor neurons in Cu/Zn superoxide dismutase-deficient mice develop normally but exhibit enhanced cell death after axonal injury. Nat Genet. 1996;13:43–7. doi:10.1038/ng0596-43.

List of figures

List of tables

Appendix

A.1 List of primers

CRISPR/Cas9 to generate VKORC1L1 mice

Oligo donor Up	ATGTGGCTGGGTTTCTGGACATCATGACACACTACTAGCCATGA CTAAACGTCCACTGATATAACTTCGTATAGCATACATTATACGAA GTTATGATATCACCAAGGTCAACACATGATAAGCAGCAGTGACT CACACTTCACTCTCGTGGTTCTCTATT
Oligo donor Dw	TTCTTTAAAAAAAAAAAAACCTGGGCTTTTTTTGGGGGGTGGGG GGTCTCATTAACCTCAATAACTTCGTATAGCATACATTATACGAA GTTATGATATCTGCGTGGAAATTGATTTCAGGGAGATAATTCAA GGAAGGACAGGTACTATAAAGAAAATG
sgRNA Up	GTTAAAGCTGAAGTGTCGTG
sgRNA Dw	TGGTATCAGTGGACGTTTAG

For genotyping of VKORC1L1 mice

RFLPprimerUp_Fw	GGGTGAGAGAATTCGTGCAT
RFLPprimerDw_Rv	AATGTGAATTGCAGCAAGCC
L1_KO_1F	ACTGTGAAGGGGTTGTCCTG
L1_KO_2R	CGAGGATTTGGTCTTTTGGGT
L1_KO_3F	TACTGGGTTCAATTCCAGCAC

For amplification of murine VKORC1L1 cDNA

mL1_Start_F	ATGGCGGCGCCCGTCCTG
mL1_Stop_R	TCAGTCTTCCTTAGGCTGCAGCTG

For quantitative PCR (TaqMan assay)

L1_TM_F_neu	CCTGGGTGAAGTGCTCCG
mL1_TM_Sonde_neu	5‘-FAM CTCGACCCCATCTGGAGGCCA BHQ1-3‘
TM_VKORC1L1_R	AGACACTGTTTGGCTGGTTTAATAC
TM_HMBS_F	AGTCATGTCCGGTAACGGC
TM_HMBS_R	CAGGGTACAAGGCTTTCAGC
S_HMBS	5’-FAM ACCGCGGAAGAAAACGGCTC BHQ1-3‘

Introduction of mutations in hVKORC1

R33E-For	CACGTGAAGGCGGCGGAGGCCCGGGACCGGGAT
R33E-Rev	ATCCCGGTCCCGGGCCTCCGCCGCCTTCACGTG
R40E-For	CGGGACCGGGATTACGAGGCGCTCTGCGACGT
R40E-Rev	ACGTCGCAGAGCGCCTCGTAATCCCGGTCCCG
R53E-For	GCCATCAGCTGTTCGGAGGTCTTCTCCTCCAGG
R53E-Rev	CCTGGAGGAGAAGACCTCCGAACAGCTGATGGC
F55A-For	GCTGTTCGCGCGTCGCCTCCTCCAGGTGGG
F55A-Rev	CCCACCTGGAGGAGGCGACGCGCGAACAGC

Introduction of mutations in hVKORC1L1

L62F-For	AAGTGCTCCGCCGCCTTTGCCTCCAGATGGG
L62F-Rev	CCCATCTGGAGGCAAAGGCGGCGGAGCACTT
60AAL-RVF-For	CCCTGGGTGAAGTGCTCCCGCGTCTTTGCCTCCAGATGGGGT
60AAL-RVF-Rev	ACCCCATCTGGAGGCAAAGACGCGGGAGCACTTCACCCAGGG
R68E-For	GCCTCCAGATGGGGTGAAGGATTTGGTCTTTTG
R68E-Rev	CAAAAGACCAAATCCTTCACCCCATCTGGAGGC
R38E_F	GCCTACCACGTGGAGGAGGAGAAGGAGCGGG
R38E_R	CCCGCTCCTTCTCCTCCTCCACGTGGTAGGC
R42E_F	GAGCGGGAGAAGGAGGAGGACCCCGAGCACC
R42E_R	GGTGCTCGGGGTCCTCCTCCTTCTCCCGCTC
R38+42E-For	TACCACGTGGAGGAGGAGAAGGAGGAGGACCCCGAGCAC
R38+42E-Rev	GTGCTCGGGGTCCTCCTCCTTTCCTCCTCCACGTGGTA

A.2 Plasmids

pX330-U6-Chimeric_BB-CBh-hSpCas9 (Plasmid #42230)

A human codon-optimized SpCas9 and chimeric guide RNA expression plasmid [89] used for generation of knockout mice. Picture taken from https://www.addgene.org/42230/ visited on 19-Jan-2018.

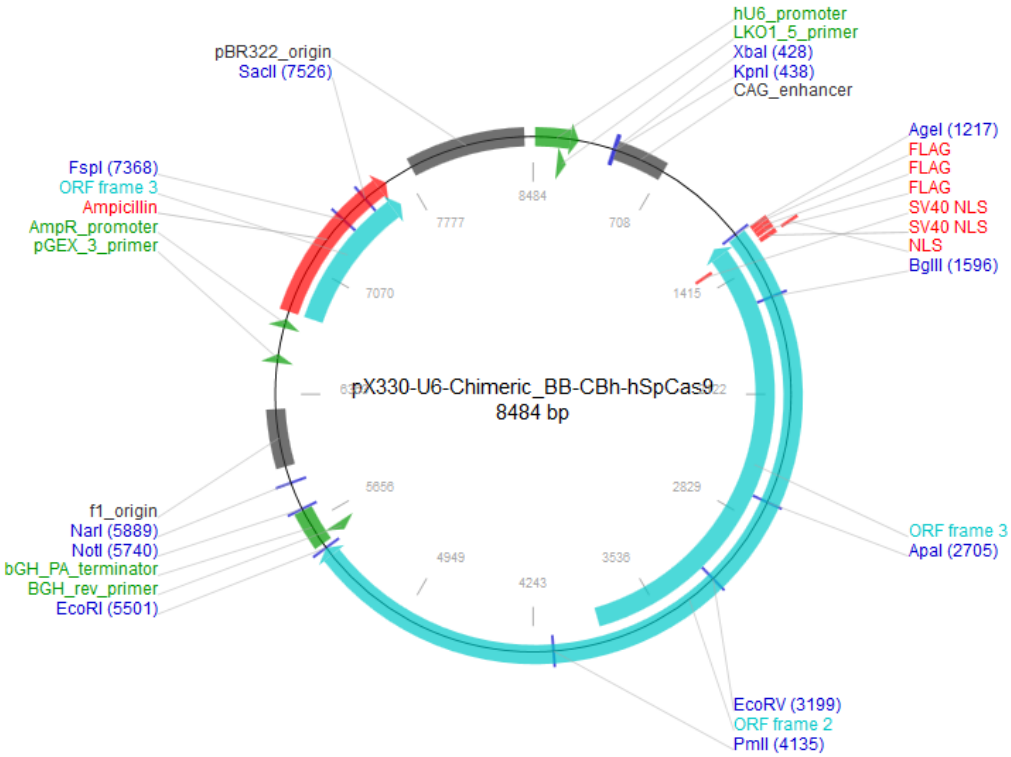

Retro Double CMV

Plasmid used for generation of HEK 293T knockout cell lines in collaboration with Klara Höning from the Institute of Molecular Medicine at the University Hospital Bonn. Picture generated with SnapGene Viewer.

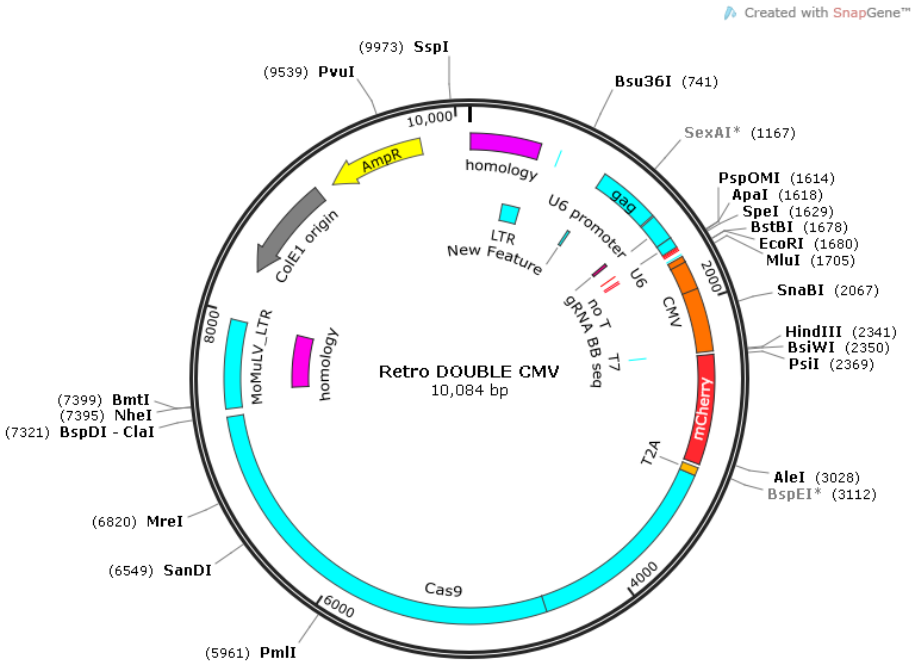

pIRES

Plasmid used for expression of *F9* and *VKORC1*/*VKORC1L1* and its variants in different HEK 293T cell lines. Vector information taken from www.clontech.com visited on 19-Jan-2018 (PR852529; published 20 May, 2008).

pIRES Vector Information PT3266-5

Cat. No. 631605

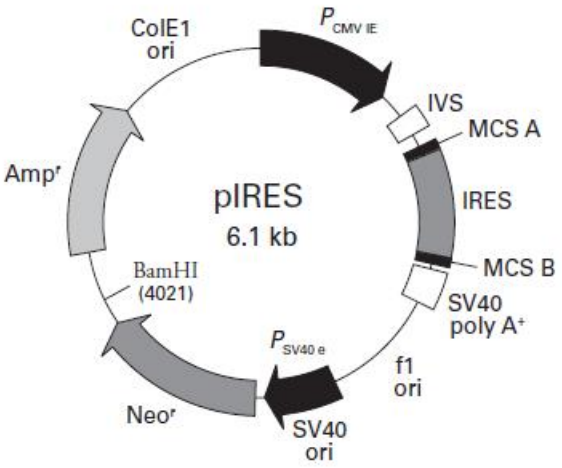

MCS A

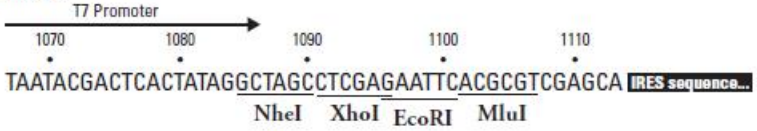

MCS B

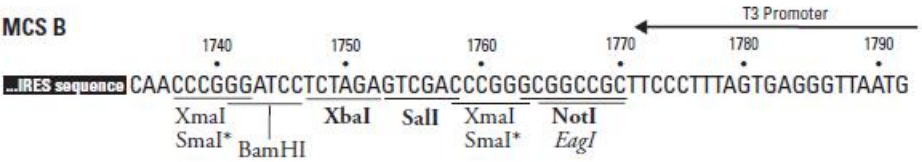

pIRES Vector Map and Multiple Cloning Sites (MCS). Unique restriction sites are in bold. The XmaI/SmaI sites can be treated as unique sites for cloning purposes.

pCMV6 XL4

Plasmid was used for expression of human *F9* and was purchased from Origene. cDNA (2.9 kb) was cloned in at *Not*I restriction sites. Vector information taken from www.origene.com visited on 19-Jan-2018.

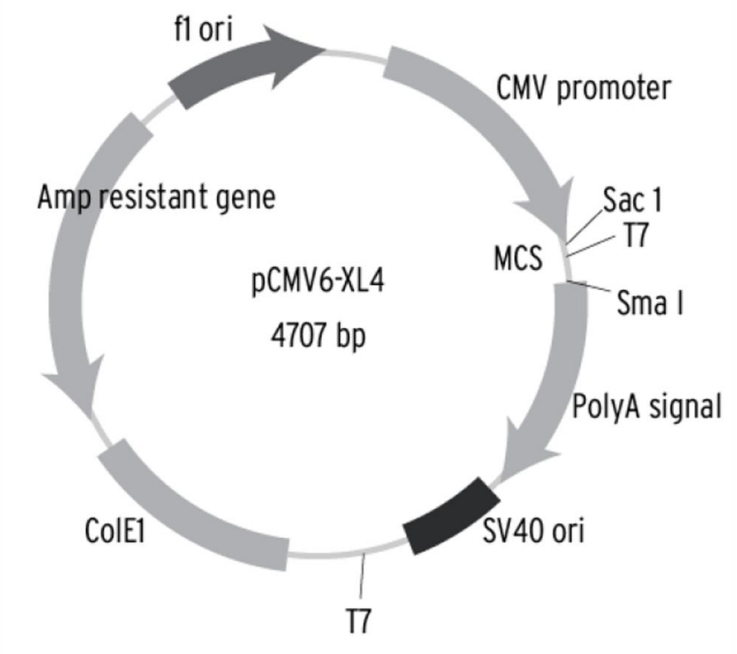

Polylinker Sequence of pCMV6-XL4, XL5, XL6, Neo and AC

A) pCMV6-XL4, XL5 and Neo

Vector Primer vp1.5 >

TTTGGCACCAAAATCAACG**GGACTTTCCAAAATGTCG**TAATAACCCCGCCCCGTTGACGCAAATGGGCGGTAGGCGTGTACG
AAACCGTGGTTTTAGTTGCCCTGAAAGGTTTTACAGCATTATTGGGGCGGGGCAACTGCGTTTACCCGCCATCCGCACATGC

T7 promoter >
Sac 1 (Not for sequencing) Not I EcoR I

GTGGGAGGTCTATATAAGCA**GAGCTC**GTTTAGTGAACCGTCAGAATTTT**GTAATACGACTCACTATAGG**GCGGCCGCGAATT
CACCCTCCAGATATATTCGT**CTCGAG**CAAATCACTTGGCAGTCTTAAAACATTATGCTGAGTGATATCC**CGCCGGCGCTTAA**

Xba 1 Not I Sma I

C----TrueClone_Insert-----CTCGAC**TCTAGA**TT**GCGGCCGC**GGTCATAGCTGTTTCCTGAACATGTGAT**CCCGGGT**
G----TrueClone_Insert-----**GAGCTGAGATCT**AA**CGCCGGCG**CCAGTATCGACAAAGGACTTGTACACTA**GGGCCCA**

GGCATCCCTGTGACCCCTCCCCAGTGCCTCTCCTGGCCCTGGAAGTTGCCACTCCAGTGCCCACCAGCCTTGTCCTAATAAA
CCGTAGGGACACTGGGGAGGGGTCACGGAGAGGACCGGGACCTTCAACGGTGAGGTCAC**GGGTGGTCGGAACAGGATTA**TTT

pcDNA 3.1 myc/His

Plasmid was used for expression of myc-tagged VKOR enzymes to verify expression by western blot. Vector information taken from www.sigmaaldrich.com visited on 19-Jan-2018.

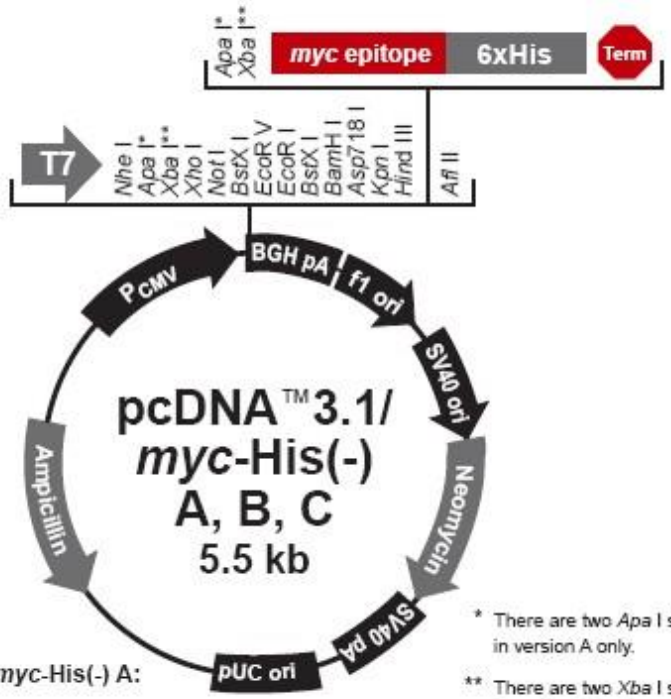

Comments for pcDNA™3.1/*myc*-His(-) A: 5522 nucleotides

CMV promoter: bases 209-863
T7 promoter/priming site: bases 863-882
Multiple cloning site: bases 895-1006
myc epitope: bases 1007-1036
Polyhistidine tag: bases 1052-1069
BGH reverse priming site: bases 1113-1130
BGH polyadenylation signal: bases 1116-1343
f1 origin: bases 1389-1817
SV40 promoter and origin: bases 1844-2152
Neomycin resistance gene: bases 2227-3021
SV40 polyadenylation signal: bases 3195-3325
pUC origin: bases 3708-4381
Ampicillin resistance gene: bases 4526-5386 (complementary strand)

List of publications

Publications:

Caspers, M., Czogalla, K.J., Liphardt, K., Muller, J., Westhofen, P., Watzka, M., and Oldenburg, J. (2015). Two enzymes catalyze vitamin K 2,3-epoxide reductase activity in mouse: VKORC1 is highly expressed in exocrine tissues while VKORC1L1 is highly expressed in brain. Thrombosis research *135*, 977-983.

Czogalla KJ, Biswas A, Höning K, Hornung V, Liphardt K, Watzka M, Oldenburg J (2017) Warfarin and vitamin K compete for binding to Phe55 in human VKOR. Nat Struct Mol Biol. Jan;24(1):77-85.

Czogalla, K.J., Liphardt, K., Hoening, K., Hornung, V., Watzka, M., and Oldenburg, J. (2018). VKORC1 and VKORC1L1 have distinctly different oral anticoagulant dose-response characteristics and binding sites. ADVANCES/2017/006775

Pezeshkpoor, B., Czogalla, KJ, Caspers, M., Berkemeier, AC, Liphardt, K, Ghosh, S., Kellner, M., Ulrich, S., Pavlova, A., and Johannes Oldenburg (2018). Variants in FIX propeptide associated with vitamin K antagonist hypersensitivity: functional analysis and additional data confirming the common founder mutations, Annals of Hematology AOHE-D-17-00776R1

Oral presentations:

FASEB Meeting Chicago (USA), 2015: Specific inhibition of VKORC1 and VKORC1L1 by 4-hydroxycoumarins

Poster presentations:

Hemophila Symposium Hamburg, 2012: Expression studies of murine VKORC1 in brain by *in situ* hybridization

GTH München, 2013: Expression pattern of the major player of vitamin K cycle VKORC1 in brain

ISTH Amsterdam (The Netherlands), 2013: Investigation on expression pattern of VKORC1 in mouse brain

GTH Wien (Austria), 2014: Screening for redox partners of vitamin K epoxide reductase complex, subunit 1-like 1 (VKORC1L1)

Hemophila Symposium Hamburg, 2014: Application of a modified $BaCl_2$ adsorption technique to identify novel vitamin K dependent proteins

Hemophila Symposium Hamburg, 2015: VKORC1 and its paralog VKORC1L1 are inhibited differently by various oral anticoagulants

ISTH Toronto (Canada), 2015: Susceptibility of VKORC1 and its paralog VKORC1L1 towards different 4-hydroxycoumarins

GTH Münster, 2016: Endogenous VKORC1 and VKORC1L1 inhibition by various oral anticoagulants in genetically engineered cells

ISTH Berlin, 2017: Specific inhibition of endogenous VKOR enzymes by oral anticoagulants reveals lower VKORC1L1 susceptibility due to different binding site

Danksagung

Ein großer Dank gebührt Prof. Oldenburg, der mir die Möglichkeit gegeben hat, diese Doktorarbeit an seinem Institut anzufertigen. Sein Interesse und Fachwissen rund ums Vitamin K bildeten die Grundlage für diese Arbeit, die durch Höhen und Tiefen (Stichwort Mäuse) gekennzeichnet war. Vielen Dank für die engagierte Förderung, auch über das Vitamin K hinaus, und die zahlreichen Möglichkeiten sich auf nationalen und internationalen Kongressen weiterzubilden.

Ein weiteres Dankeschön geht an Frau Prof. König (Institut für Pharmazeutische Biologie der Universität Bonn), die sich als Gutachterin für meine Dissertation zur Verfügung gestellt hat.

Ebenfalls möchte ich Dr. Matthias Watzka für seine Unterstützung während meiner Doktorarbeit danken.

Ein großes Dankeschön geht an Herrn Prof. Schweizer und Frau Dr. Fradejas Villar aus dem Institut für Biochemie und Molekularbiologie der Universität Bonn. Ohne ihre Hilfe wäre die Generierung der *Vkorc1l1* knockout-Mäuse so schnell nicht möglioch gewesen.

Ebenso möchte ich mich bedanken bei Herrn Prof. Hornung und Frau Dr. Höning aus dem Institut für Moleukulare Medizin der Universität Bonn. Ihre Hilfe bei der Generierung der HEK knockout Zellen war für uns Gold wert.

Natürlich darf in diesem Reigen Dr. Katrin Czogalla nicht fehlen. Ihr habe ich (wenn man ganz ehrlich ist) meine Doktorarbeit zu verdanken. Ausgehend von einer „kleinen“ Idee wuchs daraus ein Projekt welches wir bei *Blood Advances* publizieren konnten. Vielen Dank für deine Unterstützung!

Ein großes Dankeschön gilt den fleißigen Helfern im Hintergrund. Dazu gehören v.a. die Mitarbeiter und Mitarbeiterinnen aus der Gerinnung, der Molekularen Hämostaseologie und der Forschung. Vielen Dank für die tolle Zusammenarbeit, die stete Hilfsbereitschaft und bei Bedarf aufmunternden Worte.